AB-INITIO AND DFT INVESTIGATIONS OF HYDROGEN STORAGE

THESIS SUBMITTED TO
UNIVERSITY OF PUNE

FOR THE DEGREE OF
DOCTOR OF PHILOSOPHY
IN CHEMISTRY

BY
MUDIT DIXIT

RESEARCH GUIDE
DR. SOURAV PAL

PHYSICAL CHEMISTRY DIVISION
CSIR-NATIONAL CHEMICAL LABORATORY
PUNE – 411 008

NOVEMBER 2013

Ab-initio and DFT Investigations of Hydrogen Storage

Thesis submitted to

University of Pune

for the Degree of

Doctor of Philosophy in Chemistry

By

Mudit Dixit

Research Guide: Dr. Sourav Pal

Physical Chemistry Division

CSIR-National Chemical Laboratory

Pune – 411 008

November 2013

Declaration

I, Mudit Dixit, hereby declare that the work incorporated in this thesis entitled,

Ab-Inito and DFT Investigations of Hydrogen Storage

submitted by me for the degree of Doctor of Philosophy to the University of Pune is the record of the work I have carried out at the Physical Chemistry Division, National Chemical Laboratory, Pune – 411 008 from July 2008 to November 2013 under the supervision of Dr. Sourav Pal. Further, this work is original and has not formed the basis of award of any degree or diploma. Such material as has been obtained from other sources has been duly acknowledged in this thesis.

Date: _____

Mudit Dixit
Physical Chemistry Division,
National Chemical Laboratory,
Pune – 411 008

Certificate

CERTIFIED THAT the work done in the thesis entitled,

Ab-Inito and DFT Investigations of Hydrogen Storage

submitted by **Mudit Dixit** for the degree of Doctor of Philosophy to the University of Pune, was carried out by the candidate under my supervision in the Physical Chemistry Division, National Chemical Laboratory, Pune - 411008, India. Such material as has been obtained from other sources has been duly acknowledged in the thesis.

Date: _____

Dr. Sourav Pal
(Research Guide)
Physical Chemistry Division,
National Chemical Laboratory,
Pune – 411 008

To My Family

Acknowledgements

It is my pleasure to thank Dr. Sourav Pal, my Research Guide for permitting me to work in his group at National Chemical Laboratory (NCL), Pune and for offering me a stimulating problem of hydrogen storage.

I would like to thank him for his teachings, advice, guidance; quantum chemistry lectures, freedom and faith, without which this work would not have been possible. It was a great experience of working under his supervision, the knowledge gained while working in his group is valuable and significant. I am grateful to Dr. Sourav Pal, Director, NCL for providing me the foundation to carry out the work presented in this thesis. I am deeply obliged to UGC for funding my Junior and Senior Research Fellowship. I am thankful to DST for granting me the appropriate financial assistance to participate in international conference at Lille, France.

I must thank my friends and labmates, who have made my life easy during my Ph.D. work. I thank my seniors Dr. Nayana Vaval, Dr. Rahul Kar, Dr. Subhrata Banik, Lalitha, Sumantra Bhattacharya, Deepti Mishra, Dr. Bhakti Kulkarni, Dr. Tuhina Adit Maark, Dr. Sapna, Jitendra, Dr. Arijit Bag for their timely help and advice. It was a knowledge enriching experience to interact with the other scientists of our ESTG group: Dr. Kumar Vanka, Dr. Neelanjana Sengupta, and Dr. Sudip Roy. It was a great fun to interact with my batchmates and juniors, Debarati, Shantanu, Manzoor, Sayali, Achitya, Aryya and Susanta, Sudip, Deepak and Turbasu. I cannot do without thanking Mrityunjay Tiwari for his patient listening, sweet cheering, and for being a wonderful friend.

Outside my lab, I will always remember my friends Kapil, Devdutta Dandekar, Parth Patel, Krunal Patel and Atul Anand for all the moments of joyfulness, amusement and attention. I will never forget the early phase of my Ph.D, it was the time when I have learnt a lot from Sarvesh Soni and Ashwani Sharma. For this period, I must appreciate Jitendra Gupta for his togetherness and the discussion of basic quantum chemistry. I must also thank Subrata Banik and Rahul Kar for their encouragements.

I am very happy to express heartfelt thanks for togetherness and encouragement of Mrityunjay Tiwari in last phase of my Ph.D.

I do not have enough words to thank my family members for their kindness and firm support. I thank my brothers Rohit and Amit for their sincere concern and good counsel. I thank my father for his trust, patience, teachings and faith. I dedicate this thesis to my Papa. I must thank my mother for her absolute support in all the time of my life and my Ph.D. Finally, I thank my wife Kavita for her togetherness, unconditional encouragement, understanding and motivation.

Date: _____

Mudit Dixit

Contents

List of Abbreviations

The abbreviations used in this thesis (alphabetical order):

AIMD	*Ab initio* molecular dynamics
BOMD	Born-Oppenheimer molecular dynamics
BZ	Brillouin zone
CC	Coupled cluster
CI	Configuration interaction
CPMD	Car-Parrinello molecular dynamics
DFT	Density functional theory
DOS	Density of states
FC	Fuel cell
GGA	Generalized gradient approximation
HF	Hartree-Fock
HK	Hohenberg-Kohn
KS	Kohn-Sham
LDA	Local density approximation
MD	Molecular dynamics
MOF	Metal-organic framework
MP	Møller-Plesset
PW91	Perdew and Wang 1991
PAW	Projector augmented wave
PP	Pseudopotentional

QHA	Quasiharmonic approximation
TF	Thomas-Fermi
USPP	Ultra-soft pseudopotential
VASP	Vienna *ab initio* simulations package

List of Figures

List of Tables

List of Publications

This thesis is based on the following papers.

1. Ab initio and periodic DFT investigation of hydrogen storageon light metal-decorated MOF-5 **Dixit, M.**; Maark, T. A.; Pal, S. *Int. J. Hydrogen Energy* **2011**, 36, 10816−10827. (This work has been listed in ***Renewable Energy Global Innovations***)

2. Scandium-Decorated MOF-5 as Potential Candidates for Room-Temperature Hydrogen Storage: A Solution for the Clustering Problem in MOFs. **Dixit, M**.; Maark, TA.; Ghatak, K.; Ahuja, R. and Pal, S. *J. Phy. Chem. C.* ***2012****,116(33). pp. 17336-17342*

3. Why boron substitution increase the the interactions of metals with MOF-5. **Dixit, M.**; Chandrakumar, KRS. and Pal, S. (communicated JPC A)

4. Enhanced photoelectrochemical response of ZnO thin films with Mn doping: Experiments and first Principle calculations. Sharma, V.; **Dixit, M.**; Dass, S.; Shrivastav, R,; and Pal, S. (Communicated to IJHE)

5. ZIF-72 as a promising Hydrogen storage material: An ab-initio MD study. **Dixit, M.** and sourav Pal.(manuscript prepared)

The following papers are co-authored by me but are not included in this thesis:

1. Selective binding of benzoquinone with a PtII-cyclophane constructed on the skeleton of N,N'-bis(salicylidene)-p-phenylenediamine: Synthesis and spectroscopic studies. Kumari, N.: Prajapati, R.; **Dixit,**

M.; Mishra, L. "*Indian journal of chemistry A*. **2009**,48(12) 1644-1651.

2. Thiocyanato Bridged Heterodinuclear Complex[$Cu(bpy)_2$(-NCS)$Ru(bpy)_2(NO_3)$]$(PF_6)_2$ and Its Binding with Cd(II), Hg(II), Pb(II) and Ag(I) Ions. Kumari, N.; **Dixit,M.**; Herbert,WR.; and Mishra,L. *Chemistry for Sustainable Development* (**2012**) ISBN 978-90-481-8649-5 p-231

3. Kumar, K.; **Dixit, M.**; Khere, JM. and Pal, S. "Molecular Dynamics simulation on Aspargillus Niger: Insights to its unfolding pathway".(accepted)

Abstract

Hydrogen economy is a cutting edge technology which utilises the fuel cell to obtain the electrical energy by means of chemical reaction between hydrogen and oxygen. Fuel cells provide a very efficient and clean source of electrical energy. However, the need of efficient storage system is a key problem of hydrogen economy. Hydrogen storage on solid materials via adsorption is an ingenious alternative.

There are various solid-state H_2 storage materials, which are presently being investigated. However, no material is found to have all the properties required for practical storage of hydrogen. Due to the growing need of energy, it is essential to use currently existing technologies along with development of new H_2 storage materials. Experimentally, this is a time taking process. Furthermore, it requires significant individual and economic resources. Computational materials science, in comparison, is a fast and efficient way for designing novel materials. Moreover, theoretical results can also validate experimental results. Consequently, the primary motivation of this thesis is to apply computational material science to design new different classes of H_2 storage materials and to explore the fundamental interactions involved in these materials.

The motivation of this thesis is to use a computational approach to investigate different hydrogen storage materials. In the thesis we will be specifically studying Metal Organic Frameworks (MOF) based materials due to their tremendous promise for the purpose of hydrogen storage and the need for enhancing their hydrogen storage properties. To this end, in this thesis we have performed density functional theory (DFT) based calculations to study theoretically the ground state lattice structure, electronic structure; effect of dopants, new MOF and ZIF based materials via novel dopants, of these hydrogen storage materials. The effect of boron substitution followed by metals decoration has also been studied using detailed molecular orbital analysis.

Thesis organization:

Chapter 1 Introduction

In this chapter, we will give a brief introduction to fuel cells and their advantages and applications. This will be followed by explanation of the use of hydrogen as a fuel for fuel cells. Thereafter, we will provide a brief discussion on the problems associated with hydrogen storage. We will explain the various mechanisms of solid-state hydrogen storage. Furthermore, we will review few hydrogen storage materials, namely, ammonia borane, clathrate hydrates, metal organic frameworks, and complex metal hydrides. We will end the chapter by describing the motivation behind the research carried out and by presenting an outline of the thesis.

Chapter 2 Theoretical background

In this chapter we will present a brief introduction to the theory behind the methodology used in the thesis. Firstly, we will give a brief introduction to the many-body problem by using Hartree approximation, the Hartree-Fock (HF) approximation, and the methods which go beyond HF. Thereafter, we will provide a discussion on the use of density functional theory (DFT). This will be followed by a description of the concepts of molecular dynamics and *ab initio* molecular dynamics. At the end, we will discuss the implementation of the plane wave-pseudopotential molecular dynamics method in the program package of VASP.

Chapter 3 Electronic structure

In this chapter we will begin MO treatment of band theory. Later we will discuss the different tools available for studying electronic structure of solids. Our results of the charge density, band structure, and density of states (DOS) analyses on pure and Mn-doped and pure ZNO will be presented. We will illustrate from the band structure and DOS calculations that Mn doping reduces the band gaps of the three phases of Zno. By examination of the partial DOS, it will be further shown that this reduction in band gaps is due to generation of additional bands arising from the Mn impurities. Finally, the decreased

band gaps will be used to suggest that doping with Mn in ZnO makes this material suitable to be used for photoelectrochemical splitting of water to produce hydrogen.

Chapter 4 Light Metal decorated MOF

In Chapter 4, The effect of light metal (M = Li, Be, Mg, and Al) decoration on the stability of metal organic framework MOF-5 and its hydrogen adsorption is investigated by ab initio and periodic density functional theory (DFT) calculations by employing models of the form BDC:M2:nH2 and MOF-5:M2:nH2, where BDC stands for the benzenedicarboxylate organic linker and MOF-5 represents the primitive unit cell. The suitability of the periodic DFT method employing the GGAPBE functional is tested against MP2/6-311+G* and MP2/cc-pVTZ molecular calculations. A correlation between the charge transfer and interaction energies is revealed. The metal-MOF-5 interactions are analyzed using the frontier molecular orbital approach. Difference charge density plots show that H_2 molecules get polarized due to the charge generated on the metal atom adsorbed over the BDC linker, resulting in electrostatic guest-host interactions. Our solid state results show that amongst the four metal atoms, Mg and Be decoration does not stabilize the MOF-5 to any significant extent. Li and Al decoration strengthened the H2-MOF-5 interactions relative to the pure MOF-5 exhibited by the enhanced binding energies. The hydrogen binding energies for the Li- and Al-decorated MOF-5 were found to be sensible for allowing reversible hydrogen storage at ambient temperatures. A high hydrogen uptake of 4.3 wt.% and 3.9 wt.% is also predicted for the Li- and Aldecorated MOF-5, respectively.

Chapter 5 Transition metals novel dopants for MOF

Transition-metal-based systems show promising binding energy for hydrogen storage but suffer from clustering problem. The effect of light transition metal (M = Sc, Ti) decoration, boron substitution on the hydrogen storage properties of MOF-5, and clustering problem of metals has been investigated using ab initio density functional theory. Our results of solid-state calculations reveal that whereas Ti clusters strongly Sc atoms do not suffer from this problem when decorating MOF-5. Boron substitution on

metal-decorated MOF-5 enhances the interaction energy of both the metals with MOF-5. Sc-decorated MOF-5 shows a hydrogen storage capacity of 5.81 wt % with calculated binding energies of 20−40 kJ/mol, which ensures the room -temperature applicability of this hydrogen storage material. Furthermore, we have studied ZIF-72 a hydrogen storage material by studying hydrogen adsorption sites and metal decoration.

Chapter 6 Why Boron Substitution Increases the Interaction Energies of Metals with Benzene Based MOFs

To tune the interaction energies of metals with host materials and their H_2 binding energies ($E_{binding}$), boron substitution in the framework has been widely pursued. The investigation of role of boron substitution in enhancement of the interaction energies is necessary for designing new and potential storage materials. Our results demonstrate that boron substitution provides the proper symmetry in the framework to overlap with the metals orbitals. These orbital interactions increase the host-guest interactions, leading to increase in the interaction energies. We have also investigated the nature of interaction of H_2 molecules with metals in metal decorated-boronsubstituted benzene as a model system for benzene based MOFs

CHAPTER 1

Introduction

The development of sustainable energy technology is essential to satisfy the growing demand of energy. The energy demands will increase day by day. However, the natural resources are limited. Thus, it is necessary to take up the responsibility to develop and utilize the technologies that will save natural resources and protect our environment.

An innovative solution to this problem is fuel cell technology. This technology has a potential to solve the environmental needs. Hydrogen is used as efficient fuel for fuel cells. However, the storage of hydrogen is key challenge for the fuel cell technology to reduce the volume by mass ratio of hydrogen gas. To solve the problem of low density of hydrogen, it is adsorbed on active solid-state materials. Designing such active storage materials requires innovation, experimentation, and understanding of the fundamentals of hydrogen storage. The understanding can be achieved by a synergistic approach involving both theory and computation, which can be used not only to understand experimental results but also to guide them. We will begin this chapter with a brief introduction to fuel cells and their applications. We will also discuss that how hydrogen is used in the fuel cells. The practical problems associated with high pressure and

cryogenic liquid hydrogen storage is elaborated in Section 1.2. Section 1.3 explains the different mechanisms of hydrogen storage. In later sections we provide a brief summary of experimental and theoretical attempts of a few selected hydrogen storage materials. To the end of this chapter we describe the motivation of the research carried out herein and we present an outline of this thesis in Section 1.8.

1.1 Fuel Cells

A *fuel cell* (FC) is a device, which converts the electrochemical energy into electricity using hydrogen and oxygen as fuel. The FC was discovered by William Grove in 1839. He constructed a model, which comprised of four different cells of hydrogen (H_2) and oxygen. He had shown that his model of FC could produce electric current. He further used this current to split the water into H_2 and oxygen (see Fig. 1.1). However, he found that the output currents are small because of the low contact area between the gas, electrode, and the electrolyte and due to the large distance between the electrodes. This causes the electrolyte to resist the flow of electronic current. The electrodes used now a days are usually made flat with a thin layer of electrolyte sandwiched between them (Fig. 1.2). To avoid the problems found in

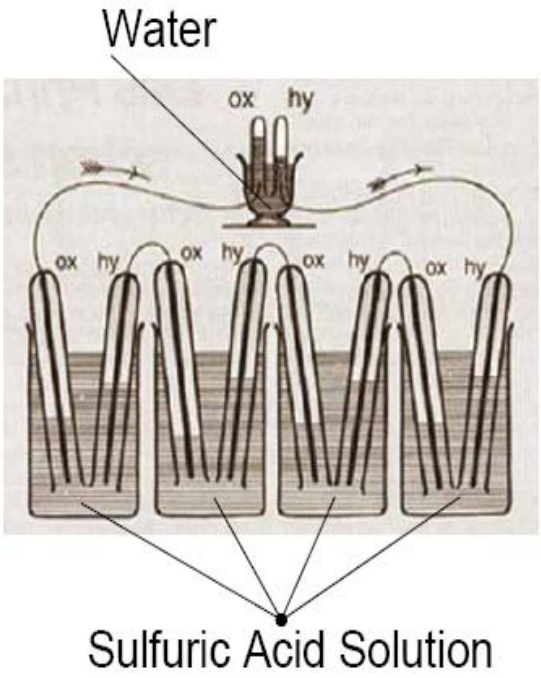

Figure 1.1 William Grove's fuel cell.

ion between hydrogen and oxygen to generate
s into the anode side of the FC where it ionizes

to release electrons and H ions.

$$2H_2 \rightarrow 4H^+ + 4e^- \qquad (1.1.1)$$

This process releases energy. The protons pass through the membrane and at the cathode react with oxygen to form water.

$$O_2 + 4e^- + 4H^+ \longrightarrow 2H_2O \qquad (1.1.2)$$

The electrons, which cannot pass through the membrane, flow from the anode to the cathode via an external circuit containing a motor, which consumes the power generated by the FC.

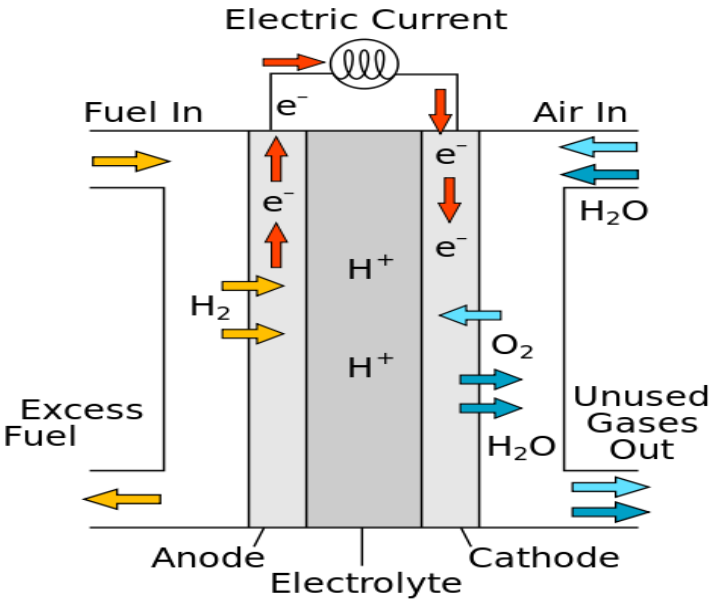

Figure 1.2 Representation of a fuel cell.

1.1.1 Fuel Cells: Applications

FCs convert one of the forms of energy to another. However, these are very different from internal combustion engines (ICE). ICEs run on high temperature explosions resulting from the release of chemical energy by burning fuel with oxygen in the air. Hence, these produce lot of noise. In comparison, FCs are very simple with few moving parts, which make these very quiet. ICEs first change chemical energy of a fuel

into thermal energy and then into mechanical energy. The second step is limited by the Carnot Cycle. On the other hand, FCs and batteries directly convert chemical energy into electrochemical energy and thus are generally more efficient than ICEs. In a battery the reactants are stored internally and when used up the battery must either be replaced or recharged. In FCs the reactants are stored externally and once refuelled, they immediately start functioning. A further advantage of using FCs is that when H_2 is used as the fuel, the only by-product is water which is environmentally benign. When used in vehicles they would result in essentially zero harmful emissions.

FCs have a wide variety of applications which are classified as transportation, portable and stationary. Polymer electrolyte membrane fuel cells (PEMFCs) which provide a continuous electrical energy supply from fuel at high levels of efficiency and power density at low operating temperature-pressure conditions are well suited for the transportation applications. PEMFCs can also be used for the purpose of portable applications such as laptops, mobile cell phones and even military communications equipment along with direct methanol fuel cells. The commercial stationary FC systems that are used for providing combined heat and power and for distributed power generation are based on molten carbonate fuel cells and solid-oxide fuel cells.

Hydrogen as an energy carrier

The usage of fuels rich in carbon such as wood and coal has been reduced, over the years. The fuels such as oil and natural gas which are rich in H_2 are being used nowadays. Currently, a transition towards a hydrogen economy is easily anticipated. Hydrogen, because of its very high energy content, excellent electrochemical reactivity and zero CO_2 emission, is indeed the most promising fuel for FCs. H_2 is the most abundant element in the universe. However, it does not occur naturally as a gaseous form. For practical FC systems, it is generated from either fossil fuels or water before it can be used as a fuel.

The widely pursued technology for large scale production of H_2 is steam

reforming. The forming reactions for a hydrocarbon of the form CnHm are:

$$C_nH_m + nH_2O \rightarrow nCO + (m/2 + n)\ H_2 \quad (1.1.3)$$

$$CO + H_2O \rightarrow CO_2 + H_2 \quad (1.1.4)$$

These are high temperature reactions (500 ^{o}C), carried out normally over a supported nickel catalyst. Partial oxidation is an alternative way of producing hydrogen, it requires even higher temperatures (1200-1500 ^{o}C) but these can handle much heavier petroleum fractions. The corresponding reaction for CH_4 is:

$$CH_4 + ½\ O_2 \rightarrow CO + H_2 \quad (1.1.5)$$

Pyrolysis or thermal cracking is another way of producing hydrogen in the absence of air. The main advantage of this process is that H_2 is produced with high purity. Removing the formed carbon, however, remains a challenge. The method of generating H_2 from H_2O using the electricity generated from sunlight via photovoltaic cells (*Photoelectrolysis*) is also used as alternative. Manufacturing H_2 from *biological processes* such as photosynthesis and fermentation using bacteria is also being explored recently.

1.2. Hydrogen Storage: The Problem

Main difficulty in H_2 storage arises because of its extremely low energy density. At normal temperature and atmospheric pressure, 1 kg of H_2 occupies a volume of 11m^3. The high volume makes it complex to store a large mass of H_2 in a small space. The improvement of energy density of gaseous hydrogen is often attempted by storing H_2 at higher pressures. A significant driving range of any vehicle can be achieved by increasing the mass of H_2 but this needs expense of increased cost and valuable space within the vehicle. The other practical challenges regarding gaseous H_2 storage are refuelling times,

heat management requirements, volumetric capacity and energy density.

Storing H_2 as a liquid increases its energy density to (8.4 MJ/L) which is almost twice that of H_2 gas compressed at 10,000 psi (4.4 MJ/L). However, liquefaction requires significant energy. Also this is done in several stages. First stage is the compression of gas, followed by cooling it to 78 K using liquid nitrogen. High pressure is then used to further cool the H_2 by expanding it through a turbine. Furthermore, liquid H_2 has a very low boiling point of -253 ^{o}C, requiring excellent insulation techniques to avoid boil-off. Thus practical applications of H_2 storage by liquefaction are severely limited.

1.1 Hydrogen storage at solid state

Storing H_2 in solid state materials is a promising alternative to classical storage of H_2 in pressurized tanks and cryogenic vessels. This method offers various advantages (i) a H_2 storage process which has low-pressure and room-temperature feasibility, (ii) the capacity to meet the requirements for on-board storage, and (iii) the highest gravimetric density. A Hydrogen storage material must exhibit reversible H_2 uptake/release, for practical applicability. The material should have a high gravimetric H_2 storage capacity. Hydrogen removal energies for this material should be optimal and can be achieved to at reasonable temperature and pressure. It should also have a fast H_2 desorption/absorption kinetics. Finally the material should be reasonably stable and can be manufactured at low cost.

There are three classical mechanisms known for hydrogen storing in materials, namely, absorption, adsorption, and chemical reaction. In *absorptive storage,* H_2 is absorbed directly into the bulk of the material. For example, in simple crystalline metal hydrides atomic hydrogen gets incorporated in the interstitial sites of the lattice (see Fig. 1.3) or low temperature hydrogen adsorption in Metal Organic Frameworks (MOFs). *Adsorptive storage* can take place via physisorption or chemisorption. Such sorptive processes typically occur on high-surface area porous materials. The *chemical reaction route for hydrogen storage* involves displacement chemical reactions, essentially by

forming new chemical bonds which may be reversible or irreversible, for both H_2 generation and H_2 storage. In the former case, H_2 generation and H_2 storage involve a simple reversal of the chemical reaction as a result of modest changes in the temperature and pressure. For irreversible H_2 storage chemical reactions, the H_2 generation reaction is not reversible under modest temperature/pressure changes, so that storage requires larger temperature/pressure changes or alternative chemical reactions. In the following sections we discuss some of the H_2 storage materials of current interest.

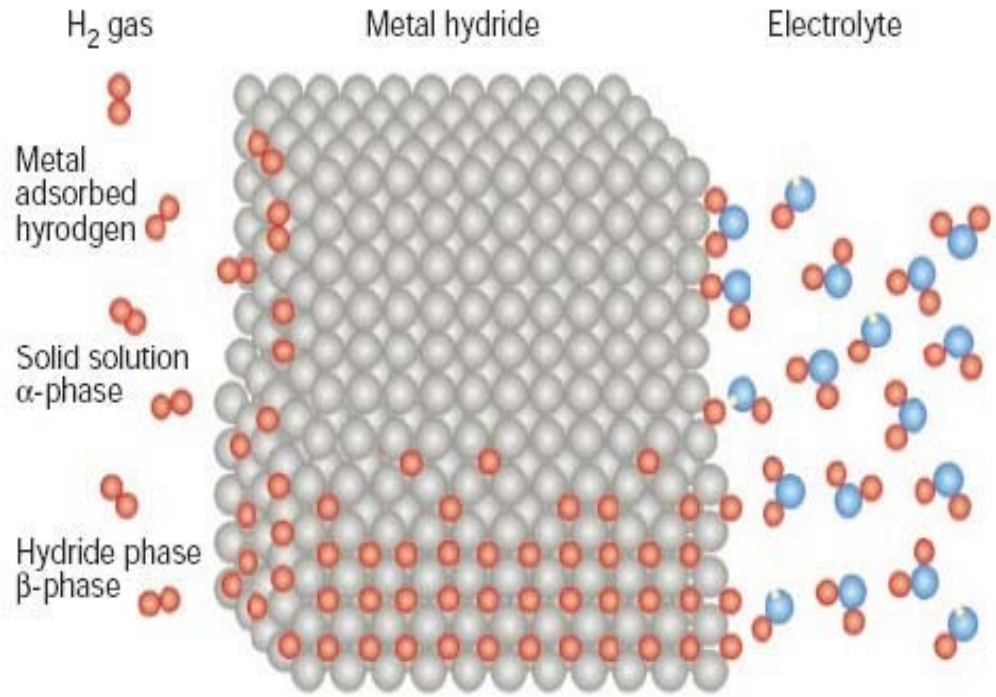

Figure 1.3 Model of a metal structure with H atoms in the interstices between the metal atoms, and H_2 molecules at the surface. (Source: ref.1)

1.4 Metal Organic Frameworks (MOFs)

Metal-organic frameworks (MOFs) are hybrid inorganic/organic crystalline materials in which metal ion clusters are linked by organic ligands to form extended frameworks that are highly stable as well as microporous. [2] With a number of organic ligands and metal ions that are available for use in the synthesis scheme a variety of networks with desired pore dimensions and metal centres can be designed.

In a path breaking work in 2003 Rosi et al. [3] reported favourable H_2 sorption properties of up to ~4.5wt.% H_2 at 78 K for MOF-5. It can be seen from Fig. 1.5 (a) that MOF-5 is built from inorganic $[OZn_4]^{6+}$ groups joined by an octahedral array of $[O_2C\text{-}C_6H_4\text{-}CO_2]^{2-}$ (1,4-benzenedicarboxylate or BDC) groups. The H_2 storage capacity however reduced to 1.0 wt.% H_2 at room temperature and 20 bar pressure. The corresponding H_2 adsorption isotherms of MOF-5 at 78 K and 298 K are displayed in Figs. 1.5 (b) and (c). MOF-177 [4, 5], IRMOF-20 [6, 7], MIL-101 [7, 8] and $[Cu(L_2)(H2O)_2]$ (L=terphenyl-3,3'',5,5'-tetracarboxylate) [9] have also been reported to show high H_2 uptake in the range of 5.0-7.5 wt.% H_2 at 77 K and moderate pressure. But at 298 K their maximum H_2 uptake falls below 1.5 wt.% H_2.

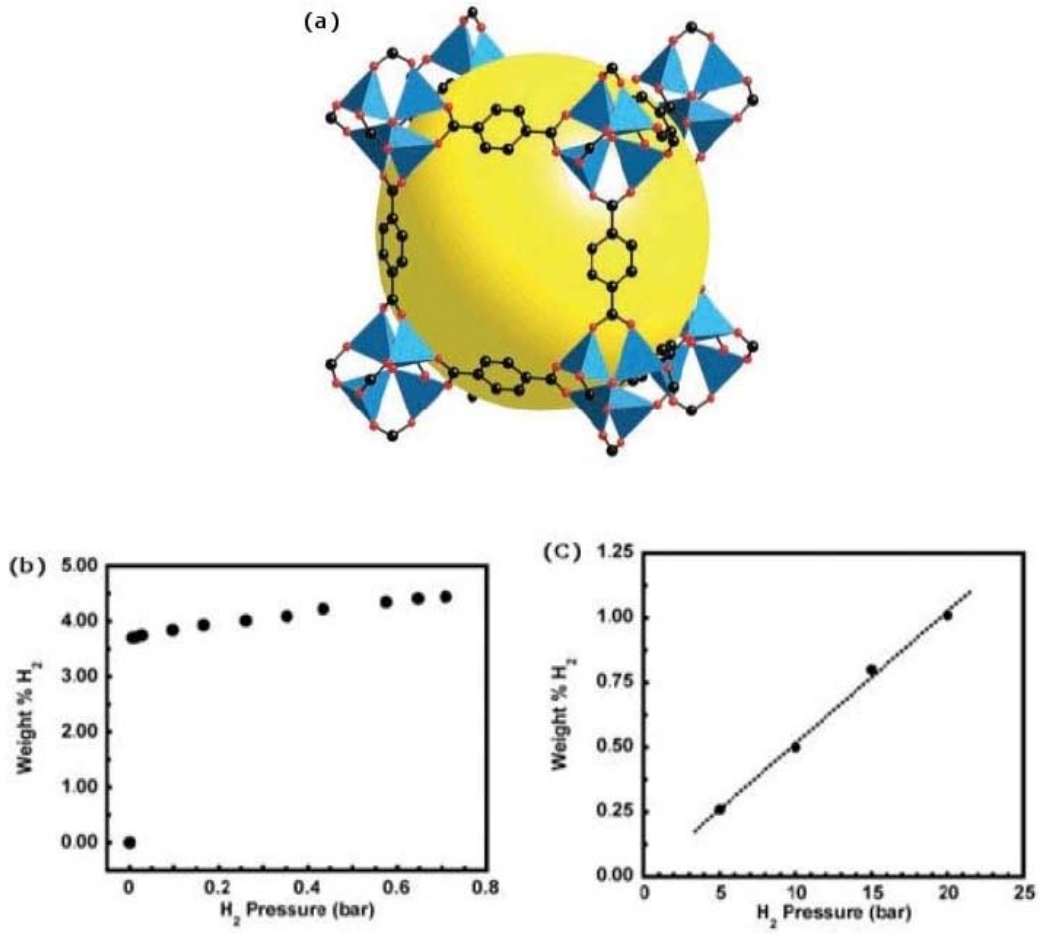

Figure 1.4 (a) MOF-5 unit cell; Hydrogen adsorption isotherms of MOF-5 at (b) 78 K and (c) 298 K. (Source: Ref. 3)

MOFs can adsorb guest molecules, and thus are good candidates for H_2 storage [10]. There is predominant contribution of Van der Waals interactions between the H_2 molecules and the MOFs. Thus, the resulting H_2 binding energies are typically in the range of 2.26-5.2 kJ/mol [11-13]. Due to these low binding energies, MOFs exhibit fast adsorption/desorption kinetics. The downside is that considerable hydrogen adsorption can only be obtained at low temperatures of ~77 K. Lochan and Head-Gordon have shown[14] that the ideal H_2 binding energy range is ~28-40 kJ/ mol at room temperature and~30-42 kJ/mol at~50℃. Thus, undoubtedly it is essential to increase the H_2 binding energy ($E_{binding}$) as well as enhance the H_2 storage capacity of MOFs to make these useful for practical and mobile applications. There are various approaches explored by researchers to improve hydrogen adsorption in MOFs, these include optimization of pore

size [15], addition of guest molecule [16] and catenation [15]. The idea of optimization of pore size is recently exploited by Li et al. [17]. Authors have shown that MOF-5 synthesized by solvothermal approach found to have the higher surface area and pore volume, when compared to the MOF-5 synthesized by conventional method. Introduction of electron donating groups within the framework and inclusion of open metals sites [18] have been attempted to enhance the H_2 binding energies. It is essential to understand the nature of main interactions involved in H_2 adsorption in order to enhance the H_2 storage and $E_{binding}$ in MOFs. Quantum mechanical studies on the linker alone have been found valuable to predict the H_2 binding sites and the orientation and to determine the binding energies. In the first computational investigation on MOF-5, Hubner et al. [19] studied simple benzene based model systems, namely, C_6H_6X (X= H, F, OH, NH_2, CH_3 and CN), naphathalene, anthracene, coranene, terethalicacid and dilithiumterephthalete. They employed MP2 method, to study these model systems. Their results revealed that the binding energy is increased with increase in ring size from 3.91 kJ/mol, for benzene to 4.28 kJ/mol, for naphthalene. Sagara et al.[20] studied both the organic linker part and zinc oxide part of MOF-5 using MP2 method. They found that H_2 preferably binds between two zinc clusters. Buda et al. [21] have illustrated that the top site had a higher $E_{binding}$ than the edge site of BDC linker in MOF-5. Han et al. [22-24] showed that accurate force fields used in Grand Canonical Monte Carlo (GCMC) calculations to determine the loading of H_2 as a function of pressure and temperature. Full periodic DFT study of MOF-5 was carried out by Mulder et al. [25] and Mueller and Ceder. [26] They found five symmetrically unique adsorption sites and concluded that the strongest interaction H_2 sites are located near the Zn_4O clusters. A recent critical review [27] sheds light on recent advances on investigation of MOFs and covalent organic frameworks (COFs) using computational methods. The authors have also discussed the different approaches which are being pursued for improving hydrogen storage in these materials. One of the interesting methods is “metal decoration” of the organic linker part of the MOFs. Formerly, many theoretical studies have been focused on the interaction of H_2 molecules with transition metal ions [28-31]. Noteworthy is the investigation by Gagliardi and Pyykko [32] which showed that bare neutral and cationic transition metals such as Cr, Mn+, W, Mo, V^+ and Ti^{2+} can bind with as many as six H_2 molecules. Maark

et al. [33] have studied the effect of metal ions, Na^{+}, Mg^{2+}, Al^{3+} and Be^{2+} using benzene as a simple model of MOF-5. A well-known study by Chandrakumar and Ghosh [34] showed that s-block metal cations could bind with even more number of H_2 molecules and form complexes of the type $M(H_2)_8$ complexes with high binding energies. The binding energies for these light metal cations were calculated to be between 56.48 kJ/mol to 753.1 kJ/mol. However, manufacturing such bare metal cations in reality is difficult. Alternatively the metal atoms can acquire charge via charge transfer by adsorption on surfaces with high electron affinity. Recently, activation of nanomaterials has also been attempted via spillover effect. H_2 adsorption in MOFs can be improved by using co-ordinately unsaturated ions such as Mg^{2+} [109], Ni^{2+} [110] and Zn^{2+} [111] in the metal oxide core. The coordinative unsaturation basically brings about stronger physisorption with a concurrent decrease in the density of the framework.

Research studies have exhibited that at moderate temperature and pressure conditions, doping of nanomaterials like nanotubes [36], nanofibers [37] and nanospheres [38] increases the $E_{binding}$ of these materials. But transition metal based materials show very high binding energy [41-43]. Zhao et al. [39], through their studies on organometallic buckyballs, found that the calculated $E_{binding}$ for transitions metals was w0.3 eV. In another well known study of transition metal decoration by Yildirim et al. [40] illustrated that Ti-decorated nanotubes can adsorb upto 8 H_2 per Ti but with a high binding energy of .43 eV/H_2. Due to these high $E_{binding}$, these materials cannot be used for reversible H_2 storage. Furthermore, transition metals have a tendency to bind among each other thereby decreasing the H_2 storage capacity [44]. This has been found to be true in case of embedding in MOFs [45-50] or attachments by strong covalent bonds with host materials [43,51]. A possible solution of this problem is to use elements with low cohesive energy, like s-block metals. The light metal decoration approach has been investigated theoretically on several systems including carbon nanotubes (CNTs), graphene and fullerenes [38,41,52-57]. In a particularly interesting work, Sun et al. [53], using de nsity functional theory, illustrated that Li-coated fullerenes do not suffer from the clustering problem of transition metal based materials discussed above. They found that an isolated $Li12C_{60}$ cluster where Li atoms are capped onto the pentagonal faces of the fullerene was not only very stable but could also store up to 120 hydrogen atoms in

molecular form with a binding energy of 0.075 eV/H_2. A similar strategy is now being widely considered for MOFs. Blomqvist et al. [58] have studied Li-decorated MOF-5 by ab initio periodic DFT calculations and shown that each Li adsorbed over each benzene ring in MOF-5 can cluster up to three H_2 molecules with binding energies between 12.0-18.0 kJ/mol H_2. It was predicted through ab initio molecular dynamics simulations that the system would exhibit a hydrogen uptake of 2.9 wt.% and 2.0 wt.% at the high temperatures of 200 K and 300 K, respectively. Han and Goddard III [59] have predicted gravimetric H_2 adsorption isotherms for several pure and Li-doped MOFs at 300 K using an ab initio based GCMC simulation. They found that Li-doped MOF-5 showed significant H_2 binding at 300 K and 100 bar. Another interesting result of their calculations was the high H2 uptake of 6.47 wt.% predicted for MOF-C30 at these conditions. Recently, Venkataramanan et al. [60] have explored isoreticular MOFs with different metals M= Fe, Cu, Co, Ni and Zn through DFT and predicted that Li doping will be possible only in Zn-based MOFs. Ab initio calculations have demonstrated that Ca can decorate organic linkers of MOF-5 with a binding energy of 1.25 eV and that the resulting hydrogen storage can be as high as 4.6 wt.% [61] Furthermore, the H_2 binding was found to be significantly stronger than the Van der Waals interactions. In a current study Zou et al. [62] have studied hydrogen storage in Ca-decorated, B-substituted MOFs through first-principles electronic structure calculations. Substitution of B atoms in place of C atoms in the benzene ring of the BDC linker increased strength of interaction of Ca with the linker as well as the interaction of H_2 molecule with Ca. A hydrogen uptake of 8 H_2 per Ca-decorated linker was found with binding energy of 20 kJ/mol rendering it suitable for reversible H_2 storage under ambient conditions. Many attempts have been made to determine the major contributing factor, the London dispersion interactions (LDI) versus interactions due to the electrostatic potential of the host materials, for H_2 adsorption in pure MOFs. Bordiga et al. [12] applied a combination of IR spectroscopy and ab initio calculations to exhibit that the adsorptive properties of MOF-5 are mainly due to the (i) dispersive interactions with the internal wall structure and (ii) weak electrostatic forces associated with $O_{13}Zn_4$ clusters. Kuc et al.[63,64] modeled IRMOF-1 by individually examining its cornerposts and linkers. Their calculations revealed that the physisorption of H_2 in MOFs is mainly due to LDI between linkers and connectors with

hydrogen while the host-guest induced electrostatic interactions were unimportant as the charge separation in the MOF is not large enough to induce significant dipole moments in H_2. It is further concluded that it is necessary to use correlation methods and large basis sets for correctly describing the LDI in these systems. Therefore, methods based on DFT which are unable to correctly describe dispersion forces and Van der Waals interactions face challenges in studying pure MOFs. But it is also known that ab initio methods such as MP2 and CCSD(T) are not practical for application to the full structure.

1.5 Metal Hydrides

Metal hydrides formed by metal atoms that represent a host lattice and hydrogen atoms. Generally there are two kinds of hydrides, α phase and β-phase. At α phase only some hydrogen is absorbed and at β-phase the hydride is fully formed. Hydrogen storage capacity of metal hydrides and their potential depends on depends on different parameters. Different metals have different ability to dissociate hydrogen; this ability is dependent on electronic structure, morphology, purity and surface structure [65]. A potential hydrogen-storage material must have the following properties. High gravimetric storage, this represents the amount of available energy, low desorption temperature, reversibility, fast kinetics, high stability against O_2 and moisture and recyclability. Hydrogen-storage as metal hydride has been the studied intensively over the last decade [66–72]. The light metals like Li, Be, Na, Mg, B and Al, form a various hydrides. They are very attractive due to their high gravimetric wt. % of hydrogen. Currently, there are various studies on modifying and optimizing their properties to use these as practical hydrogen storage materials. In a detailed critical review by Guo et. al[73] they have explored material challenges associated with hydrogen storage and the effect of mechanical milling and chemical additives on metal hydride properties. Recently in another review Shevlin and Guo [74] outlined the fundamentals behind density functional theory (DFT) and expounded upon its applications for calculating quantities such as hydrogen binding energies, enthalpies and free energies of formation, diffusion and reaction pathways, activation barriers and transition states of metal hydride mixtures.

1.5.1 Complex Metal Hydrides

Complex metal hydrides are widely explored in last two decades; these are very attractive hydrogen storage candidates. These are formed by the combination of hydrogen with light metals to form stable hydrides of the form $NaAlH_4$, Na_3AlH_6, $LiBH_4$, $LiNH_2$, and Li_2NH. These are called complex hydrides because in these hydrides the hydrogen atoms are covalently bonded to the central atoms in the "complex" anions.

$NaAlH_4$ is one of the widely studied complex aluminium hydride or alanate which releases H_2 via a two-step process:

$$3NaAlH_4 \rightarrow Na_3AlH_6 + 2Al + 3H_2 \quad (1.5.1)$$

$$Na_3AlH_6 \rightarrow 3NaH + Al + \frac{3}{2}H_2 \quad (1.5.2)$$

It has reasonably good gravimetric H_2 storage capacity of about 5.5 wt.%. These reactions have high desorption temperatures (185-230^oC and 260^oC, respectively.) and thus have high kinetic barriers. Due to these high barriers and irreversibility these reactions do not seems practical of real life applications. An important research study [75] demonstrated that Ti doping in $NaAlH_4$ kinetically enhances the dehydrogenation reactions. Also on Ti doping these desorption reactions became reversible under moderate conditions in solid state. However, the H_2 storage capacities were found to reduce rapidly upon recycling the reactions. Furthermore, the desorption kinetics was still insufficient for practical application H_2 storage.

Many theoretical studies attempted to interpret the role played by Ti in reducing the dehydrogenation temperature of $NaAlH_4$. However, most of these gave inconsistent results about the favorable substitution site for Ti in the material.[76-79] Araújo et. Al[80] found that the desorption of two hydrogen atoms from this material a system was in fact exothermic in nature with respect to formation of a H_2 molecule. In another similar work by Li et al.[82] studied the effect of Ti and metal vacancies on the electronic

structure, stability, and dehydrogenation of Na_3AlH_6. [81] Subsequently, Blomqvist et al. [83] studied the effect of other transition metal atoms on dehydrogenation of $NaAlH_4$. They found that Cr and Fe more effective dopants than Ti.

A combined experimental and theoretical approach demonstrated that fullerenes, nanotubes and graphene are good catalysts for hydrogen uptake and release in $NaAlH_4$. [84] It was concluded that the electron affinities of these carbon based catalysts were playing important role in the hydrogen sorption. They have also demonstrated that the curvature of these carbon nanostructures also affects the catalytic process. They found that fullerene is better catalyst than carbon nanotubes.

Many other complex metal hydrides are studied for hydrogen storage, some of these are $LiAlH_4$, $KAlH_4$ and $Mg(AlH_4)_2$.

1.6 Clathrate hydrates

Crystalline inclusion compounds of hydrogen bonded water cages are called *Clathrate hydrates*. These materials can bind to certain molecules hence these can be potentials host of small molecules like hydrogen.

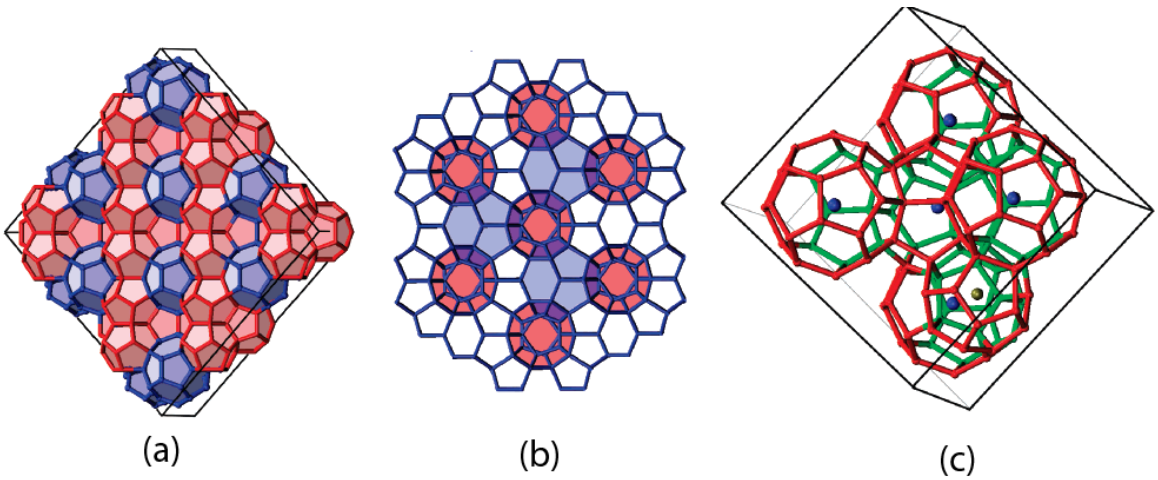

Fig. 1.5. (a) Clathrate *sII* structure (b) Layer of the clathrate *sII* structure (c) Cubic unit cell of the clathrate *sII* structure130 (source ref 135)

In a classical study Dyadin et al.[85] studied the H_2O-H_2 system and found a temperature region with anomalous melting behavior with kinetics of ice melting at H_2 pressures of 100-360 MPa. They proposed this state as a clathrate phase of hydrogen hydrate. Subsequently, Mao et al. [86] have discovered first H_2 clathrate hydrates in 2002. They found these in classical sII structure with a unit cell containing 136 H_2O molecules. They suggested that four hydrogen molecules are stored in a large *sII* clathrate cage, and two hydrogen molecules are stored in a smaller cage. This clathratewas found in frameworks around eight hexakaidodecahedron ($5^{12}6^4$) and 16 pentagonal dodecahedron 5^{16} cages. Following this work, Lokshin et al.[87] studied the composition of this clatharate phase and found that there is only one hydrogen molecule in small cages of *sII* clathrate corresponding to the 3.9 mass % hydrogen content in the clathrate. It was later thought that each cage of hydrate can accommodate only one guest molecule.

The potential of the clathrates as a hydrogen storage material were further explored by Mao et. al [88]in 2004. These prior investigations were later followed by other studies by the broader community. There are five main obstacles in the practical applications of H_2 clathrate hydrates, namely, (a) slow kinetics (b) enclathration, (c) high pressures required for clathrate formation and stabilization, and (d) relatively low H_2 storage capacities (e) low stability of clatharate hydrates.

One of the approaches to enhance the kinetics of clathrate formation is to increase the surface-to-volume ratio of clathrate hydrates by using small crushed ice particles [88]. However, the use of crushed ice is problematic for multiple cycles, also the material would go back to the bulk state on melting. Efficient mechanical mixing or multiple temperature cycles are known to can accelerate clathrate formation small scale, however, these process are incompatible for on-board H_2 storage. In a recent investigation by Su et al. [89], they have shown a polymerized high internal phase emulsion (polyHIPE) material as support to improve the kinetics and recyclability for gas hydrates. It has been shown that the pressure required for clathrate formation can be reduced significantly by introducing promoter molecules such as tetrahydrofuran into the larger $5^{12}6^4$ cage. [90]

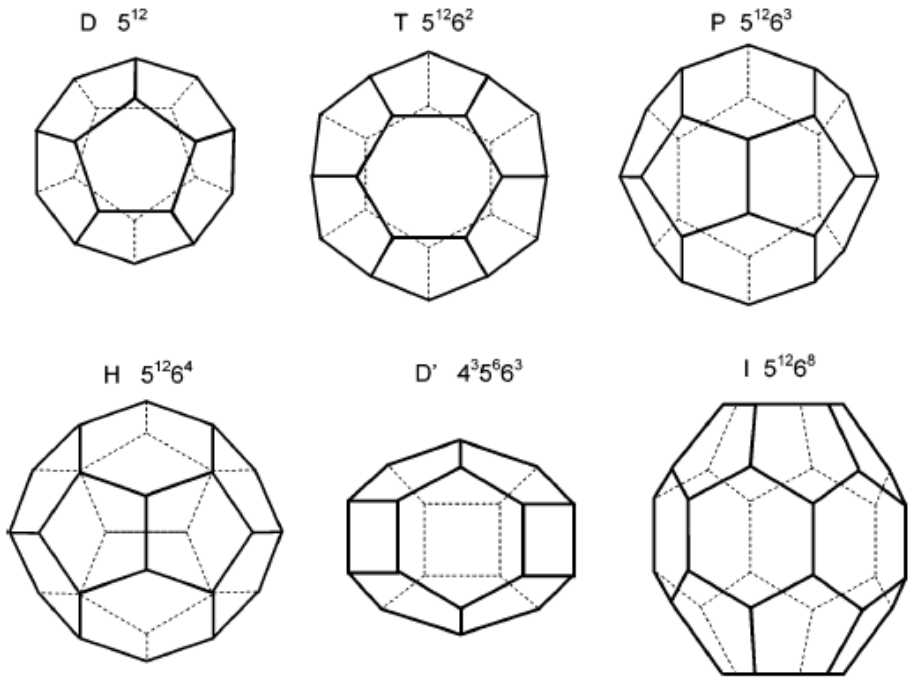

Figure 1.6. The major building blocks of the clathrate lattices *D*, pentagonal dodecahedron (12 pentagonal faces); *T*, tetrakaidecahedron (12 pentagonal and 2 hexagonal faces); *P*, pentakaidecahedron (12 pentagonal and 3 hexagonal faces); *H*,hexakaidecahedron (12 pentagonal and 4 hexagonal faces); *D*¢,irregular dodecahedron (3 square, 6 pentagonal, and 3 hexagonalfaces); *I*, icosahedron (12 pentagonal and 8 hexagonal faces). (source ref 153)

However, this method leads to reduced H_2 storage capacity. THF-containing binary-clathrate hydrates are found to increase the storage to ~4 wt.% H_2[91] at modrate pressures. The compositions of these binary clathrate hydrates are changed to allow the H_2 guest molecules to enter in all the cages. The above reports led to several attempts to improve the clathrates for practical hydrogen storage applications.[92-96] Recently [97] it was shown that the H_2–absorption rate of tetrahydrothiophene and furan hydrates was much greater than that of tetrahydrofuran hydrate. Their H_2 storage capacities however were remained unaltered. A detailed review on the structures, stabilities, occupancies, and dynamics of hydrogen clathrates and their developments towards hydrogen storage is provided in Ref. [98].

Water clusters have been studied intensively. However, the stability and structural features of clusters of water have always been of great interest. [99-102] In an *ab initio* investigation, Ludwig and Appelhagen [103] studied clathrate-like water clusters with

buckminsterfullerene as the guest species. In a complimentary study by Shameema et. al.[104] they have investigated the effect of encapsulation of water and other molecules when encapsulated in a C_{60} fullerene cage. It demonstrated that larger water clusters adopt different structures, the stability of these structures driven by molecular environment. [105, 106] Many other clatharate like structures are also being explored theoretically, one such study is by Parthasarathi et al. They have studied hydrogen bonding in protanted water molecules using atoms-in molecules (AIM) approach. [107] Recently, the authors [108] have studied the of linear water chains $(H_2O)_n$, n = 5-20 using *ab initio* DFT. Subsequently, Kirov and co-authors [109] have offered a new model to identify the most stable networks in polyhedral water clusters. Their models was based on screening of the energy of the local network, also using the concept of "strong" or "weak" nearest neighbour interactions according to their trans or cis orientation and their connectivity. To investigate properties governing the thermodynamic stability of clathrate hydrates many theoretical studies have also been attempted. Research efforts have been made to relate the thermodynamic stability with the cage occupancy, the nature bonding in the H_2 molecules and the clustering of H_2 molecules inside the cages. Patchkovskii et. al. have demonstrated that the stability of the clathrate is primarily due to the dispersive interactions of H_2 molecules with the cages. Their conclusions were based on first-principles calculations. [110] The multiple occupancies in the clathrate cages are confirmed by theoretical investigations of Sluiter et al. [111] at the experimental conditions of 200 MPa and 250 K. They have employed electronic density functional theory to show that the enclathration of H_2 molecules in clathrates is based on physisorption with energy of the order of 20-25 meV/H_2. They have dismissed possibility of stable H_2 clusters inside the clatharate cages and shown that the H_2 interaction energies with the cage walls are much larger than that with other H_2 molecules. It was concluded that the H_2 molecules in a cage preferably bind to the cage walls. Conclusions made in this study were based on the quantum effects of rotational movement only however the translational motions were not taken in considerations.

The extension of this work was carried out by Inerbaev et al. [112] they employed the quasiharmonic approximation (QHA) and considered all types of molecular vibrations. They studied the consequences of cage occupancy and temperature on the

structural, dynamic and thermodynamic properties of sII clathrate hydrate. Lokshin et al. [65] validated the experimental results theoretically using the experimental conditions. Their results were in good agreements at the equilibrium pressure of the H_2 clathrate hydrate. They have further demonstrated that cage occupancy can be as high as $3H_2$ per cage for large cages and at temperatures above as ~125 K with affecting the host lattice stability. Furthermore, their results suggest that the zero-point vibrations are fundamentally important to calculate the thermodynamic properties of clathrate hydrates.

All the above results provide insight that it essential to investigate various possible promoter molecules which can enhance the interaction of H_2 molecules with the clathare cage and can reduce the high pressure requirement of the clathrates, maintaining the stability of host structure. The molecular understanding of the nature of interaction and binding mechanism of such promoter molecules can be gained with the help of quantum chemical calculations. The insight gained by these calculations can guide the design and development of new and stable clatharte for practical hydrogen storage. Clearly, computational science can play important role in the development of novel hydrogen storage materials.

1.7 Boron-based hydrides

The boron based hydrides are very attractive candidates to solve the key problems of hydrogen economy. These offer the chemical hydrogen storage via chemisorptions and these are know have very promising properties. The boron based hydrides have H_2 in high gravimetric densities. The hydrogen stored in these materials can be used for practical applications via dehydrogenation. The dehydrogenation is often achieved by hydrolysis or thermolysis. However, these materials have certain technical barriers like high dehydrogenation temperatures and low purity of the produced hydrogen. To deal with these issues, many research efforts are made to modify these and find new materials.

The most commonly studied hydrides are $LiBH_4$, $NaBH_4$, KBH_4 and ammonia borane (NH_3BH_3). The hydrolysis of $LiBH_4$, $NaBH_4$, and KBH_4 takes as follows:

$$LiBH_4 + 4H_2O \rightarrow LiBO_2.2H_2O + 4H_2 \quad (1.7.1)$$

$$NaBH_4 + 4H_2O \rightarrow NaBO_2.2H_2O + 4H_2 \quad (1.7.2)$$

$$KBH_4 + 4H_2O \rightarrow LiBO_2.2H_2O + 4H_2 \quad (1.7.3)$$

$LiBH_4$ and KBH_4 have various practical barriers spontaneous H_2 desorption, slow kinentics, spontaneous dehydrogenation, and hygroscopicity. Because of various problems associated with very few research efforts have been made to study to $LiBH_4$ and KBH_4 in comparison to $NaBH_4$ [113,114–118].

$NaBH_4$ was synthesized in the 1950s [119]. It has a stable cubic crystal structure (space group Fm3m) and is synthesized on industrial scale for various catalytic applications. [120] However, recently, it emerged as a promising chemical hydrogen storage candidate [121]. NaBH4 also faces several problems as practical storage material like low gravimetric capacities and catalyst recyclability. Dehydrogenation of $NaBH_4$ via hydrolysis is often done in presence of active catalyst. The reactivity of cobalt-based catalysts, for $NaBH_4$ dehydrogenation, has attracted vast research interest [122,123–129].

The most critical issues with boron-based hydride are low release H_2 and the formation of borate by-products, like $MBO_2.2H_2O$ and $MBO_2.4H_2O$. Recently, ammonia borne (NH_3BH_3) has emerged as a new hydrogen storage candidate. It undergoes hydrolysis as follows:

$$NH_3BH_3 + (2+x)H_2O \rightarrow NH_4BO_2.xH_2O + 3H_2 \quad (1.7.4)$$

At normal temperature and pressure, it is a white crystalline solid; it adopts body centered tetragonal crystal structure. NH_3BH_3 is often synthesized from $NaBH_4$ by salt metathesis :

$$2NaBH_4 + (NH_4)SO_4 \rightarrow 2NH_3BH_3 + Na_2SO_4 + 2H_2 \quad (1.7.5)$$

The hydrolysis of NH_3BH_3 normally takes place in the presence of a suitable catalyst. It has high hydrogen content with gravimetric H_2 capacity of 19.6 wt% of H_2. However, the hydrogen from NH_3 group is difficult to be removed via hydrolysis reducing the effective hydrogen release of NH_3BH_3. Furthermore, the hydrated by-products are also reduces the net H_2 capacities.

NH_3BH_3 favorably offers $3H^{\delta+}$ and $3H^{\delta-}$ these H_2 molecules can easily combine together through via both intermolecular and intermolecular interactions to give $3H_2$ (Figure 1).

At temperatures below -40℃, ammonia borane also exists in the form of NH_4BH_4 (ammonium borohydride). NH_4BH_4 has higher hydrogen content than NH_3BH_3 [130]. This material has very high gravimetric density of 24.3wt%. However, it is unstable at normal temperatures . At temperature higher than -40℃ it decompose to form B_2H_6 $[BH_2(NH_3)_2][BH_4]$ and H_2 [131]. In contrast, ammonia bor ane is significantly stable with melting point of 112-114℃. The intermolecular interaction between the hydrogen atoms of BH_3 unit and NH_3 units, makes this materials stable.

The thermolysis of NH_3BH_3 is often done at high temperatures (~100-200℃), it goes as follows:

$$NH_3BH_3 \rightarrow [NH_2BH_2] + H_2 \quad (1.7.6)$$

$$[NH_2BH_2] \rightarrow [NHBH] + H_2 \quad (1.7.7)$$

$$[NHBH] \rightarrow BN + H_2 \quad (1.7.8)$$

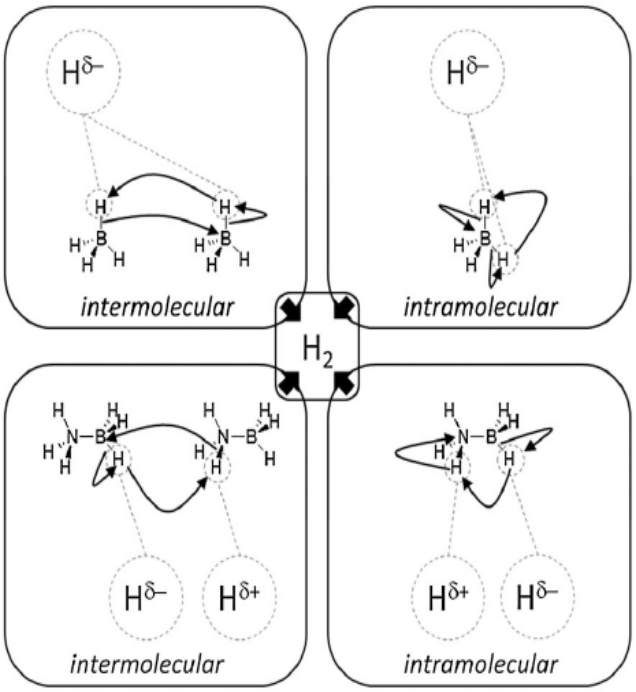

Fig 1.7. Qualitative mechanism thermolysis and illustration of intermolecular and intermolecular interactions of ammonia borane.(source ref 154)

Reaction 1.7.8 requires temperature higher than 500℃. These interactions are responsible for slow kinetics, the formation of side products like borazine ($B_3N_3H_6$) and B_2H_6, and the high dehydrogenation temperatures.

Various research attempts have been made to reduce the dehydrogenation temperatures of ammonia borane. Different approaches have been pursued, and many milestones have been achived [131,132,133,134]. To dehydrogenate NH_3BH_3 at room temperature few strategies are adopted, the first strategy is to dissolve NH_3BH_3 in a solvent organic solvent or in an ionic liquid. It is observed that NH_3BH_3 dehydrogenates effectively, at reasonably low temperatures without using any catalyst [135-137]. Interestingly, the use of ionic liquids facilitates the formation of polyborazylene materials.[136] These polyborazylene materials can be used for borane regeneration [138]. Organic solvents reduce the dehydrogenation temperature also improves the H_2 release kinetics. Homogeneous catalyst brings additional improvements [139,140,141]. Boron-based hydrides are considerably important candidate for hydrogen storage. However, onboard application requires recyclability of the solid by-products.

1.8 Graphene

Carbon based materials like fullerenes and nanotubes are attractive chemical hydrogen storage candidates. However, their production and high cost are main barriers for practical applications. Recently, graphene has emerged as a promising candidate for hydrogen storage. It is a two-dimensional flat monolayer of carbon atoms packed into a honeycomb lattice, has come into prominence because of the developments in its experimental fabrication techniques. Due to its fascinating physics for fundamental studies and its potential applications for the next-generation electronic devices and H_2 storage materials graphene attracts a lot of attention.

Lu et al. [142] have recently investigated in detail the electronic structure of tetracyanoethylene (TCNE) on graphene using the first-principles method based on DFT. It was demonstrated that the electronic structure of graphene can be controlled over a wider range by organic molecules, and that it is possible to build graphenebased electronic devices by modifying the graphene with patterned organic molecules, without the need for cutting or etching graphene. Another route that has been recently suggested for tuning the electronic structure involves growing graphene on a substrate. [143, 144] In many computations polycyclic aromatic hydrocarbons (PAHs) are chosen to model graphene. Heine et al. [145] calculated the physisorption energy of H_2 as a function of the PAH size and the adsorption site. The adsorption energies were found to be between 4-7 kJ/mol and these results were then extrapolated to graphene layers. A similar *ab initio* study was also carried out by the authors for modelling N_2 adsorption on grapehene platelets which revealed that the trends for H_2 and N_2 adsorption on PAHs and graphene were same but with N_2 binding twice as strongly as H_2. [146] At room temperature quantum effects are significant and need to be accounted for. This nontrivial task was performed by Patchkovskii and co-workers [147] who found that H_2 storage in graphene depended on the interlayer distance. For distances less than 5 Å the H_2-graphene interaction potential was repulsive which prevented the penetration of H_2 in between the graphite layers. The storage capacity peaked at an interlayer distance of 6 Å and then reduced continuously with increasing distance. For the limit of a single graphene sheet an insignificant uptake of H_2 on the layer surface was predicted. It was concluded that with

an appropriate interlayer the H_2 storage in graphene could be tuned to reach reasonable values. Introduction of spacers was suggested as a possible route for achieving this such uniform interlayer distances. In an interesting study C60-intercalated graphite (CIG) was simulated. [148] Between 50-300 K temperatures CIG was found to have double the interaction free energy with H_2 than the empty structure. Compared to Li-doped carbon nanotubes and Li-doped graphite, CIG was able to achieve a high H_2 storage capacity at low temperatures.

More recently a combined experimental and theoretical investigation has been performed on the H_2 and CO_2 uptake of graphene. [149] Graphene samples with different surface areas prepared by exfoliation of graphitic oxide or conversion of nanodiamond showed significant absorption of H_2 and CO_2. The maximum H_2 uptake was found to be 3.1 wt.% at 100 atm and 298 K. The theoretical calculations yielded a 7.7 wt.% of H_2 uptake by a single-layer graphene both in the parallel and perpendicular orientations. Current advancements in experiments have now permitted production of finite sized graphene layers or graphene nanoribbons (GNRs) with varying widths. Depending up on where the layers are terminated one can have two different edge geometries, namely, zigzag and armchair edges which vary largely in their electronic properties. Their electronic and magnetic properties have only recently been explored using a many-body description. In this regard the detailed configuration interaction and density functional studies of undoped and doped GNRs done by Pati and coworkers are noteworthy. [150-152] In another fresh study Lu et al. have investigated effects of hydrogen passivation of edges of armchair GNRs on their electronic properties using first-principles method. [153]

1.9 Motivation and outline of the thesis

There are various solid-state H_2 storage materials, which are presently investigated; however, no material is found to have all the properties required for practical storage of hydrogen. Due to the growing need of energy, it is essential to use currently existing technologies along with development of new H_2 storage materials. Experimentally, this is a time taking process. Furthermore, it requires significant individual and economic resources. Computational materials science, in

comparison, is a fast and efficient way for designing novel materials. Moreover, theoretical results also validate experimental results. Consequently, the primary motivation of this thesis is to apply computational material science to design new different classes of H_2 storage materials and to explore the fundamental interactions involved in these materials.

The motivation of this thesis is to use a computational approach to investigate different hydrogen storage materials. In the thesis we will be specifically studying Metal Organic Frameworks (MOF) based materials due to their tremendous promise for the purpose of hydrogen storage and the need for enhancing their hydrogen storage properties. To this end, in this thesis we have performed density functional theory (DFT) based calculations to study theoretically the ground state lattice structure, electronic structure; effect of dopants, new MOF based materials via novel dopants, of these hydrogen storage materials. The effect of boron substitution followed by metals decoration has also been studied using detailed molecular orbital analysis.

The outline of this thesis is as follows, in chapter 2 we will present an brief introduction to the theory behind the methodology used in the thesis. We will describe the implementation of the plane wave-pseudopotential molecular dynamics method in the program package of VASP for performing solid-state calculations. In chapter 3 we discuss different tools available for studying electronic structure of solids. Our results of the charge density, band structure, and density of states (DOS) analyses on pure and Mn-doped and pure ZNO will be presented. In Chapter 4, the effect of light metal (M = Li, Be, Mg, and Al) decoration on the stability of metal organic framework MOF-5 and its hydrogen adsorption is investigated by ab initio and periodic density functional theory (DFT) calculations. Chapter 5 illustrates The effect of light transition metal (M = Sc, Ti) decoration, boron substitution on the hydrogen storage properties of MOF-5, and clustering problem of metals has been investigated using ab initio density functional theory Furthermore, we study the crystal structure of standard ZIF, calculate H_2 different adsorption and propose Sc and Ca decorated ZIF as a potential hydrogen storage candidate. In Chapter 6 we explore that why boron substitution increases the interaction energies of metals with benzene based MOFs.

References

1. L. Schlapbach and A. Züttel, *Nature* **2001**, *414*, 353.
2. M. Eddaoudi, H. Li, T. Reineke, M. Fehr, D. Kelley, T. L. Groy, and O. M. Yaghi, *Top. Catal.* **1999**, *9*, 105.
3. N. L. Rosi, J. Eckert, M. Eddaoudi, D. T. Vodak, J. Kim, M. O'Keeffe, and O. M. Yaghi, *Science* **2003**, *300*, 1127.
4. J. L. C. Roswell, A. R. Milward, K. S. Park, and O. M. Yaghi, *J. Am. Chem. Soc.* **2004**, *126*, 5666.
5. G. Wong-Foy, A. J. Matzger and O. M. Yaghi, *J. Am. Chem. Soc.* **2006**, *128*, 3494.
6. J. L. C. Roswell and O. M. Yaghi, *J. Am. Chem. Soc.* **2006**, *128*, 1304.
7. .M. Latroche, S. Surblè, C. Serre, C. Mellot-Draznieks, P. L. Llewellyn, J. H. Lee, J. S. Chang, S. H. Jhung and G. Fèrey, *Angew. Chem., Int. Ed.* **2006**, *45*, 8227.
8. .O. I. Lebedev, F. Millange, C. Serre, G. van Tendeloo, and G. Fèrey, *Chem. Mater.* **2005**, *17*, 6525.
9. Eddaoudi M, Li H, Reineke T, Fehr M, Kelley D, Groy T, et al. *Top Catal*. **1999**, 9, 105.
10. J. L. C. Roswell and O. M. Yaghi, *J. Am. Chem. Soc.* **2006**, *128*, 1304.
11. Bordiga S, Vitillo JG, Ricchiardi G, Regli L, Cocina D, Zecchina A, et al. *J Phys Chem B.* ***2009,*** 109, 18237.
12. Kaye SS, Long JR. *J. Am. Chem. Soc.* **2005**, 127, 6506.
13. Lochan RC, Head-Gordon M. *Phys. Chem.Chem. Phys.* **2006**,8,1357.
14. Yaghi OM, Chen B, Ockwig NW, Millward AR, Contreras DS. *Angew. Chem. Int. Ed.* **2005**, 44, 4670.
15. Chae HK, Siberio-Perez DY, Kim J, Go Y, Eddaoudi M, Matzger AJ, et al. *Nature.* **2004**, 427, 523.
16. Li J, Cheng S, Zhao Q, Long P, Dong J. *Int. J. Hydrogen. Energy.* **2009**, 34, 1377.
17. Chen B, Eddaoudi M, Reineke TM, Kampf JW, O'Keeffe M, Yaghi OM. *J. Am. Chem. Soc.* **2000**, 122, 11559.

18. Hubner O, Gloss A, Fichtner M, Klopper W. *J. Phys. Chem. A.* **2004**, 108, 3019.
19. Sagara T, Klassen J, Ganz E. *J. Chem. Phys.* **2004**, 121, 12543.
20. Buda C, Dunietz BD. *J. Phys. Chem. B.* **2006**, 110, 10479.
21. Han SS, Deng WQ, Goddard W. *Angew. Chem. Int. Ed.* **2007**, 119, 6405.
22. Han SS, Furukawa H, Yaghi OM, Goddard WA. *J. Am. Chem. Soc.* **2008**, 130, 11580.
23. Han SS, Goddard WA. High *J. Phys. Chem. C.* **2008**, 112, 13431.
24. Mulder F, Dingemans T, Wagemaker M, Kearley G. *Chem. Phys.* **2005**, 317, 113.
25. Mueller T, Ceder G. *J. Phys. Chem. B.* **2005**, 109, 17974.
26. Han SS, Mendoza-Corte´s JL, Goddard III WA. *Chem. Soc. Rev*. 2009, 38, 1460
27. Niu J, Rao BK, Jena P. Phys. Rev. Lett. **1992**, 68, 2277.
28. Charles J, Bauschlicher W, Walch SP. *J. Chem. Phys.* **1982**,76,4560.
29. Niu J, Rao BK, Khanna SN, Jena P. *Chem. Phys. Lett*. **1991**, 230, 299.
30. Maseras F, Lledos A, Clot E, Eisenstein O. *Chem. Rev*. **2000**, 100, 601.
31. Gagliardi L, Pyykko P. J. Am. Chem. Soc. **2004**,126, 15014.
32. Maark TA, Pal S. *Int. J. Hydrogen. Energy.* **2010**, 35, 12846.
33. Chandrakumar KRS, Ghosh SK. *Chem. Phys. Lett* **2007**, 447, 208.
34. 111.Y. Liu, H. Kabbour, C. M. Brown, D. A. Neumann, and C. C. Ahn, *Langmuir* **2008**, *24*, 4772.
35. Suttisawat Y, Rangsunvigit P, Kitiyanan B, Williams M, Ndungu P, Lototskyy M, et al. *Int. J. Hydrogen. Energy.* **2009**, 34, 6669.
36. Kim BJ, Lee YS, Park SJ. *Int. J. Hydrogen. Energy.* **2008**, 33, 4112.
37. Zubizarreta L, Menndez J, Pis J, Arenillas A. *Int. J. Hydrogen. Energy.* **2009**, 34, 3070.
38. Zhao Y, Kim YH, Dillon AC, Heben MJ, Zhang SB. Phys. Rev. Lett. **2005**, 94, 155504.
39. Yildirim T, Ciraci S. *Phys. Rev. Lett.* **2005**,94,175501.
40. Lee H, Choi WI, Ihm J. Phys. Rev. Lett. **2006**,97,056104.
41. Kim G, Jhi SH, Park N. *Appl. Phys. Lett.* **2008**, 92, 013106.
42. Sun Q, Wang Q, Jena P, Kawazoe Y. *J. Am. Chem. Soc.* **2005**, 127, 14582.

43. Forster PM, Eckert J, Heiken BD, Parise JB, Yoon JW, Jhung SH, et al. *J. Am. Chem. Soc.* **2006**, 128, 16846.
44. Ma S, Zhou H-C. *J. Am. Chem. Soc.* **2006**, 128, 11734.
45. Dinca M, Dailly A, Liu Y, Brown CM, Neumann DA, Long JR. *J. Am. Chem. Soc.* **2006**, 128, 16876.
46. Dinca M, Han WS, Liu Y, Dailly A, Brown CM, Long JR. *Angew. Chem. Int. Ed.* **2007**, 46, 1419.
47. Dinca M, Long JR. *J. Am. Chem. Soc.* **2007**, 129, 11172.
48. Vitillo JG, Regli L, Chavan S, Ricchiardi G, Spoto G, Dietzel PDC, et al. *J. Am. Chem. Soc.* **2008**, 130, 8386.
49. Hamaed A, Trudeau M, Antonelli DM. *J. Am. Chem. Soc.* **2008**, 130, 6992.
50. Patchkovskii S, Tse JS, Yurchenko SN, Zhechkov L, Heine T, Seifert G. *Proc. Natl. Acad. Sci.* **2005**, 102, 10439.
51. Heine T, Zhechkov L, Seifert G. *Phys. Chem. Chem. Phys.* **2004**, 6, 980.
52. Sun Q, Jena P, Wang Q, Marquez M. *J. Am. Chem. Soc.* **2006**, 128, 9741.
53. Chandrakumar KRS, Ghosh SK. Nano. Lett. **2007**, 8, 13.
54. Forst CJ, Slycke J, Van Vliet KJ, Yip S. *Phys. Rev. Lett.* **2006**, 96, 175501.
55. Kim YH, Zhao Y, Williamson A, Heben MJ, Zhang SB. *Phys. Rev. Lett.* **2006**, 96, 016102.
56. Chen P, Wu X, Lin J, Tan KL. *Science*. **1999**, 285, 91.
57. Blomqvist A, Arajo CM, Srepusharawoot P, Ahuja R. *Proc. Natl. Acad. Sci.* **2007**, 104, 20173.
58. Han SS, Goddard WA. *J. Am. Chem. Soc.* **2007**, 129, 8422.
59. Venkataramanan N, Sahara R, Mizuseki H, Kawazoe Y. *Int. J. Mol. Sci.* **2009**, 10, 1601.
60. Sun YY, Lee K, Kim YH, Zhang SB. *Appl. Phys. Lett.* **2009**, 95, 033109
61. Zou X, Cha M-H, Kim S, Nguyen MC, Zhou G, Duan W, et al. *Int. J. Hydrogen. Energy.* **2010**, 35, 198.
62. Kuc A, Heine T, Seifert G, Duarte HA. *Chem. Eur. J.* **2008**, 14, 6597.
63. Kuc A, Heine T, Seifert G, Duarte HA. *Theor. Chem. Accounts.* **2008**, 120, 543.
64. David E. *J. Mater. Process. Technol.* **2005**, 162, 169.

65. Zhou L. Progress and problems in hydrogen storage methods. *Renew. Sustain. Energy. Rev*. **2005**, 9, 395.
66. Schlapbach L, Züttel A. *Nature* **2001**, 414, 353.
67. Zuttel A. *Mater. Today*. 2003, 24, 33.
68. Zhou L, Zhou Y, Sun Y. *Int. J. Hydrogen. Energy*. **2006**, 31, 259.
69. Grochala W, Edwards PP. *Chem. Rev*. 2004,104,1283.
70. Eberle U, Arnold G, Helmholt RV. *J. Power. Sour*. 2006,154,456.
71. Latroche M. *J. Phys. Chem. Solids*. 2004,65,517.
72. Z. X. Guo, C. Shang, and K. F. Aguey-Zinsou, *J. Eur. Ceramic Soc.* **2008**, *28*, 1467.
73. S. A. Shevlin and Z. X. Guo, *Chem. Soc. Rev*. **2009**, *38*, 211.
74. B. Bogdanović and M. Schwickardi, *J. Alloys Compd.* **1997**, *253-254*, 1.
75. J. Íñiguez and T. Yildirim, *Appl. Phys. Lett*. **2005**, *86*, 103109.
76. J. Íñiguez, T. Yildirim, T. J. Udovic, M. Sulic, and C. M. Jensen, *Phys. Rev. B* **2004**, *70*, 060101.
77. O. M. Løvvik and S. M. Opalka, *Phys. Rev. B* **2005**, *71*, 054103.
78. O. M. Løvvik and S. M. Opalka, *Appl. Phys. Lett*. **2006**, *88*, 161917.
79. C. M. Araújo, R. Ahuja, J. M. O. Guillén, and P. Jena, *Appl. Phys. Lett*. **2005**, *86*, 251913.
80. C. M. Araújo, S. Li, R. Ahuja, and P. Jena, *Phys. Rev. B* **2005**, *72*, 165101.
81. S. Li, P. Jena, and R. Ahuja, *Phys. Rev. B* **2006**, *73*, 214107.
82. A. Blomqvist, C. M. Araújo, P. Jena, and R. Ahuja, *Appl. Phys. Lett*. **2007**, *90*, 141904.
83. P. A. Beresth, A. G. Harter, R. Zidan, A. Blomqvist, C. M. C. M. Araújo, R. H. Scheicher, R. Ahuja, and P. Jena, *Nano Lett*. **2009**, *9*, 1501.
84. Dyadin, Y. A. Larionov, E. G. Manakov, A. Y. Zhurko, F. V.Aladko, E. Y. Mikina, T. V. Komarov, V. Y. *Mendeleev Commun.***1999**, 171.
85. W. L. Mao, Ho-kwang Mao, A. F. Goncharov, V. V. Struzhkin, Q. Guao, J. Hu, J. Shu, R. J. Hemley, M. Somayazulu, and Y. Zhao, *Science* **2002**, *297*, 2247.
86. Lokshin K. A, Zhao Y, He D, Mao W.L, Mao H.-K, Hemley R. J, Lobanov, M. V.; Greenblatt, M. *Phys. Re*V. *Lett*. **2004**, *93*,125503.

87. Mao W. L, Mao H. K. *Proc. Natl. Acad. Sci.* **2004**, *101*, 708.

88. T. A. Strobel, C. J. Taylor, K. C. Hester, S. F. Dec, C. A. Koh, K. T. Miller, and E. D. Sloan, *J. Phys. Chem. B* **2006**, *110*, 17121.

89. F. Su, C. L. Bray, and A. I. Cooper, *Adv. Mater.* **2008**, *20*, 2663.

90. L. J. Florusse, C. J. Peters, J. Schoonman, K. C. Hester, C. A. Koh, S. F. Dec, K. N. Marsh, and E. D. Sloan, *Science* **2004**, *306*, 469.

91. Jong-won Lee, D. Y. Kim, J. Park, Yu-Taek Seo, H. Zeng, I. L. Moudrakovski, C. I. Ratcliffe, and J. A. Ripmeester, *Nature* **2005**, *434*, 743.

92. Do-Youn Kim, Y. Park, and H. Lee, *Cat. Today* **2007**, *120*, 257.

93. T. A. Strobel, C. A. Koh, and E. D. Sloan, *Fluid Phase Equilib.* **2007**, *261*, 382.

94. S. Hashimoto, T. Sugahara, M. Moritoki, H. Sato, and K. Ohgaki, *Chem. Eng. Sci.* **2008**, *63*, 1092.

95. Ji-Ho Yoon, J. Han, J. Park, S. Choi, Sun-Hwa Yeon, and H. Lee *J. Phys. Chem. Solids* **2008**, *69*, 1432.

96. T. Tsuda, K. Ogata, S. Hashimoto, T. Sugahara, M. Moritoki, and K. Ohgaki, *Chem. Eng. Sci.* **2009**, *64*, 4150.

97. T. A. Strobel, K. C. Hester, C. A. Koh, A. K. Sum, and E. D. Sloan Jr., *Chem. Phys. Lett.* **2009.**

98. S. Maheshwary, N. Patel, N. Sathyamurthy, A. D. Kulkarni, and S. R. Gadre, *Phys. Chem. A* **2001**, *105*, 10525.

99. J. D. Cruzan, L. B. Braly, K. Liu, M. G. Brown, J. G. Loeser, and R. J. Saykally, *Science* ***1*996,** *271*, 59.

100. J. D. Cruzan, L. B. Braly, K. Liu, M. G. Brown, J. G. Loeser, and R. J. Saykally, *J. Phys. Chem. A* **1997**, *101*, 9022.

101. 90. J. Kim and K. S. Kim, *J. Chem. Phys.* **1998**, *109*, 5886.

102. R. Ludwig, and A. Appelhagen, *Angew. Chem., Int. Ed.* **2005**, *44*, 811.

103. O. Shameema, C. N. Ramachandran, and N. Sathyamurthy, *J. Phys. Chem. A* **2006**, *110*, 2.

104. S. K. Ghosh and P. K. Bharadwaj, *Angew. Chem., Int. Ed.* **2004**, *116*, 4490.

105. S. K. Ghosh and P. K. Bharadwaj, *Inorg. Chem.* **2004**, *43*, 3771.

106. R. Parthasarathi, V. Subramanian, and N. Sathyamurthy, *J. Phys. Chem. A Lett.* **2007**, *111*, 13287.

107. R. Parthasarathi, M. Elango, V. Subramanian, and N. Sathyamurthy, *J. Phys. Chem. A* **2009**, *113*, 3744.

108. M. V. Kirov, G. S. Fanourgakis, and S. S. Xantheas, *Chem. Phys. Lett.* **2008**, *461*, 180.

109. S. Patchkovskii and J. S. Tse, *Proc. Natl. Acad. Sci. U.S.A.* **2003**, *100*, 14645.

110. M. H. F. Sluiter, H. Adachi, R. V. Belosludov, V. R. Belosludov, and Y. Kawazoe, *Mater. Trans.* **2004**, *45*, 1452.

111. T. M. Inerbaev, V. R. Belosludov, R. V. Belosludov, M. Sluiter, and Y. Kawazoe, *Comp. Mater. Sci.* **2006**, *36*, 229.

112. Li C, Peng P, Zhou DW,Wan L. *Int. J. Hydrogen. Energy*, **2011,** 36, 14512.

113. Kojima Y, Kawai Y, Kimbara M, Nakanishi H,Matsumoto S. *Int. J. Hydrogen. Energy*. **2004**, 29,1213.

114. Zhu L, Kim D, Kim H, Masel RI, Shannon MA. *J. Power Sources,* **2008**, 185, 1334.

115. Goudon JP, Bernard F, Renouard J, Yvart P. *Int. J. Hydrogen. Energy*. **2010**,35,11071–11076.

116. Sahin Ö, Dolaş H, Özdemir M. *Int. J. Hydrogen. Energy*. **2007**, 32,2330.

117. Xu D, Wang H, Guo Q, Ji S. *Fuel. Process. Tech*. **2011**,92,1606.

118. Schlesinger HI, Brown HC, Finholt E, Gilbreath JR,Hoekstra HR, Hyde EK. *J. Am. Chem. Soc.* 1953, 75, 215.

119. Çakanyıldırım Ç, Gürü M. *Int. J. Hydrogen Energy*, **2008**, 33,4634.

120. Amendola SC, Sharp-Goldman SL, Saleem Janjua M, Spencer NC, Kelly MT, Petillo PJ, Binder M. *Int. J. Hydrogen Energy*, **2000**, 25, 969.

121. Akdim O, Demirci UB, Miele P. *Int. J. Hydrogen Energy,* 2011, 36,13669.

122. Wee JH. *J. Power Sources,* 2006, 155,329.

123. Liu BH, Li ZP. *J. Power Sources*, 2009; 187:527.

124. Umegaki T, Yan JM, Zhang XB, Shioyama H, Kuriyama N, Xu Q. *Int. J. Hydrogen Energy,* **2009**, 34,2303.

125. Marrero-Alfonso EY, Beaird AM, Davis TA,Matthews MA. *Ind. Eng. Chem. Res.* **2009**, 48, 3703–3712.

126. Demirci UB, Akdim O, Andrieux J, Hannauer J, Chamoun R, Miele P. *Fuel Cells* **2010**, 10, 335.

127. Jiang HL, Singh SK, Yan JM, Zhang XB, Xu Q.. *Chem. Sus. Chem.* **2010**, 3,541.

128. Muir SS, Yao X. Int. J. Hydrogen Energy. **2011**, 36,5983.

129. Parry RW, Schulz DR, Girardot PR. *J. Am. Chem. Soc*. **1958**, 80,1.

130. Staubitz A, Robertson APM, Manners I. *Chem. Rev*. **2010**, 110,1079.

131. Hamilton CW, Baker RT, Staubitz A, Manners I. *Chem. Soc. Rev*. **2009**, 38,279.

132. Wang P, Kang XD. *Dalton Trans.* **2008**, 5400.

133. Stephens FH, Baker RT, Matus MH, Grant DJ, Dixon DA. *Angew. Chem. Int. Ed.* **2007**, 46,746.

134. Bluhm ME, Bradley MG, Butterick R III, Kusari U, Sneddon LG. *J. Am. Chem. Soc*. **2006**, 128,7748.

135. Himmelberger DW, Alden LR, Bluhm ME, Sneddon LG. *Inorganic Chemistry* **2009**, 48,9883.

136. Ahluwalia RK, Peng JK, Hua TQ. *Int. J. Hydrogen Energy* **2011**, 36, 15689.

137. Sutton A, Burrell AK, Dixon DA, Garner EB III, Gordon JC, Nakagawa T, Ott KC, Robinson JP, Vasiliu M. *Science* **2011**, 331,1426.

138. Jaska CA, Temple K, Lough AJ, Manners I. *J. Am. Chem. Soc.* **2003**, 125, 9424.

139. Denney MC, Pons V, Hebden TJ, Heinekey DM, Goldberg KI. *J. Am. Chem. Soc.* **2006**, 128,12048.

140. Kim SK, Han WS, Kim TJ, Kim TY, Nam SW, Mitoraj M, Piekos L, Michalak A, Hwang SJ, Kang SO. *J. Am. Chem. Soc.* **2010**, 132, 9954.

141. K. P. Prasanth, H. C. Bajaj, H. D. Chung, K.Y. Choo, T. H. Kim, and R. V. Jasra, *Int. J. Hydrogen Energy* **2009**, *34*, 888.

142. A. Zecchina, S. Bordiga, J. G. Vitillo, G. Ricchiardi, C.Lamberti, G. Spoto, M.

Bjorgen, and K. P. Lillerud, *J. Am. Chem. Soc.* **2005**, *127*, 6361.

143. L. Chen, R. K. Singh, and P. Webley, *Micropor. Mesopor. Mater.* **2007**, *102*, 159.
144. M. Armandi, B. Bonelli, C. O. Arean, and E. Garrone, *Micropor. Mesopor.Mater.* **2008**, *112*, 411. Z. Yang, Y. Xia, and R. Mokaya, *J. Am. Chem. Soc.* **2007**, *129*, 1673.
145. A. Lachawiec and R.T. Yang, *Langmuir* **2008**, *24*, 6159.
146. C. Guan, X. Zhang, K. Wang, and C. Yang, *Sep. and Purification Tech.* **2009**, *66*, 565.
147. C. Guan. K. Wang, C. Yang, and X. S. Zhao, *Micropor. Mesopor. Mater.* **2009**, *118*, 503.
148. T. Roussel, C. Bichara, K. E. Gubbins, and R. J. –M. Pellenq, *J. Chem. Phys.* **2009**, *130*, 174717.
149. H. Nishihara, Peng-Xiang Hou, Li-Xiang Li, M. Ito, M. Uchiyama, T. Kaburagi, A. Ikura, J. Katamura, T. Kawarada, K. Mizuuchi, and T. Kyotani, *J. Phys. Chem. C* **2009**, *113*, 3189.
150. Y. H. Lu, W. Chen, Y. P. Feng, and P. M. He, *J. Phys. Chem. B* **2009**, *113*, 2.
151. Y. H. Lu, P. M. He, and Y. P. Feng, *J. Phys. Chem. C* **2008**, *112*, 12683.
152. Z. H. Ni, T. Yu, Y. H. Lu, Y. Y. Wang, Y. P. Feng, and Z. X. Shen, *ACS Nano* **2008**, *2*, 2301.
153. Viktor V. Struzhkin, Burkhard Militzer, Wendy L. Mao, Ho-kwang Mao,and Russell J. Hemley. *Chem. Rev*. **2007,** 107, 4133-4151
154. Georges Moussa, Romain Moury, Umit B. Demirci, Tansel Şener and Philippe Miele. *Int. J. Energy Res*. **2013** DOI: 10.1002/er

CHAPTER 2

Theoretical Background

Most of the properties of physics, chemistry and biology can be calculated from total energies or the difference of total energies. Quantum chemistry and computational material science can precisely calculate these total energies. Clearly, these methods can be easily applied to explore various properties molecules and materials. Therefore, computational calculations based on a quantum mechanics have considerably important impact on solid-state physics and chemistry and on materials science. These approaches are not only providing deeper understanding to molecular and crystal structures but also offering an economic and effective route to design new and materials for various applications. This chapter briefly abstracts these theoretical approaches. These methods are used in the work been presented in this thesis.

We start with a concise introduction to electronic structure; this will be followed by discussion of fundamentally important theoretical methods like Born-Oppenheimer approximation, Hartree approximation, Hartree-Fock theory, and methods beyond Hartree-Fock. In the later section, we will provide a succinct introduction of density functional theory (DFT). Further, we will discuss Hohenberg-Kohn theorems and Kohn-Sham equations details, as these theorems gave the basis to DFT namely. In the succeeding section, we have offered detailed discussion on exchange-correlations functionals. A detailed overview of the concepts of molecular dynamics (MD) is given in In Section 2.3 and the fundamentals of ab initio MD are elaborated in Section 2.4. Born-Oppenheimer molecular dynamics (BOMD) and Car-Parrinello molecular dynamics (CPMD) are explained and contrasted in this Section. To this end, we will offer a

discussion of plane wave pseudopotential approach and the implementation these methods in Vienna ab initio simulation package (VASP).

2.1 Electronic structure

For any N electrons system with M nuclei, total energy can be calculated by solving the Schrödinger equation. The time-independent *Schrödinger wave equation* [1] given as

$$H\psi = E\psi \tag{2.1.1}$$

Where ψ is the wavefunction, the energy (E) of the system is eigenvalue and Hamiltonian operator(H). Hamiltonian operator can be written as the sum of kinetic and potential energy operators.

$$H = -\sum_{i}^{N}\frac{\hbar^2}{2m_e}\nabla_i^2 - \sum_{\alpha=1}^{M}\frac{\hbar^2}{2m_\alpha}\nabla_A^2 + \frac{1}{2}\sum_{i\neq j}^{N}\frac{e^2}{r_{ij}} + \frac{1}{2}\sum_{\alpha\neq\beta}^{N}\frac{Z_\alpha Z_\beta e^2}{R_{\alpha\beta}} - \sum_{i}^{N}\sum_{\alpha}^{M}\frac{Z_\alpha e^2}{r_{i\alpha}} \tag{2.1.2}$$

The first two terms are the kinetic energies of *N* electrons and the third term is electrostatic repulsion, fourth term is the electrostatic repulsion and the last term is the Columbic attraction between electrons and nuclei. Where r_{iA} is the distance between electrons and nuclei, r_{ij} is the between electrons and $R_{\alpha\beta}$ is the distance between the nuclei.

2.1.1 Born-Oppenheimer (BO) approximation

Due to the larger masses of nuclei when compared to electrons, their velocities are therefore smaller than electrons. Under the Born-Oppenheimer approximation [2] it is assumed that the nuclei are fixed. This approximation removes the terms involving internulear distances in Equation (2.1.2). This simplification allows splitting the total Hamiltonion into two terms, the electronic Hamiltonion and a constant term. Furthermore, the fourth term in the above said equation is included in the total energy after calculating the wavefunction. The electronic Hamiltonian operator is given as:

$$H_e = -\sum_i^N \frac{\hbar^2}{2m_e}\nabla_i^2 + \frac{1}{2}\sum_{i\neq j}^N \frac{e^2}{r_{ij}} - \sum_i^N \sum_\alpha^M \frac{Z_\alpha e^2}{r_{i\alpha}} \quad (2.1.3)$$

The second term of equation (2.1.3) is due to electron-electron interactions, this is term involves two electron operator, thus, it is the most challenging to deal with. Without this term, the electronic Hamiltonians is similar to the Hamiltonians of non interacting system.

.

2.1.2 Hartree theory

Hamiltonian of any non interacting electron can be expressed as the linear combination of one electron operators, describing the kinetic energy and potential energy of electrons.

$$H_{non-\text{int}} = \sum_i h_i \quad (2.1.4)$$

Then the total non-interacting wavefunction $\Psi_{non-\text{int}}$ becomes a product of *N* one-electron wavefunctions ψ_i. This wavefunction is called *Hartree product.*

$$\Psi_{non-\text{int}} = \psi_1(r_1)\psi_2(r_2)\psi_3(r_3)....\psi_n(r_n) \quad (2.1.5)$$

The electron-electron interactions assumed to be depend only on the positions of the electron under consideration which moves in an electronic field of other electrons. Two electron term in Equation (2.1.3) can consequently be approximated as a sum of one-electron potentials v_i

$$\sum_{i\neq j}^N \frac{1}{r_{ij}} \approx \sum_{i=1}^N v_i(r_i) = \sum_{i=1}^N \int \frac{\rho(r_j) - \left|\psi_i\left(r_j\right)\right|^2}{\left|r_i - r_j\right|} dr_j \quad (2.1.6)$$

However, Hartree product is not antisymmetric with respect to exchange of electrons and does not account for the Pauli Exclusion Principle. To get a wavefunction which comply with Pauli Exclusion Principle, it is essential to go beyond the Hartree approximation

2.1.3 Hartree-Fock theory

To overcome the shortcomings of Hartree theory, the introduction of anti symmetrise wavefunction was done within Hartree-Fock theory. This theory adopts single Slater determinant to represent the wavefunction. Slater determinant is an antisymetric wavefunction which is composed of an antisymmetrized product of N orthonormal spin orbitals $\psi_i(x)$ for all the electrons

$$\Psi_{HF} = \frac{1}{\sqrt{N!}} \begin{vmatrix} \psi_1(x_1)\psi_2(x_1).....\psi_N(x_1) \\ \psi_1(x_2)\psi_2(x_2).....\psi_N(x_2) \\ ..... \\ ..... \\ \psi_1(x_N)..\psi_2(x_N).....\psi_N(x_N) \end{vmatrix} \tag{2.1.7}$$

In the *Hartree-Fock (HF) theory* [3] the orthonormal spin orbitals are minimize using the variation principle

$$E\left[\Psi_{HF}\right] = \frac{\left\langle \Psi_{HF} \middle| H \middle| \Psi_{HF} \right\rangle}{\left\langle \Psi_{HF} \mid \Psi_{HF} \right\rangle}$$

The normalization integral $\left\langle \Psi_{HF} \mid \Psi_{HF} \right\rangle$ is equal to unity.

$$E_{HF} = \left\langle \Psi_{HF} \middle| H \middle| \Psi_{HF} \right\rangle = \sum_{i=1}^{N} H_i + \frac{1}{2}\sum_{i,j}^{N} (J_{ij} - K_{ij}) \tag{2.1.8}$$

$$H_i = \left\langle \psi_i(x) \middle| -\frac{1}{2}\nabla^2 = v(x) \middle| \psi_i(x) \right\rangle \tag{2.1.9}$$

$$J_{ij} = \int\int \psi_i(x_1)\psi_i^*(x_1)\frac{1}{2}\psi_j^*(x_2)\psi_j(x_2)dx_1dx_2 \tag{2.1.10}$$

$$K_{ij} = \int\int \psi_i^*(x_1)\psi_j(x_1)\frac{1}{2}\psi_i(x_2)\psi_j^*(x_2)dx_1dx_2 \tag{2.1.11}$$

Where J_{ij} and K_{ij} are called Coulomb integrals and exchange integrals respectively.

Above equation is solved using the orthonoramlity condition. The Fock operator is given as:

$$F(\Psi_i(x)) = \sum_{j=1}^{N}\varepsilon_{ij}\psi_j(x) \tag{2.1.12}$$

$$F(\psi_i) = -\frac{1}{2}\nabla_i^2 - \sum_{A}^{M}\frac{Z_A}{r_{iA}} + v^{HF}(i) \tag{2.1.13}$$

Here v^{HF} is the effective potential experienced by i^{th} election due to the presence of other electrons. In HF approximation, the many electron problem is simplified to single electron problem, by considering the interaction of each electron in average way. The Hartree-Fock potential V^{HF} depends on the spin orbitals of other electrons. Clearly, the Hartree-Fock equations are non linear equations, hence, these should be solved iteratively. The self consistent filed (SCF) procedure is employed to solve Hartree-Fock equations. In the SCF procedure initial guess of spin orbitals is used to calculate the Hartree-Fock potential. The calculated Hartree-Fock potential is used to obtained new spin orbitals. These new spin orbitals are used to calculate new Hartree-Fock potential. This process is repeated unit the Hartee-Fock potential no longer changes on repeating the procedure.

The Hartree-Fock theory offers alternative way of treating the multielectron by single electron picture using the field approximation. This approximation takes care of exchange completely. However, the correlation of anti parallel elections is completely missing. Consequently, even if the HF equations are correctly solved, the method eventually turns out to be theoretically incomplete. The correlation energy is defined as the difference between the correct energy and that of the HF solution i.e.

$$E_{corr} = E - E_{HF}\,.$$

2.2 Density functional theory (DFT)

Various properties of any system can be determined by solving the time-independent Schrödinger equation (2.1.1). However, ψ depends on 3N coordinates, hence it is difficult to deal with.

Density can be measured experimentally, it is a physical observable. Most of physical observables can be expressed in terms of electron density matrix.

$$\rho^{(1)}(r,r') = N\int \psi^*(r_1,r_2....,r_N)\psi(r_1',r_2.....,r_N)dr_2...dr_N \quad (2.2.1)$$

$$\rho^{(2)}(r_1,r_2,r_1',r_2') = \frac{N(N-1)}{2}\int \psi^*(r_1,r_2,r_3....,r_N)\psi(r_1',r_2',r_3.....,r_N)dr_3...dr_N \quad (2.2.2)$$

$$\rho^{(1)}(r) = \rho(r,r) \quad (2.2.3)$$

Where, $\rho^{(1)}(r,r')$, $\rho^{(2)}(r_1,r_2,r_1',r_2')$, $\rho^{(1)}(r)$ are one-electron density matrix, two-electron density matrix, real space electron density resperively.

The *density functional theory* (DFT) [7] offers different formalism where complete knowledge of *N*-electron wavefunction **Ψ** can be skipped and uses much simpler electron density *ρ(r)* and its corresponding calculation scheme. The first attempt of using electron density as the basic variable began with the revolutionary work of Thomas and Fermi.

2.2.1 Thomas-Fermi Model

The idea of using statistical considerations to estimate the distribution of electrons in an atom is proposed by Thomas [8] and Fermi [9]. In this model Kinetic energy is approximated functional of density of non-interacting electrons in a homogeneous gas. In this model the exchange and correlation terms are completely ignored. The Thomas-

Fermi total energy of an atom is given as:

$$E_{TF}[\rho(r)] = C_F \int \rho^{\frac{5}{3}}(r)dr - Z\int \frac{\rho(r)}{r}dr + \frac{1}{2}\int \int \frac{\rho(r)\rho(r')}{|r-r'|}drdr' \quad (2.2.4)$$

Where the Fermi coefficient $C_F = 2.871$. This equation is minimised under the constraint

$$N = N[\rho(r)] = \int \rho(r)dr \quad (2.2.5)$$

Assuming that atom is in its ground state.

Lagrange multipliers is used to incorporate the constraint that the ground-state electron density must satisfy the variational principle

$$\delta\left[E_{TF}[\rho] - \mu_{TF}(\int \rho(r)dr - N)\right] = 0 \quad (2.2.6)$$

$$\mu_{TF} = \frac{\delta E_{TF}[\rho]}{\delta\rho(r)} = \frac{5}{3}C_F\rho^{\frac{2}{3}}(r) - \left[\frac{Z}{r} - \int \frac{\rho(r_2)}{|r-r_2|}dr_2\right] \quad (2.2.7)$$

In this model the Thomas Fermi energy is calculated by solving the Equation (2.2.7) by imposing the constraint (2.2.5). The calculated electron density is used to solve Equation (2.2.6) to give the total energy. This method was the first method to use kinetic energy as a functional of electron density. TF model is inaccurate for the total energies of atoms and molecules due to oversimplification and ignorance of exchange and correlation.

2.2.2 Hohenberg-Kohn theorems

The current density functional theory was originated with the fundamental ideas based on the theorems of Hohenberg and Kohn [10]. The first Hohenberg-Kohn *(HK1)*

theorem states that: "*The external potential v(r) is determined, within a trivial additive constant, by the electron density* $\rho(r)$. The electronic Hamiltonian can be completely defined if the number of electron N and external potential v(r) is known. Since $\rho(r)$ determines the number of electrons, it follows that $\rho(r)$ also determines the ground-state wavefunction **Ψ** and all other properties such as kinetic energy $T[\rho(r)]$, potential energy $V[\rho(r)]$ and total energy $E[\rho(r)]$ of the system. Hence the ground state expectation value of any observable, including the total energy, is a unique functional of the ground-state electron density $\rho(r)$.

$$E_v[\rho] = T[\rho] + V_{ne}[\rho] + V_{ee}[\rho] = \int \rho(r) v(r)\, dr + F_{HK}[\rho] \tag{2.2.8}$$

where

$$F_{HK}[\rho] = T[\rho] + V_{ne}[\rho] \tag{2.2.9}$$

The second HK theorem states that: *For a trial density* $\rho(r)$ *such that* $\tilde{\rho}(r) \geq 0$ *and* $\int \rho(r) dr = N$ *the actual ground state energy can be given as*

$$E_0 \leq E_v[\tilde{\rho}] \tag{2.2.10}$$

The second HK theorem is essentially a variational approach to search of the ground state wavefunction**.** The electron density $\rho_0(r)$ can be used to search the lowest energy. Hence, the ground-state energy E_0 is given as the minimum of the functional $E[\rho(r)]$.

The classical part of the electron-electron interaction $V_{ee}[\rho]$ in Equation (2.2.9) is the Coulomb potential energy

$$J[\rho] = \frac{1}{2} \int\int \frac{\rho(r_1)\rho(r_2)}{r_2 - r_1} dr_1 dr_2 \tag{2.2.11}$$

In the TF theory $V_{ee}[\rho]$ is replaced by $J[\rho]$ and kinetic energy $T[\rho]$ is taken from the theory of a non-interacting uniform electron gas. This constitutes a direct approach for calculating $T[\rho]$ and therefore the total energy if the electron density is known but only approximately. It would however be preferable to correctly calculate $T[\rho]$ as it forms the

leading part of the total energy. Kohn and Sham proposed the introduction of orbitals into the problem allowing more accurate computation of $T[\rho]$ with a small residual correction that is handled separately.

2.2.3 Kohn-Sham equations

Kohn and Sham have used new approach to solve the problem of calculating the total energy E as a functional of electron density $E[\rho(r)]$ by solving a set of single-particle Schrödinger-like equations. They used previously existing Thomas-Fermi model, however, the treatment of the kinetic energy term was totally different in their formalism. In Thomas-Fermi theory the kinetic energy term was an effective local potential. Kohn-Sham theory replaces this term kinetic energy operator non interaction electrons. The kinetic energy of the interacting system is calculated from the projection on to the non-interacting system with equal density of the interacting system.

For a system of non interacting electrons the kinetic energy is

$$T_0 = \sum_{i=1}^{N} n_i \left\langle \psi_i \left| -\frac{1}{2}\nabla^2 \right| \psi_i \right\rangle \tag{2.2.12}$$

and the electron density is

$$\rho(r) = \sum_{i=1}^{N} n_i \left|\psi_i(x)\right|^2 \tag{2.2.13}$$

with x including both space and spin coordinates. Here ψi and ni are the natural spin orbitals and their occupation numbers respectively. Using orbitals to calculate the kinetic energy is an indirect though accurate approach.

The electron-electron Coulomb repulsion written as;

$$E_C = \frac{e^2}{2}\iint \frac{\rho(r_1)\rho(r_2)}{|r_1 - r_2|} dr_1 dr_2 = \frac{1}{2} V_C(r)\rho(r) dr$$

(2.2.14)

Consequently, the total energy functional can be written as:

$$E[\rho] = T[\rho] + \int [V_{ext}(r) + \frac{1}{2} V_C(r)]\rho(r) dr + E_{XC}[\rho]$$

(2.2.15)

Kohn and Sham [11] replaced the interacting many-body problem by a corresponding noninteracting particle system with the same density in an appropriate external potential. The total energy functional can be rewritten as:

$$E\left[\rho(r)\right] = T_0\left[\rho(r)\right] + \frac{1}{2}\int\int \frac{\rho(r)\rho(r')}{|r - r'|} dr dr' + E_{XC}\left[\rho(r)\right] + \int \rho(r) v(r)\, dr \quad (2.2.14)$$

In the above equation the first term is the kinetic energy functional of the system of noninteracting electrons with the same density, the second term is the classical Coulomb energy for the electron-electron interaction, the third term is energy functional incorporating all the many-body effects of exchange and correlation and the last term is the attractive Coulomb potential provided by the fixed nuclei.

The construction of the *Kohn-Sham (KS) functional* is based on the assumption that the exact ground state density can be represented by the ground state density of an auxiliary system of noninteracting particles. The solution of the KS auxiliary system can be viewed as the minimization problem of the KS functional with respect to the density. This leads to *N* KS equations

$$\left[-\frac{1}{2}\nabla^2 + v_{eff}(r)\right]\psi_i(r) = \varepsilon_i \psi_i(r) \quad (2.2.15)$$

$$\rho(r) = \sum_i^N \sum_s |\psi_i(r,s)|^2 \quad (2.2.16)$$

Here ε_i are eigenvalues, ψ_i are KS orbitals and *veff* is the effective potential

$$v_{eff}(r) = v(r) + \int \frac{\rho(r')}{|r - r'|} dr' + v_{XC}(r) \tag{2.2.17}$$

that is the sum of potential from the nuclei, a Hartree-style potential and the potential for exchange and correlation. The latter is defined as

$$v_{XC} = \frac{\partial E_{XC}[\rho(r)]}{\partial \rho(r)} \tag{2.2.18}$$

In Equation (2.2.18) v_{eff} depends on $\rho(r)$. Hence the KS Equations (2.2.14), (2.2.15) and (2.2.16) have to be solved self-consistently. Therefore, in a DFT calculation one begins with a guess for $\rho(r)$ for constructing v_{eff} from Equation (2.2.14). After the first iteration we get a new electron density from which the Hartree and exchange-correlation potentials are generated to yield a new potential. This process is repeated until self-consistency is achieved.

2.2.4. Solutions of Kohn-Sham equations

The Kohn-Sham equations are solved using self-consistent calculations. The effective potential corresponding to electron density $\rho(r)$ is first calculated then the single electron wavefunctions are constructed. These wavefunctions are used to estimate new charge density. Within the iterative procedure when at a given cut-off there is no change in the input and output charge density, the self-consistent solution is said to be achieved.

The idea of using the charge density instead of wavefunctions to determine the electronic structure makes computation easier and cost effective. This is very advantageous when compared to wavefunction based methods, particularly for heavy atoms and reasonably big systems. In the implementations of DFT, the wavefunction ψ_i is expressed in a basis to treat the potentials accurately.

$$\psi_i(r) = \sum_j^N c_{ij} \phi_j(r) \tag{2.2.19}$$

Where $\phi_j(r)$ are the basis functions used in the calculation.

Then the charge density can be written as:

$$\rho(r) = \sum_i^N \sum_j^M c_{ij}^* c_{ik} \phi_{ij}^*(r) \phi_k(r) \tag{2.2.20}$$

It is impossible to write the exchange correlation term in an analytical form in most basis sets, consequently, the calculation of matrix elements is impossible. Auxiliary basis functions are thus used to calculate these matrix elements. The charge density expressed in terms of auxiliary functions:

$$\rho(r) \approx \tilde{\rho}(r) = \sum_i^M c_i^\rho f_i^\rho(r) \tag{2.2.21}$$

The basis functions $\phi_j(r)$ and the auxiliary functions $f_i(r)$ are used for calculations involving following steps.

1. The specification of nuclear coordinates.
2. Start with guess of potentials Hartree potential and exchange correlation potential.
3. Hamiltonian and overlap matrix are calculated using these potentials and the selected basis

$$S_{ik} = \left\langle \phi_i \mid \phi_j \right\rangle \tag{2.2.22}$$

$$H_{ij} = \left\langle \phi_i \left| \frac{-\hbar^2}{2m} \nabla^2 + V_{Hartree} + V_{XC} \right| \phi_j \right\rangle \tag{2.2.23}$$

4. The formation and diagonalization of secular equation to get the Kohn-Sham energies ε_i and the orbitals ψ_i.

$$Hc_i = \varepsilon_i S c_i \tag{2.2.24}$$

5. Charge density is calculated from new potentials $V_{Hartree}$ and V_{XC} and start from step 3 again.

6. Once the convergence criteria have met, V_{XC} physical quantities are calculated.

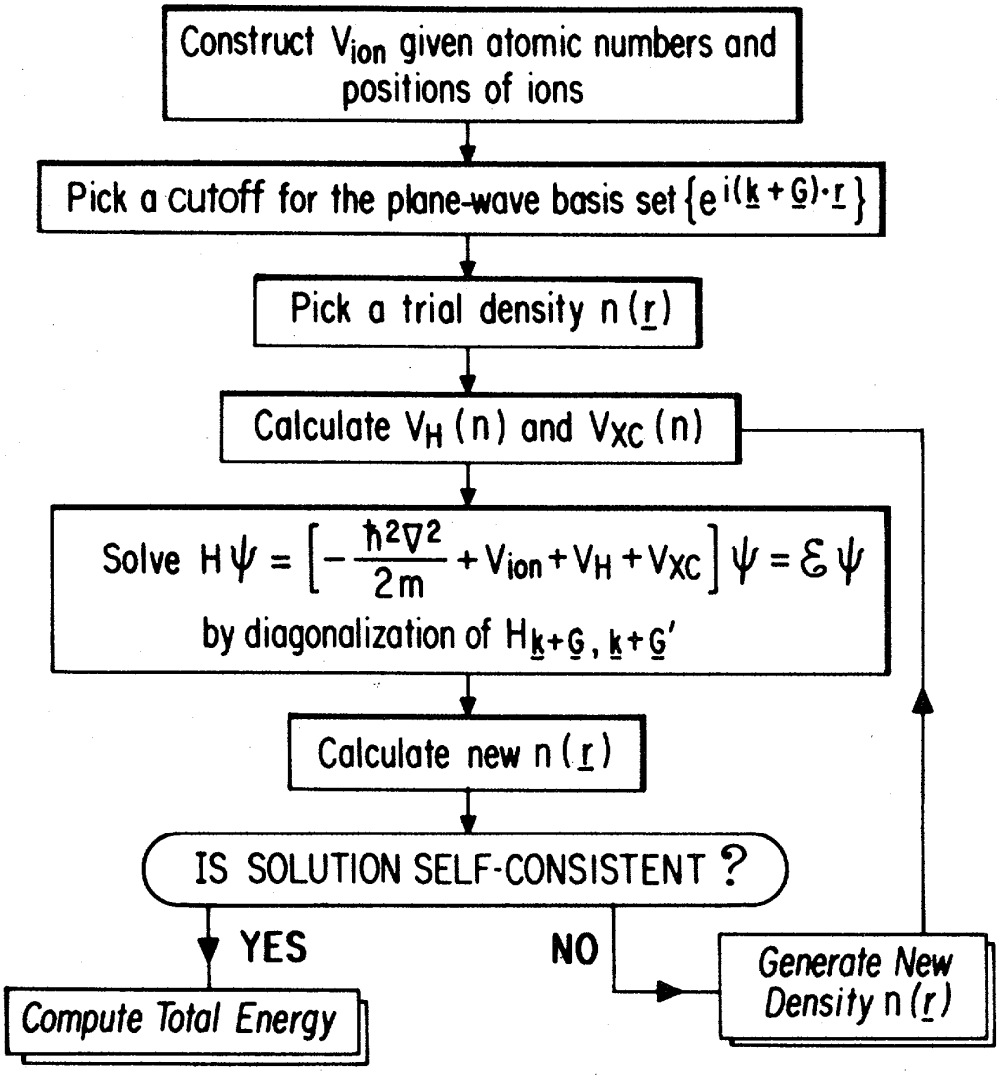

Figure 2.1. The flow chart of self-consistent solutions for the Kohn-Sham equations.(source:ref 23)

2.2.5 Exchange-correlation functionals

The KS equations provide the basis to calculate the kinetic energy correctly. However, the main challenge in DFT is to accurately calculate the exchange correlation energy. Clearly it is essential to find a good approximation of the exchange-correlation functional $E_{XC}[\rho(r)]$. Local Density Approximation *(LDA)* [11] is one of the many

exchange correlation functional available within DFT. It is given as:

$$E_{XC}^{LDA}[\rho] = \int \rho(r)\varepsilon_{XC}[\rho(r)]dr \tag{2.2.25}$$

where $\varepsilon_{XC}[\rho(r)]$ is the exchange-correlation energy per particle of a uniform electron gas of density $\rho(r)$.The exchange part of $\varepsilon_{XC}[\rho(r)]$ can be expressed analytically by that of a homogeneous electron gas.

$$\varepsilon_X\left[\rho(r)\right] = -C_X\rho(r)^{\frac{1}{3}} \tag{2.2.26}$$

$$C_X = \frac{3}{4}\left(\frac{3}{\pi}\right)^{\frac{1}{3}} \tag{2.2.27}$$

The correlation part may be obtained from perturbation theory or from Quantum Monte Carlo method. The corresponding exchange-correlation potential and KS equation then become

$$v_{XC}^{LDA}(r) = \frac{\delta E_{XC}^{LDA}}{\delta\rho(r)} = \varepsilon_{XC}\left[\rho(r)\right] + \rho(r)\frac{\partial\varepsilon_{XC}\left[\rho(r)\right]}{\partial\rho} \tag{2.2.28}$$

$$\left[-\frac{1}{2}\nabla^2 + v(r) + \int\frac{\rho(r')}{|r-r'|}dr' + v_{xc}^{LDA}(r)\right]\psi_i(r) = \varepsilon_i\psi_i(r) \tag{2.2.29}$$

The self-consistent solution of Equation (2.2.19) defines the *LDA method*. Application of LDA amounts to assuming that the exchange-correlation energy for a nonuniform system can be obtained by applying uniform electron gas results to infinitesimal portions of the nonuniform electron distribution and then summing over all individual contributions.

LDA is expected to work for systems with slowly varying electron densities. However it was successful for even semiconductors and insulators due to large cancellations in the exchange part. Hence further improvements are called for. A route to bring about this improvement is to take into account the gradient of the electron density. The idea is to include $\partial\rho(r)/\partial r$ as well as $\rho(r)$ to describe the exchange hole. This is

implemented via the method of *generalized gradient approximation* (GGA) in which the exchange-correlation energy functional is written as

$$E_{XC}^{GGA}\left[\rho(r)\right]=\int \rho(r)F[\rho(r),\nabla\rho(r)]dr \tag{2.2.30}$$

In 1986 the exchange part of $E_{XC}^{GGA}\left[\rho(r)\right]$ was proposed by Perdew and Wang (PW86) [12] and another correction was developed by Becke in 1988 (B88) [13]. Gradient corrections to the correlation part were proposed in 1986 by Perdew (P86) [14], in 1991 by Perdew and Wang (PW91) [15], in 1988 by Lee, Yang and Parr (LYP) [16] and in 1996 by Perdew, Burke and Ernzerhof (PBE) [17]. In all our density functional calculations the PW91 GGA functional has been employed.

2.3 Molecular dynamics

The aim of *molecular dynamics* (MD) is to model the detailed microscopic dynamical behavior of many different types of systems as found in chemistry, physics or biology. In such a scenario, the motions of nuclei must be taken care from the beginning. In the MD method, nuclear motion of the particles is described using the laws of Newton's mechanics whereby every new distribution is derived from the previous one by using the interactions between the particles. For an i^{th} particle of the system, the total potential energy at time t0=0 is computed as a sum of all pair interactions u_{ij}

$$u(\vec{r}_i)=\sum_j u_{ij}(\vec{r}_i,\vec{r}_j) \tag{2.3.1}$$

Once this is obtained the force acting on the particle can be calculated as

$$\vec{f}_i=-\nabla u(\vec{r}_i) \tag{2.3.2}$$

which causes an acceleration

$$\vec{a}_i=\frac{\vec{f}}{m} \tag{2.3.3}$$

This in turn modifies the initial velocity $\vec{v}_i$ to $\vec{v}_i'$ and then every particle is allowed to move with that velocity over a short period of time Δt. This produces new positions r'_i for all the particles at time $t_1 = t_0 + \Delta t$. Next the potential energies u'_i, forces $\vec{f}_i'$ and velocities $\vec{v}''_i$ are calculated for this new distribution. This procedure is repeated for a large number of times. Therefore, MD simulations can describe systems that evolve in time. The new positions are derived from the Newtonian laws of motion and are therefore deterministic.

2.3.1 Equations of motion

The Hamiltonian for a system of N particles moving under the influence of a potential function $U(R^N)$ is given by

$$H(R^N, P^N) = \sum_{I=1}^{N} \frac{P_I^2}{2M_I} + U(R^N) \tag{2.3.4}$$

where R^N and P^N are the sets containing all the positions and momenta respectively. The forces are derived from the potential

$$F_I(R^N) = -\frac{\partial U(R^N)}{\partial R_I} \tag{2.3.5}$$

The equations of motion are according to Hamilton's equations

$$\dot{R}_I = \frac{\partial H}{\partial P_I} = \frac{P_I}{M_I} \quad \dot{P}_I = \frac{\partial H}{\partial R_I} = -\frac{\partial U}{\partial R_I} = F_I(R^N) \tag{2.3.6}$$

From which the Newton's second law is obtained

$$M_I \ddot{R}_I = F_I(R^N) \tag{2.3.7}$$

The equations of motion are integrated and atomic trajectories are followed on the potential energy surface.

2.3.2 Numerical integration

The numerical integration techniques are based on a discretization of time and a repeated calculation of the forces on the particles. These methods must have the properties of (a) long time energy conservation to ensure that we stay on the constant energy hypersurface and short time reversibility and (b) short time reversibility so that the discrete equation still exhibit the time reversible symmetry of the original differential equations.

A computationally efficient scheme is the *Verlet algorithm* [18]. To derive it $\vec{r}_i(t)$ is expanded forward and backward in time in the third order of Taylor expansion.

$$\vec{r}_i(t+\delta t) = \vec{r}_i(t) + \vec{v}_i(t)\delta t + \frac{1}{2m_i}\vec{f}_i(t)(\delta t)^2 + \frac{1}{6}\vec{b}_i(t)(\delta t)^3 + O((\delta t)^4) \tag{2.3.8}$$

$$\vec{r}_i(t-\delta t) = \vec{r}_i(t) - \vec{v}_i(t)\delta t + \frac{1}{2m_i}\vec{f}_i(t)(\delta t)^2 - \frac{1}{6}\vec{b}_i(t)(\delta t)^3 + O((\delta t)^4) \tag{2.3.9}$$

Adding,

$$\vec{r}_i(t+\delta t) = 2\vec{r}_i(t) - \vec{r}_i(t+\delta t) + \frac{1}{m_i}\vec{f}_i(t)(\delta t)^2 + O((\delta t)^4) \tag{2.3.10}$$

Subtracting,

$$\vec{v}_i(t) = \frac{1}{2(\delta t)}[\vec{r}_i(t+\delta t) - \vec{r}_i(t-\delta t)] + O((\delta t)^4) \tag{2.3.11}$$

A MD simulation is usually performed for a fixed number of particles N inside a fixed volume. The initial values for positions and velocities are chosen together with an appropriate time step. The first part of the simulation is the equilibration phase in which strong fluctuations may occur. Once all the important quantities are sufficiently equilibrated, the actual simulation is performed. The time evolution of such a microcanonical ensemble is accumulated over many time steps. Finally observables are calculated from the trajectory as time averages which are thought of as being comparable to experimentally observed ensemble averages.

2.4 Ab-inito Molecular Dynamics

The basic idea underlying every *ab intio molecular dynamics* (AIMD) method is to compute the forces acting on the nuclei from electronic structure calculations that are performed on-the-fly as the MD trajectory is generated. In this way the electronic variables are not generated beforehand, but are considered as active degrees of freedom. This implies, that given a suitable approximate solution of the manyelectron problem, chemically complex systems can also be handled by MD. This implies that now, one has to select a particular approximation for solving the Schrödinger equation.

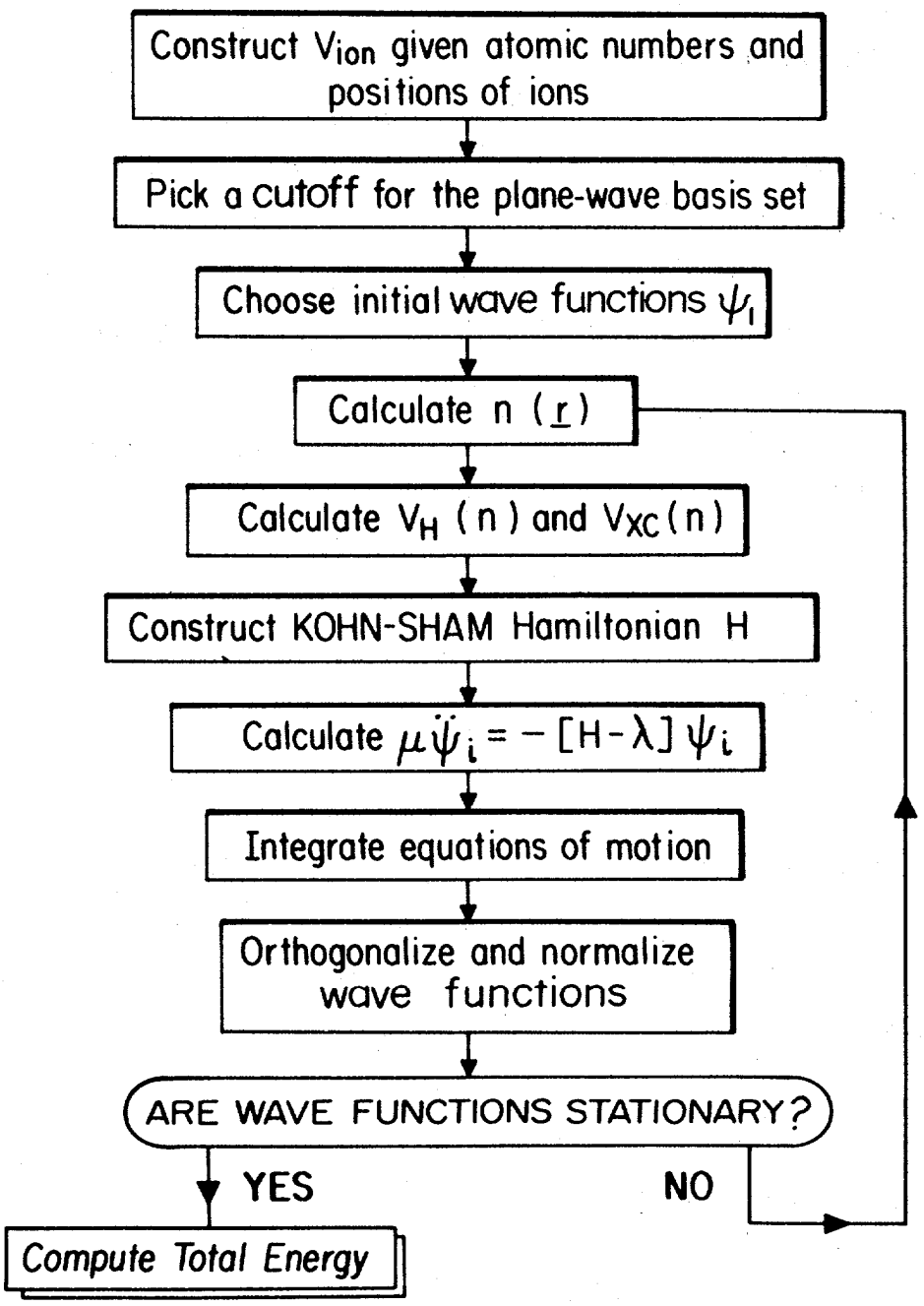

Figure 2.2 Flow chart for computational procedure on *ab initio* molecular dynamics calclations. (source:ref23)

2.4.1 Born-Oppenheimer molecular dynamics

The most commonly employed approach to AIMD is the *Born-Oppenheimer molecular dynamics* (BOMD) in which the electronic problem is solved using DFT for obtaining the ground state eigenvalue. For an interacting system of electrons with classical nuclei fixed at positions $\{\mathrm{R}^{\mathrm{N}}\}$, the total ground state energy can be found by minimizing the KS energy functional (as defined in Equation 2.2.11)

$$\underset{\Psi_0}{Min}\{\langle \Psi_0 | H | \Psi_0 \rangle\} = \underset{\{\phi_i\}}{Min} E^{KS}\left[\{\phi_i\}, R^N\right] \tag{2.4.1}$$

with respect to orbitals which are subject to the orthonormality constraint

$$\langle \phi_i \mid \phi_i \rangle = \delta_{ij} \tag{2.4.2}$$

The corresponding Lagrangian for BOMD is therefore

$$M_I R_I = -V_I[\underset{\{\phi_i\}}{Min} E^{KS}\left[\{\phi_i\}, R^N\right] \tag{2.4.3}$$

The forces between nuclei needed for the implementation of

$$\frac{d}{dR_I}[\underset{\{\phi_i\}}{Min} E^{KS}\left[\{\phi_i\}, R^N\right] \tag{2.4.4}$$

Once the initial forces are calculated they are next fed into a numerical integration procedure together with a set of initial velocities for the nuclei, and a step of molecular dynamics is carried out, yielding a new set of positions and velocities. At the new nuclear positions, the energy functional is minimized again and a new set of forces is obtained and used to perform another step of MD propagation. This procedure is repeated until an entire trajectory has been generated.

These steps involved in BOMD are displayed in the form of a flowchart presented in fig. 2.2

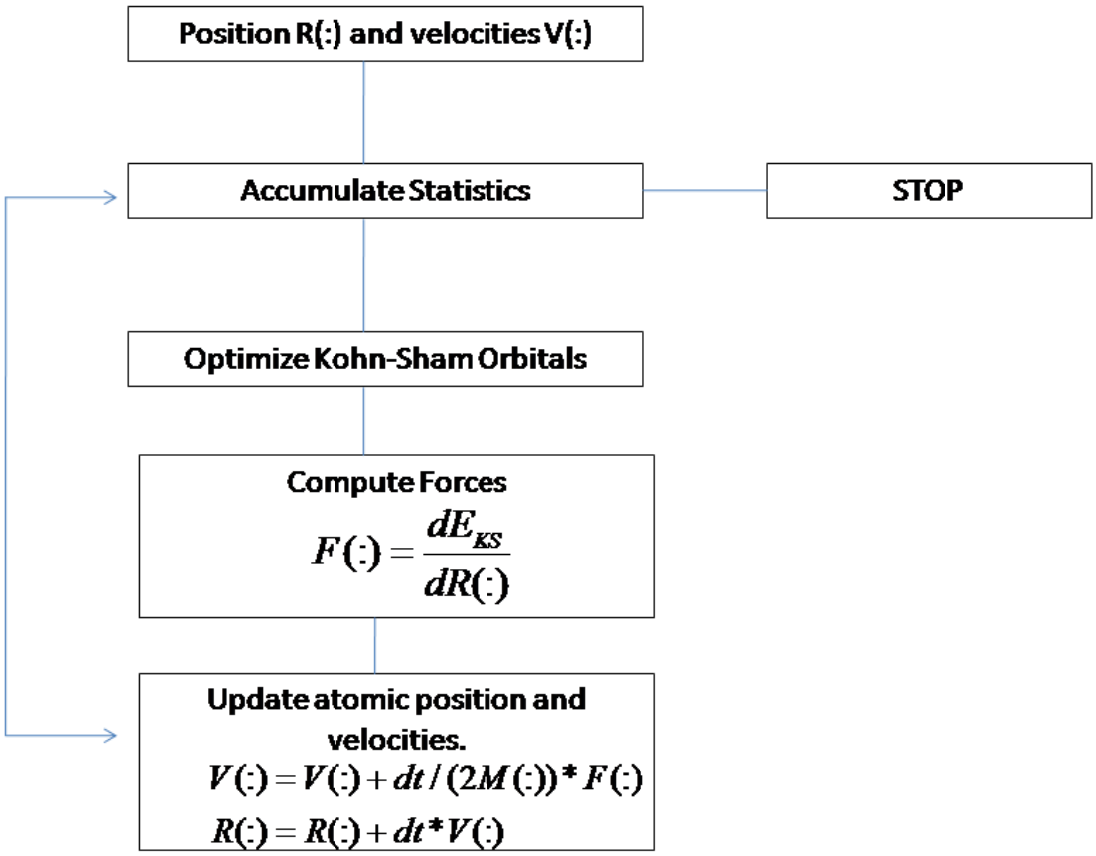

Figure 2.3. Flowchart displaying the steps involved in the Born-Oppenheimer Molecular Dynamics algorithm.

Fig.2.2.Clearly explains that BOMD requires a full self-consistent density functional minimization of energy and its derivative at each point. For cutting down computational expenses it would therefore be appealing to have an approach that does not require exact calculation of ground state energy at every step. An elegant alternative to BOMD was proposed by Car and Parrinello [24].

2.4.2 Car-Parrinello molelcular dynamics

Car-Parrinello molecular dynamics (CPMD) [19] is an efficient way to combine a quantum chemical description of electron dynamics and a classical description of nuclei dynamics in a unique framework. The Car-Parinello approach exploits the time-scale separation of fast electronic and slow nuclear motion. This is achieved by mapping the

two-component quantum/classical problem onto a two-component purely classical problem with two separate energy scales.

In CPMD the extended energy functional ε^{KS} is considered to be dependent on $\{\Phi i\}$ and R^N. In classical mechanics the force of the nuclei is obtained as the derivative of a Lagrangian with respect to the nuclear positions. Similarly, a functional derivative with respect to the orbitals, which if also interpreted as classical fields, would yield the force on the orbitals. Car and Parinello postulated the following Lagrangian using ε^{KS}

$$L_{CP}(R^N, \dot{R}^N, \{\phi_i\}, \{\dot{\phi}_i\}) = \sum_{I=1}^{N} \frac{1}{2} M_I \dot{R}_I^2 + \sum_i \frac{1}{2} \mu \left\langle \dot{\phi}_i \mid \dot{\phi}_i \right\rangle - \varepsilon^{KS}[\{\phi_i\}, R^N] \tag{2.4.5}$$

and the equations of motion are

$$M_I \ddot{R}_I(t) = \frac{\partial E^{KS}}{\partial R_I} + \sum_{ij} \Lambda_{ij} \frac{\partial}{\partial R_I} \left\langle \phi_i \mid \phi_j \right\rangle \tag{2.4.6}$$

where μ is the "fictitious mass" or inertia parameter assigned to the degrees of freedom. The forces needed for the implementation of CPMD can be obtained as the partial derivatives of the KS energy functional with respect to both the nuclear positions and the KS orbitals

$$F\left(\phi_i\right) = -f_i H^{KS} \phi_i \tag{2.4.7}$$

$$F\left(R_I\right) = -\frac{\partial E^{KS}}{\partial R_I} \tag{2.4.8}$$

The forces in Equation (2.4.13) are the same forces as in BOMD but in BOMD these were derived under the condition that the wavefunctions are optimized and are therefore are only correct up to the accuracy achieved in the wavefunction optimization. In CPMD these are the correct forces and calculated from analytic energy expressions are correct to machine precision.

In CPMD we begin with a starting configuration for which the KS equation is solved for the electrons. Next the forces are evaluated as the derivative of E^{KS} with respect to nuclear positions as given in Equation (2.4.13). In the same nuclear step the fictitious forces acting on the orbitals are calculated as the functional derivative of E^{KS}

with respect to orbitals (see Equation (2.4.12)). This is followed by an update of the forces in Equation (2.4.13) are the same forces as in BOMD but in BOMD these were derived under the condition that the wavefunctions are optimized and are therefore are only correct up to the accuracy achieved in the wavefunction optimization. In CPMD these are the correct forces and calculated from analytic energy expressions are correct to machine precision.

In CPMD we begin with a starting configuration for which the KS equation is solved for the electrons. Next the forces are evaluated as the derivative of E^{KS} with respect to nuclear positions as given in Equation (2.4.13). In the same nuclear step the fictitious forces acting on the orbitals are calculated as the functional derivative of E^{KS} with respect to orbitals (see Equation (2.4.12)). This is followed by an update of the nuclear and electronic configurations and another step of MD is performed. For generating a trajectory these steps are continuously repeated.

The flowchart of the above CPMD algorithm is shown in Fig. 2.2. It is noticeable that only one electronic step is performed for all the nuclear steps and hence the computationally demanding full electronic minimization is executed only for the starting configuration. If μ is small then the new electronic configuration corresponding to the new nuclear configuration will be already near enough to the exact ground state. On the other hand if μ is large then it ensures the use of reasonably large time steps, in order to have a fast integration of the equations.

2.5 Plane wave-pseudopotential method

In this section we discuss plane wave-pseudopotential method within the code VASP [20,21] This code is extensively used to carry out this work. The plane wave pseudopotential approach uses plane waves as basis set. The computational challenges of solving Schrödinger equation are simplified by exploiting the symmetry and periodic boundary conditions.

2.5.1 The plane wave basis sets

The external potential and the ground state density is periodic solid are translationally invariant under a lattice translation T, thus

$$v_{eff}(r+T) = v_{eff}(r) \tag{2.5.1}$$

Bloch's theorem states that each electronic wavefunction ψ_i(k,r) can be written as a product of a function $u_i(k,r)$ that has the periodicity of the lattice and a *plane wave* $e^{ik.r}$ with k being a vector in the first *Brillouin zone* (BZ), i.e.

$$\psi_i(k,r) = e^{ik.r} u_i(k,r) \tag{2.5.2}$$

Thus,

$$\psi_i(k,r+T) = e^{ikT} \psi_i(k,r) \tag{2.5.3}$$

The periodic function can be expanded in the plane wave basis as

$$u_i(r,k) = \frac{1}{\sqrt{\Omega_{cell}}} \sum_G c_i(G,K) e^{iG.r} \tag{2.5.4}$$

where Ω_{cell} is the volume of the primitive cell and G are the reciprocal lattice vectors. In the above form the $\psi_i(k,r)$'s are k-dependent. The complete set of G vectors is infinite and evaluating sums over all such vectors would be computationally expensive. Since orbitals and densities tend to become smooth at small scales, i.e. the plane wave components become negligible for large G vectors, therefore during calculations the infinite sums over G vectors and cells can be truncated.

2.5.2 Pseudopotentials

To accurately represent a system within the plane wave basis, because of the orbitals oscillations, a larger basis is required compare to localized basis set. These rapid oscillations can only be accounted with large kinetic energy cut-off. The pseudopotentials

replace the core potentials with an effective soft potential to solve this problem. Hence the core electrons can be considered to be "frozen" while keeping intact the core electron distribution of the isolated atom in the crystal environment. In turn, the long range interactions of the core are accounted for by PPs. Conventionally the PP is constructed by satisfying four general criteria:

(a) the valence pseudo-wavefunction Φl^{PS} must be the same as the all-electron (AE) wavefunction Φl^{AE} outside a given cut-off radius Rcut,

(b) the charge enclosed within Rcut must be equal for the two wavefunctions, i.e.

$$\int_0^{R_{cut}} \left|\Phi_l^{PS}(r)\right|^2 dr = \int_0^{R_{cut}} \left|\Phi_l^{AE}(r)\right|^2 dr \tag{2.5.4}$$

and is normalized such that

$$\int_0^{\infty} \left|\Phi_l^{PS}(r)\right|^2 dr = \int_0^{\infty} \left|\Phi_l^{AE}(r)\right|^2 dr = 1 \tag{2.5.5}$$

This is commonly referred to as *norm-conservation*, (c) ΦPS must not have any radial nodes within the core region and, (d) the valence AE and PP eigenvalues must be equal. These features are illustrated in Fig. 2.3.

Application of PPs has various advantages. It leads to a reduction in the number of electrons in the system and thereby allows for faster calculations and a simplified treatment of bigger systems. PPs also allow for a considerable reduction of the basis set size. The pseudized valence wavefunctions are nodeless functions and therefore require less basis functions for an accurate description. Furthermore the relativistic effects connected to the core electrons are incorporated into the PPs without complicating the calculations of the final system. Most importantly, PPs are transferable which implies that the same PP would be adequate for an atom in all possible chemical environments. This proves particularly useful during a simulation in which a change of environment is

expected, such as in case of chemical reactions and phase transitions.

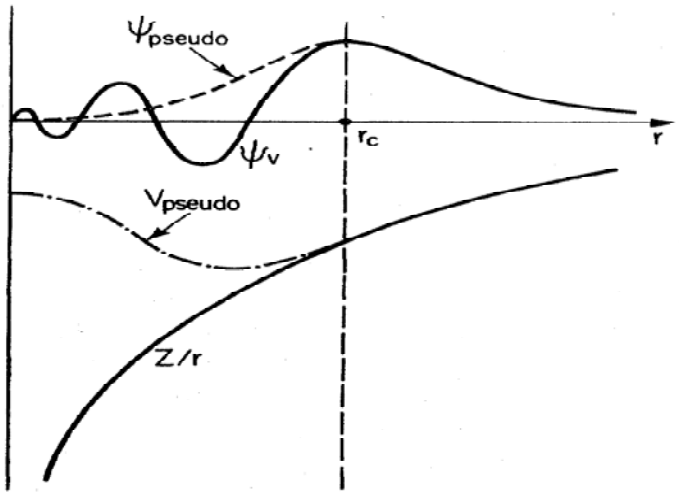

Figure 2.4. Schematic representation of all electron potentials (solid line) and pseudo potentials (dashed lines). r_c is the radius at which pseudo potential and all electron potential matches.(source ref 23)

References

1. E. Schrödinger, *Ann. Phys.* **1926**, *79*, 361.

2. M. Born and J. R. Oppenheimer, *Ann. Phys.* **1927**, *84,* 457.

3. C. C. J. Roothaan, *Rev. Mod. Phys.* **1951**, *23*, 69.

4. C. Møller and M. S. Plesset, *Phys. Rev.* **1934**, *46*, 618.

5. C. D. Sherrill and H. F. Schaefer, *Adv. Quantum Chem.* **1999**, *34*, 143.

6. R. J. Bartlett, *J. Phys. Chem.* **1989**, *93*, 1697.

7. R. G. Parr and W. Yang, *Density functional theory of atoms and molecules*, Clarendon Press, New York **1989**.

8. L. H. Thomas, *Proc. Cambr. Phil. Soc.* **1927**, *23*, 542.

9. E. Fermi, *Z. Phys.* **1928**, *48*, 73.

10. P. Hohenberg and W. Kohn, *Phys. Rev.* **1964**, *136*, 864.

11. W. Kohn and L. J. Sham, *Phys. Rev.* **1965**, *140*, 1133.

12. J. P. Perdew and Y. Wang, *Phys. Rev. B* **1986**, *33*, 8800.

13. A. D. Becke, *Phys. Rev. A* **1988**, *38*, 3098.

14. J. P. Perdew, *Phys. Rev. B* **1986**, *33*, 8822.

15. J. P. Perdew and Y. Wang, *Phys. Rev. B* **1992**, *45*, 13244.

16. C. Lee, W. Yang, and R. G. Parr, *Phys. Rev. B* **1988**, *37*, 785.

17. J. P. Perdew, S. Burke, and M. Ernzerhof, *Phys. Rev. Lett.* **1996**, *77*, 3865.

18. L. Verlet, *Phys. Rev.* **1969**, *57*, 98; *Phys. Rev.* **1967**, *165*, 201.

19. R. Car and M. Parrinello, *Phys. Rev. Lett.* **1985**, *55*, 2471.

20. G. Kresse and J. Hafner, *Phys. Rev. B* **1993**, *47*, 558.

21. G. Kresse and J. Furthmüller, *Phys. Rev. B* **1996**, *54*, 11169.

22. F. Bloch, *Z. Phys.* **1928**, *52*, 555.

23. M. C. Payne, *Rev.Mod.Phys.*,**1992**,64,4.

CHAPTER 3

Electronic structure

Resembling the molecules and atoms, the electronic structure in solid is of fundamental importance. The electron distributions, van der Waals and electrostatic interactions are responsible for the formation of solids. The valence electrons play crucial role in the bonding of solids. Also, the electronic distribution can be considerably modified from the isolated atom. Consequently, for a description of solid electronic structure must be taken into account carefully. Thus, in this chapter we will begin MO treatment of band theory. Later we will discuss the different tools available for studying electronic structure of solids. Our results of the charge density, band structure, and density of states (DOS) analyses on pure and Mn-doped and pure ZNO will be presented. We will illustrate from the band structure and DOS calculations that Mn doping reduces the band gaps of the three phases of Zno. By examination of the partial DOS, it will be further shown that this reduction in band gaps is due to generation of additional bands arising from the Mn impurities. Finally, the decreased band gaps will be used to suggest that doping with Mn in ZnO makes this material suitable to be used for photoelectrochemical splitting of water to produce hydrogen.

.

Introduction

3.1 Band theory and molecular orbitals

Molecular orbitals are formed by splitting the atomic orbitals to give discrete energy levels. However, when a large number of atomic orbitals are mixed, the resulting energy levels no longer remain distinct. In solids, a large number of atomic orbitals interact with each other to form crystal orbitals; these are often called as bands.

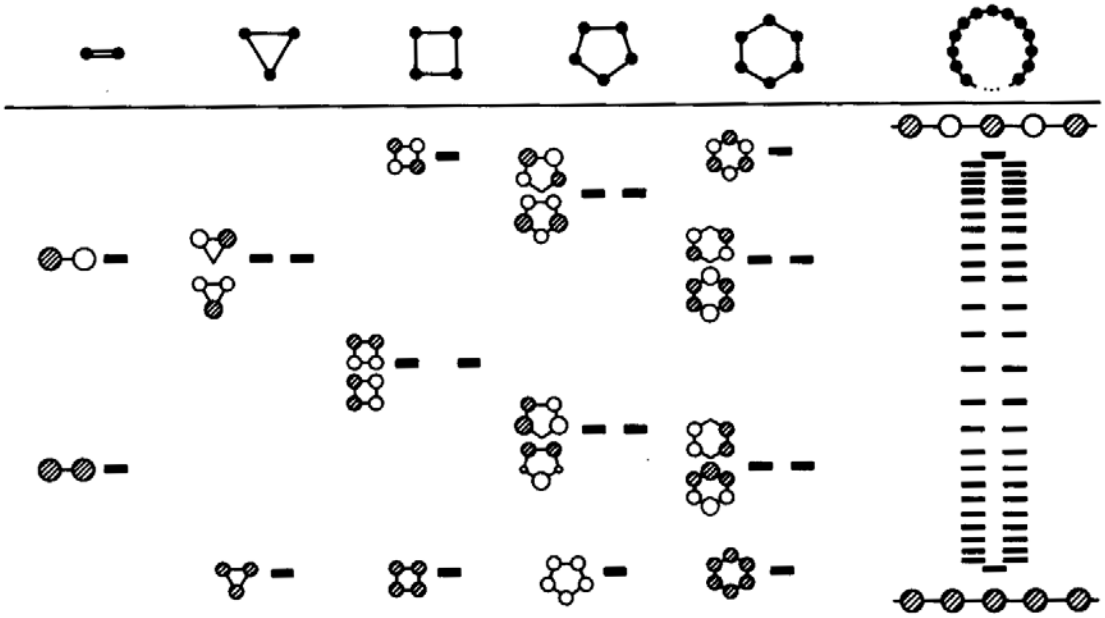

Figure 3.1. Schematic representation of bands from molecular orbitals. (Source ref 1)

The formation of these bands can be understood by taking a simplistic example of linear chains of Hydrogen atoms.

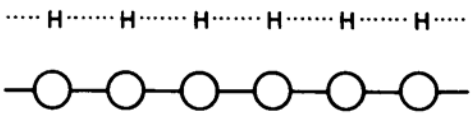

Linear Hydrogen chain

The symmetry adopted linear combination give the bonding and anti bonding orbitals as follows:

$$\psi_{bonding} = \chi_1 + \chi_2 + \chi_3 + \chi_4 \cdots \tag{3.1.1}$$

$$\psi_{anti-bonding} = \chi_1 - \chi_2 + \chi_3 - \chi_4 \cdots \tag{3.1.2}$$

In solids, the formation of these symmetry-adopted linear combination is done by formation of Bloch's equations.

$$\psi_k = \sum_n e^{ikna} \chi_n \tag{3.1.3}$$

For k=0 $\psi_0 = \chi_1 + \chi_2 + \chi_3 + \chi_4 \cdots$

For k= $\frac{\pi}{a}$ $\psi_{\frac{\pi}{a}} = \chi_1 - \chi_2 + \chi_3 - \chi_4 \cdots$ (3.1.4)

Clearly, the Bloch's fuction at 0 and $\frac{\pi}{a}$ represents the bonding(valance band) and anti-bonding orbitals(conduction band) respectively.

The band structure is calculated as follows:

$$E_k = \frac{\langle \psi_k | H | \psi_k \rangle}{\langle \psi_k | \psi_k \rangle} \tag{3.1.5}$$

The calculations of band structure (BS) and Density of sates (DOS) are central to computational material science. BS and DOS are very useful to predict various properties of solids. These are qualitatively explored using the basic molecular orbital picture to obtain useful information about that structure, reactivity and molecular interactions. BS

represents the molecular orbitals in a solid. It is a plot of energy verses k, where k is the wave vector that represents the phase of atomic orbital and the wave length of electronic wavefunction. The number of lines in a bandstructure plot is equal to the number of orbitals in the unit cell. Molecular orbitals can be used as a guide to predict and interpret the BS and DOS. The center of gravity of each band is determined qualitatively using the MO diagram. Molecular overlap determines that whether a band will run uphill or downhill or flat. The band picture can also predict that the electons are localized or delocalized within the solid. Wide band represents delocalization of electons with the large intermolecular overlap. Whereas narrow bands represents the localization of electrons with weak intermolecular overlap.

Using the above discussed tools, we have performed charge density, band structure and DOS calculations for pure and Mn- doped ZnO in order to develop an understanding photoelectrochemical behavior for possible use in photosplitting of water to produce hydrogen.

3.2 Mn doped ZnO: Hydrogen production

The problem of hydrogen production is clearly another big hurdle to practically utilize the hydrogen economy. A possible solution to overcome this difficulty is to use the solar light driven photoelectrochemical (PEC) splitting of water. Many research efforts have been made to produce the hydrogen by using such PEC approaches [1-6]. The most important issue in such process is to optimize the semiconductor properties of the working electrode. The electrode should be modified in a way that will facilitate not only the efficient absorption of solar light but also quick separation and migration of photogenerated charge carriers across electrode – electrolyte junction in the desired direction. After the first report by Fujishima and Honda, who used single crystal TiO_2 as photoanode to demonstrate the feasibility of PEC splitting of water, considerable progress has occurred [7]. Gerischer presented a thorough overview of the theory of the process [8], while Nozik provided a good account of the various PEC devices [9]. Heller made an

excellent analysis of efficiencies of various PEC systems involving the use of different semiconductors [10]. Yet, the development of an efficient and commercially viable PEC device for this purpose remains an unfinished task, and the quest for a semiconductor having ideal optical properties and well aligned band edge energetic still continues [6].

Zinc oxide (ZnO) finds a wide range of scientific and technological applications [11-13]. Most applications depend on its defect chemistry. The interest in doping ZnO arises from the possibility of tailoring its electrical, magnetic and optical properties for such applications [14-17]. The doping of transition metal elements into ZnO offers a feasible mean for fine tuning its optical behavior, particularly the band gap. Mn doped ZnO has currently attracted much attention for its potential use in the novel memory and optical devices, varistor in multicomponent systems, ferromagnetism and magneto-optical applications at room temperature [18-20]. However, severe suppression of the luminescence of $Zn_{1-x}Mn_xO$ even at very low doping levels is also reported [21]. Mn doping in ZnO is known to reduce its band gap for low concentration doping (< 3 mol% of Mn). For higher concentrations (> 3 mol%) the band gap increases as expected on the basis of virtual crystal approximation (VCA), as the band gap of MnO is ~ 4.2 eV [22]. There are only few reports on Mn incorporated ZnO nanostructures and nanostructured thin films and their optical and structural properties still need to be explored [23]. Besides, the behavior of Mn incorporated nanocrystalline ZnO in PEC splitting of water possibly remains unstudied so far. In our previous reports we presented the PEC splitting of water using Cr, Ni, Cu and Ru incorporated ZnO [15-17]. As thorough experimental anlysis of zinc oxide with each type of dopant is quite demanding, it can be quite effective to use first priciple based density functional theory calculations in short listing of dopants that have promise for enhaced photoelectrochemical property of ZnO. Such calculations[25-28] are quite useful in for determination of the trends in band gap upon doping of given material. The recent investigation with Mn incorporated ZnO has also shown that it is an even better choice for above application.

3.3 Methodology

All calculation were performed using VASP (Vienna ab- Intio simulation packages) implementation of DFT within the generalized gradient approximations (GGA). We have used projector augmented wave (PAW) approach to evalute all the properties.

We simulated the effects of Mn doping using 2x2x2 (32 atoms) ZnO supercell and replacing one Zn atom by MN atom, amounting 12.5% doping amount. Calculated crystal parameter of the unit bulk wurtzite ZnO are a = 3.28 A and c = 5.28 A, in a good agreement with experimental data. A Monkhorst-Pack mesh of 2x2x2 K points was used in sampling. The intregals over the brillouin zone, and a much finer mesh was used in accurate determination of the density of electronic states. Kohn Sham wave functions were represented in plane-wave basis with an energy cutoff of 520 eV, and the charge density was represented with a plane-wave basis with the cutoff energy of 460 eV. Structural optimization was carried out by using Hellman-Feyman Forces to minimize total energy. To check the convergence of our results, we carried our test calculation with higher energy cutoff on the plane-wave basis and finer mesh of K-points, making sure that there are negligible changes in energy and in the electronic structure. We have emplayed DFT with plane wave pseudopotential based approach using projector augmented wave (PAW) as implemented in VASP code. A kinetic energy cutoff of 520 eV was employed for primitive cell calculation, where as 460 eV cutoff was taken for full unit cell.

Calculations all geometry optimization were carried out without geometry constraint. All forces were calculated using Hellman-Feyman theorm. Geometries were considered and optimized with maximum force found smaller than 0.01 eV/A. Real space projection were used to evalute PAW character of wave functions. The primitive cell of ZnO was built from the crystal structure of ZnO that was take from experimental data and 2x2x2 K-Points grid generated by Monkhorst-Pack scheme was applied to it.

3.4 Results and Discussions

In order to identify the way Mn doping influences the electronic states of ZnO, the first-principle DFT computations were made to explore the band structures of doped and undoped ZnO (Fig. 8, Table 5). Since, DFT considers the electronic ground state, the band gap predictions from it are approximate. One needs to use hybrid functional or self interaction corrections in DFT to accurately estimate the absolute bandgap energies. While, valence band properties and offsets are described accurately well with DFT, the conduction band properties cannot be portrayed properly. The present set of computations was focused more towards the qualitative understanding on the way band gap energy of Mn doped ZnO.

a (Å)	c/a	Remark
3.2495	1.6024	Experimental [24]
3.28	1.61	GGA-PBE [this work]

Table 3.1 Lattice parameters of wurtzite ZnO.

As is clear from the Fig3.2 that top of the valence band and bottom of the conduction band is at G point of Brillouin zone, suggesting that doped and Undoped ZnO is a direct band gap material.

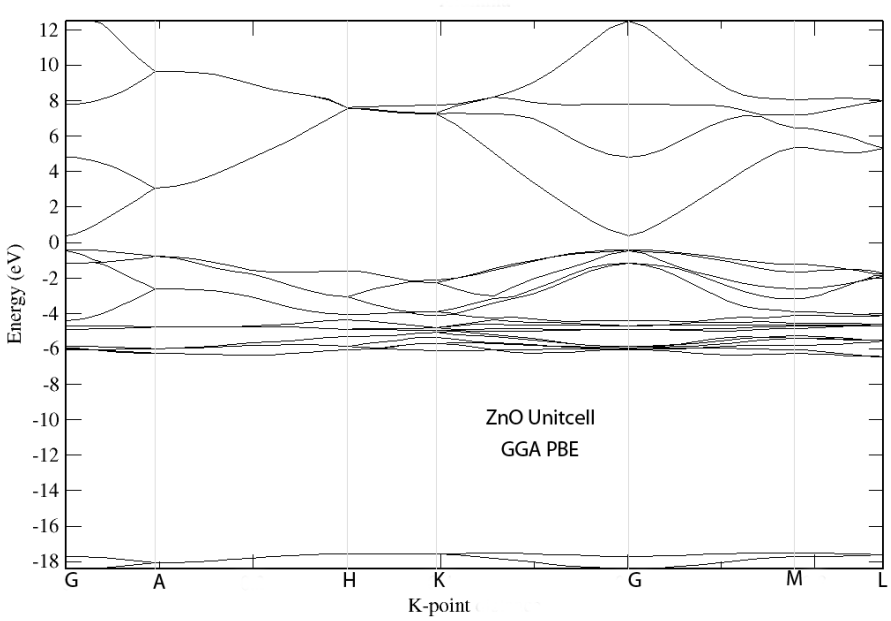

Figure 3.2. Bandstructure of ZnO unit cell at GGA PBE method.

Figure 3.2 illustrates the bandsture of ZnO unitcell, the peaks the conduction band are priarily formed by p orbital of Oxygen atoms. However the band near -18 e v is due the s orbital of oxygen. The conduction band is formed by the overlap of d orbitals of Zn and p orbitals of p orbitals of Oxygen. The calculated band gap at GGA PBE method was found to be 0.78eV. The calculated band is in agrement to the priviously reported values. However, the claculated band gap is significantly underestimted. It is well established that GGA method underestimates the band gap.

ZnO Density of States shows clear agement with band structure. The femi level is set to zero in all density of states and bandstructure calculations. Figure 3.3 showcase the projected density of states (PDOS) of ZnO unitcell. PDOS clearly supports the bandstructure with clearly identifying the contribution of different orbitals. PDOS confirms that the conduction band of ZnO is mainly formed by Zn(d) and O(p) orbitals.

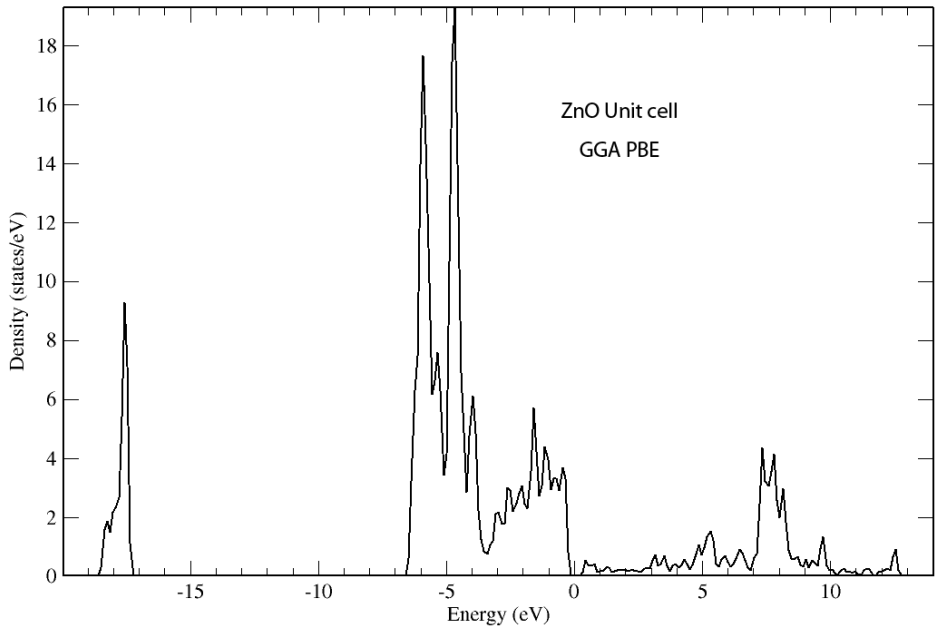

Figure 3.3 Total density of states of ZnO unit cell at GGA PBE level.

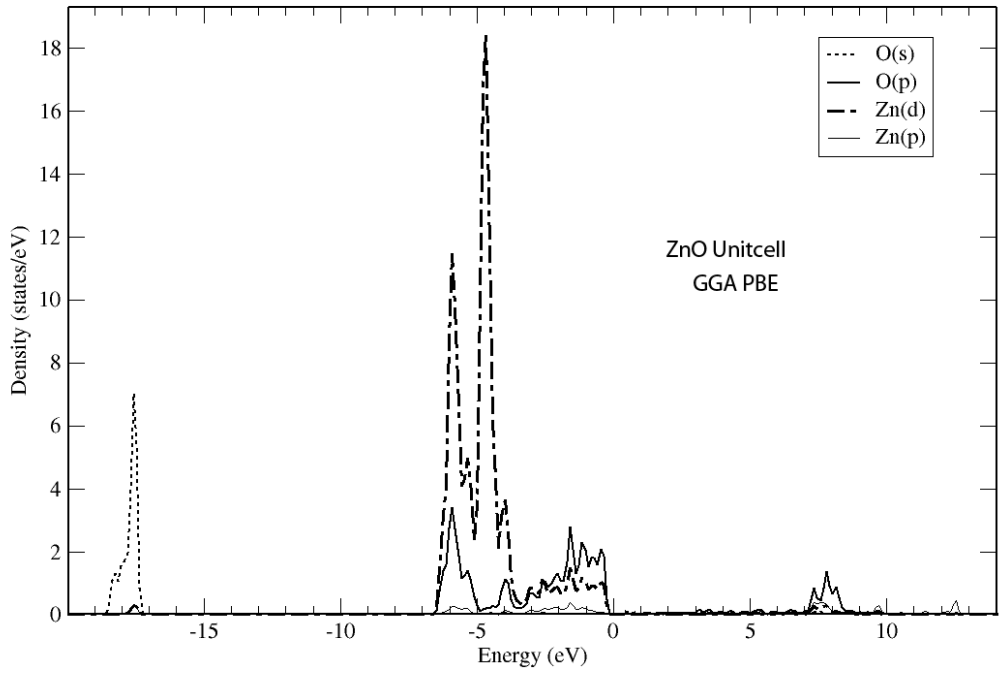

Figure 3.4 PDOS of ZnO unit cell at GGA PBE level.

The exchange and correlation functionals within DFT are based on various approximations. LDA is based on homogeneous electron gas approximation. Furthermore, the interactions are calculated based on mean field approximation. This approximation cannot calculate highly sensitive properties like band gaps.

Various attempts are made to deal with the problem in DFT. One effective approach is use many body formalism. Another widely used method is LDA (or GGA) + U method. The LDA+U method is used to take care strong electronic correlation by adding Hubbard-like Hamiltonian. Resulting energy depends on the site specific electronic occupancy. The band gaps calculated by LDA+U methods are improved when compared to experimental values.

Figure 3.5 illustrates the bandstructure of ZnO unitcell at GGA+U level, the band gap by GGA+U found to be 1.27 eV. This band gap is clearly improved when compared to without the introduction of U.

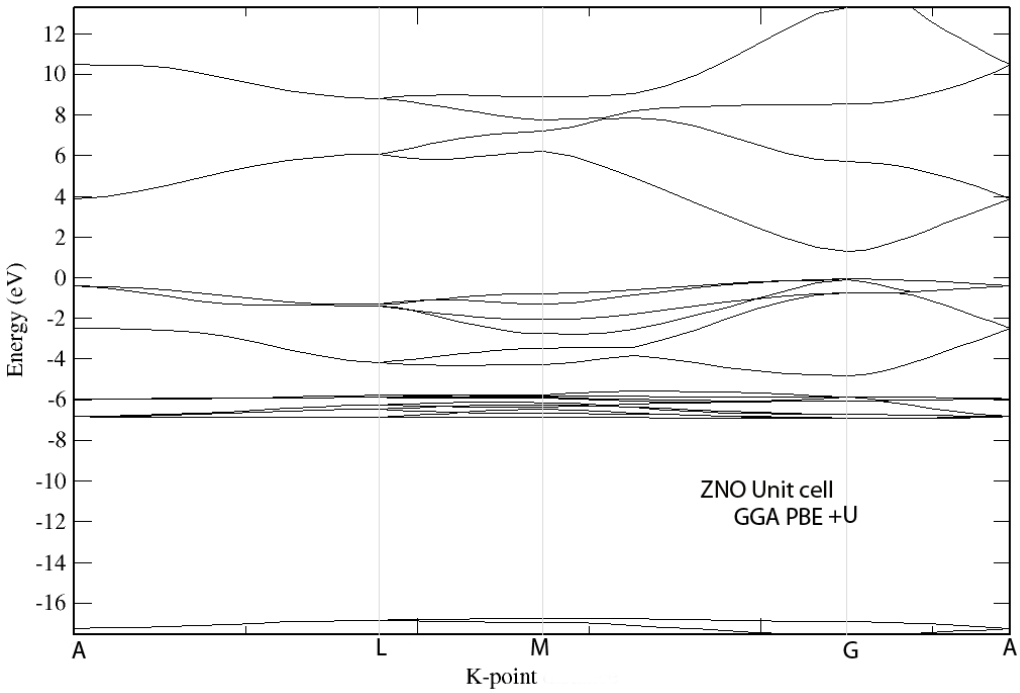

Figure 3.5 Band structure of ZnO unit cell at GGA+U PBE level.

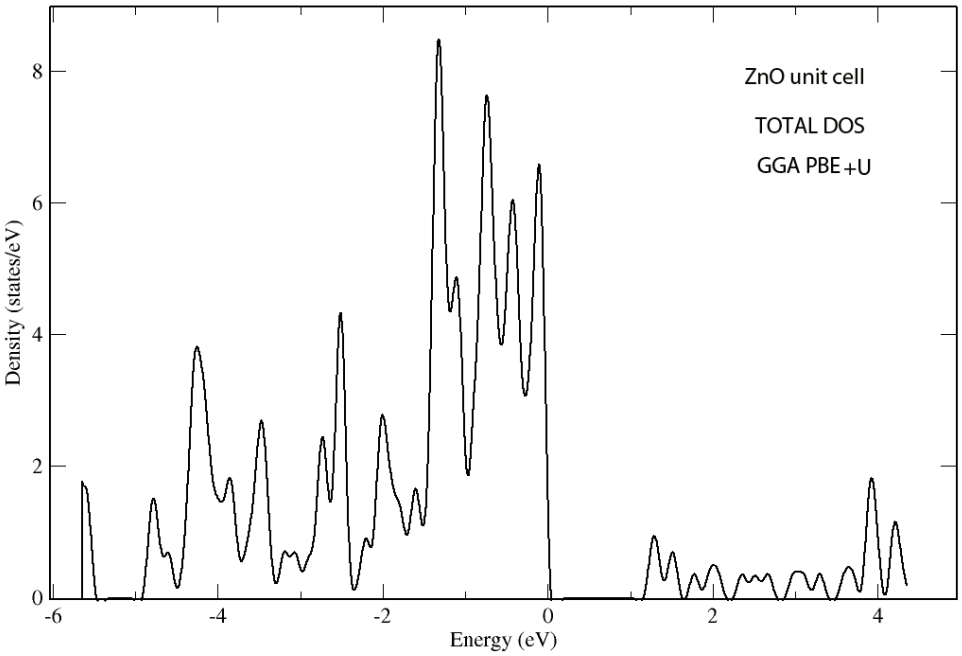

Figure 3.6 Total density of states of ZnO unit cell at GGA+U PBE level.

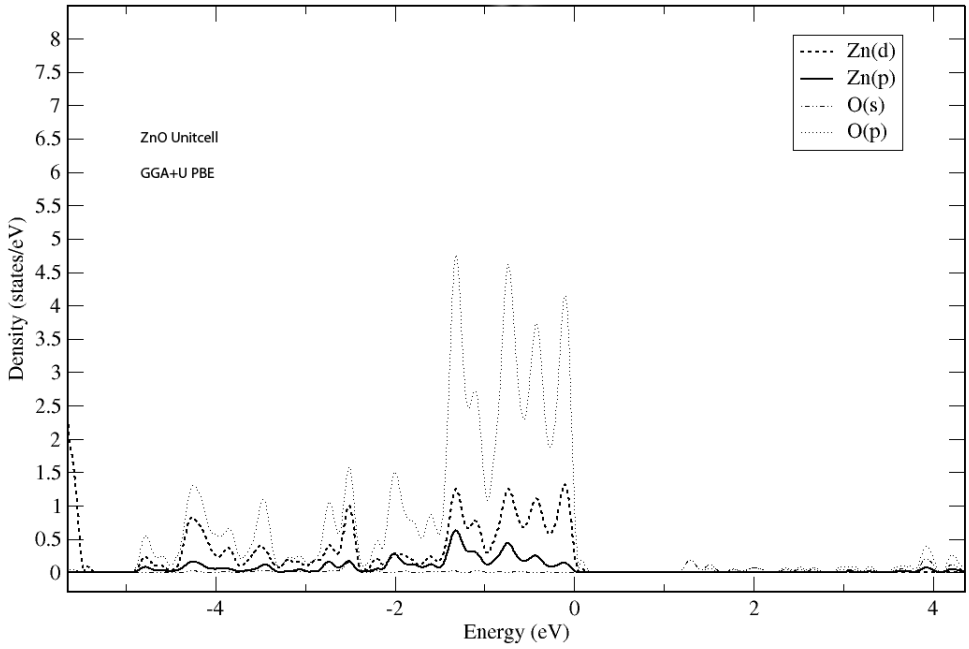

Figure 3.7 PDOS of ZnO unit cell at GGA+U PBE level.

The effect of U electronic structure can be exploed by comparing the PDOS of ZnO unit cell with and without inclusion of U. It is clear from figure 3.7 and figure 3.4 that inculsion of U shifts the Zn(d) peaks near fermi level.

The bandstructure of ZnO 2x2x2 is presented in figure 3.8. when compareing the band structure of unitcell and supper cell, the band of supercell are overlaped. Due to this opverlaing it becomes difficult to interpret the band structure of supper cells. This overlapping of bands aries due to the band folding.

However, the band gap does not change with the size of cell. Figure 3.9 shows the total DOS of ZnO 2x2x2 super cell. The projected DOS of ZnO supercell are similar to that of PDOS of unit cell.

Figure 3.10 shows the charge density slice of ZnO 2x2x2 super cell and Mn doped ZnO. From the charge density slice of Mn doped ZnO its clear that charge density on Mn atom is lower when compared to the charge density on Zn atom. Also, the charge density on oxygen atoms surrounding Mn atoms is higher when compared to oxygen atoms surrounding Zn atoms. Clearly, Mn doping significantly enhance the charge transfer.

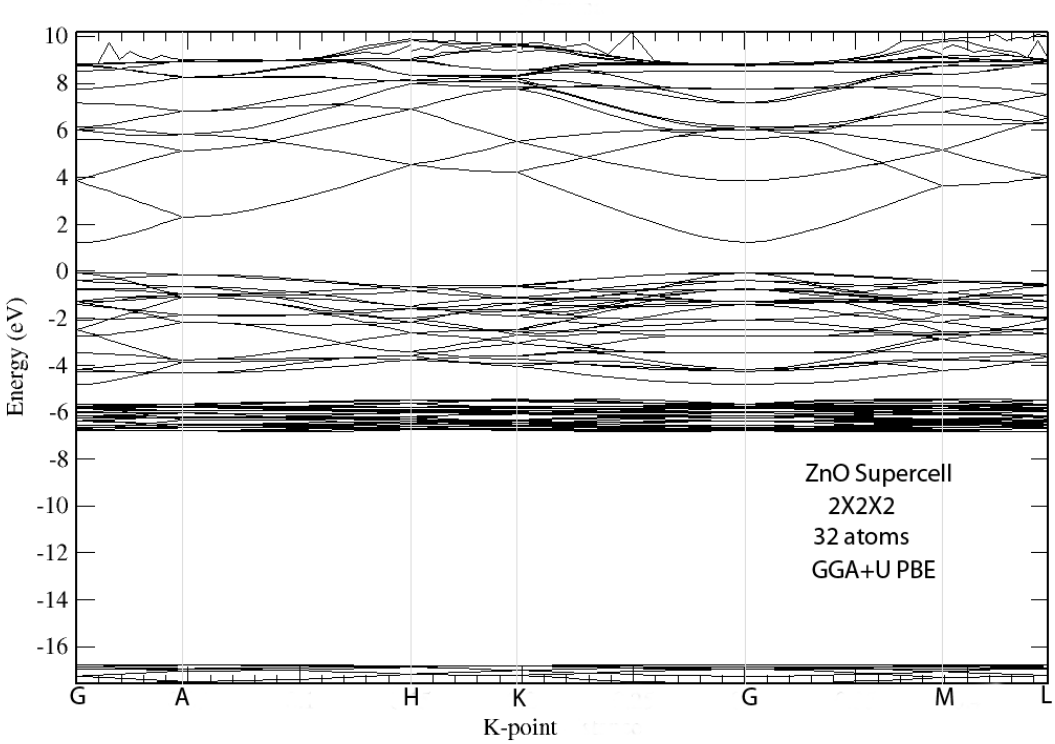

Figure 3.8 Bandstructure of ZnO 2x2x2 supercell GGA+U PBE level.

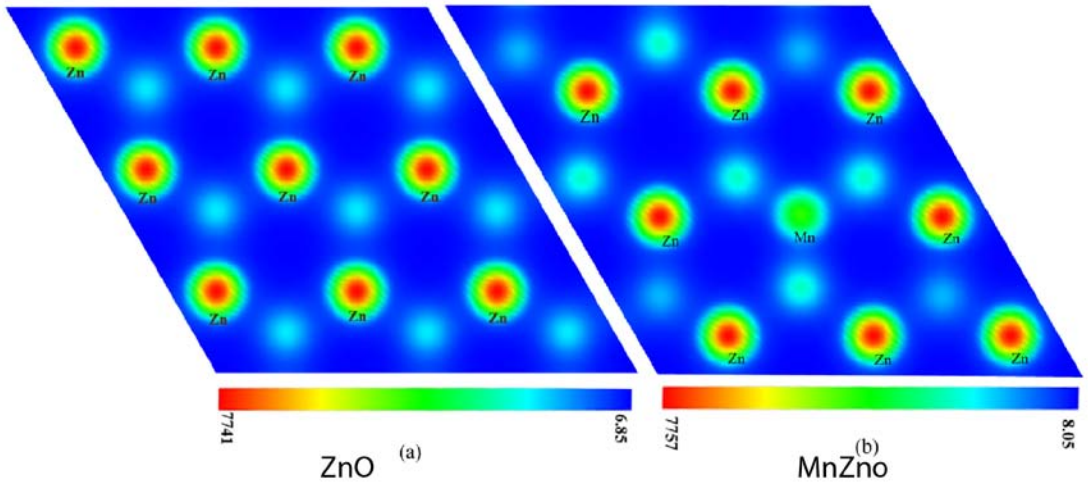

Fig. 3.9 Charge density slice of (a) 2x2x2 super cell (6) 2x2x2 Mn doped ZnO 6.25% Mn.

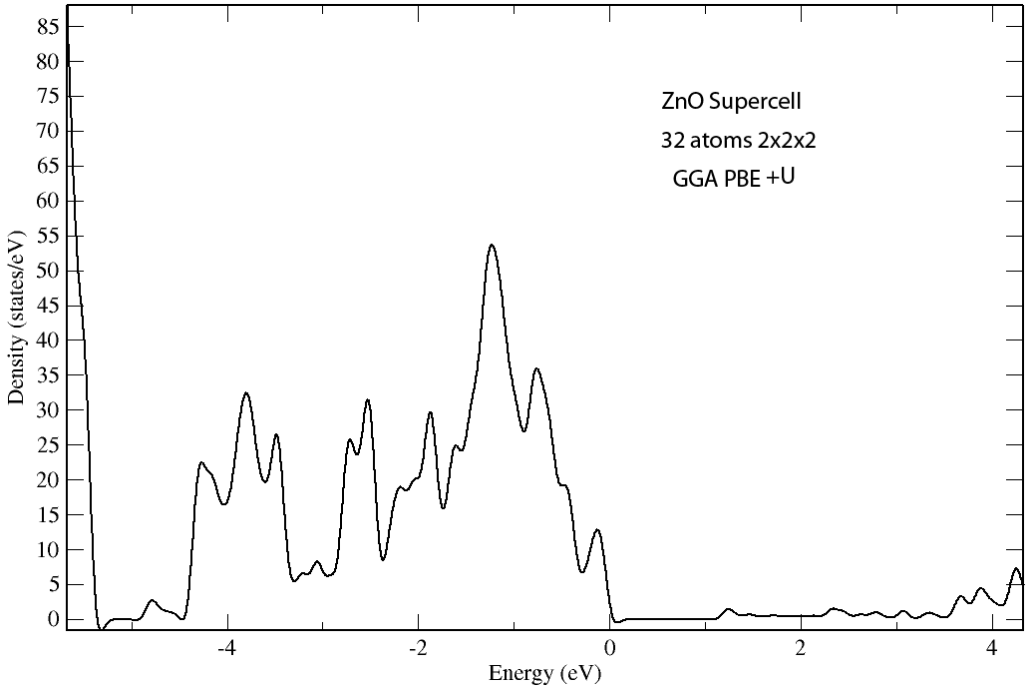

Figure 3.10 Total DOS of ZnO 2x2x2 supercell GGA+U PBE level.

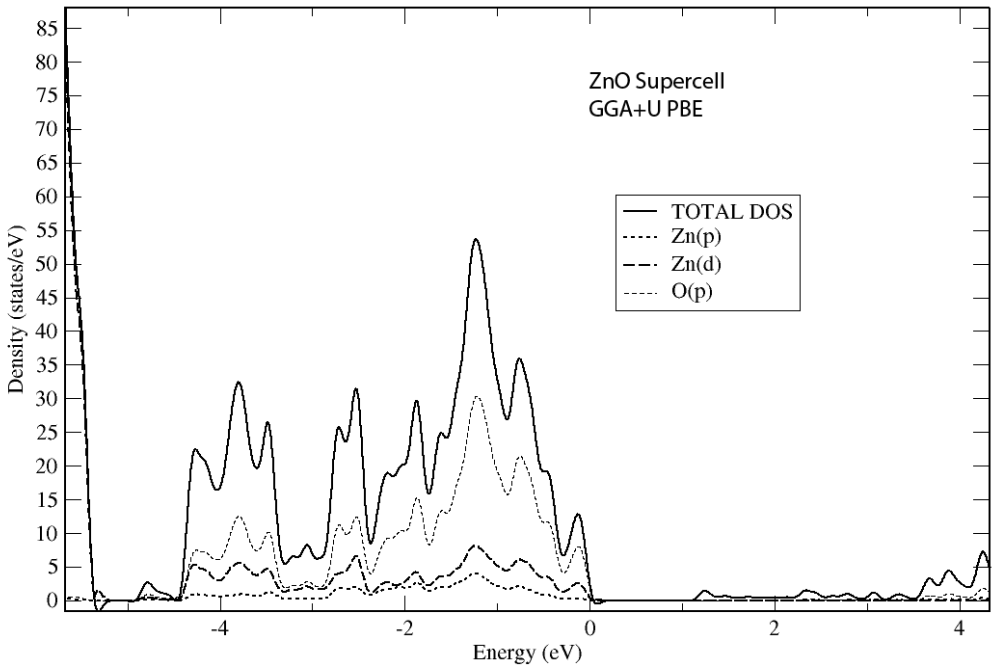

Figure 3.11 PDOS of ZnO 2x2x2 supercell GGA+U PBE level.

Form the above discussion it clear that Mn doping influences the charge transfer in ZnO. Motivated by the charge transfer we study the bandstructure and DOS of Mn doped ZnO, To reduce the ZnO band gap and make this material suitable for photoelectrochemical splitting of water for H_2 production. Produced H_2 can be stored by suitable storage material.

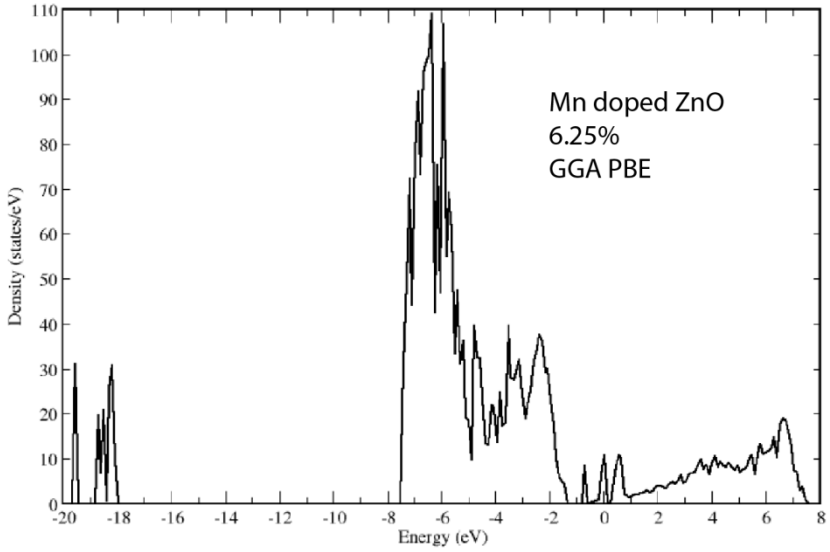

Figure 3.12 Total DOS of Mn doped ZnO by GGA PBE method.

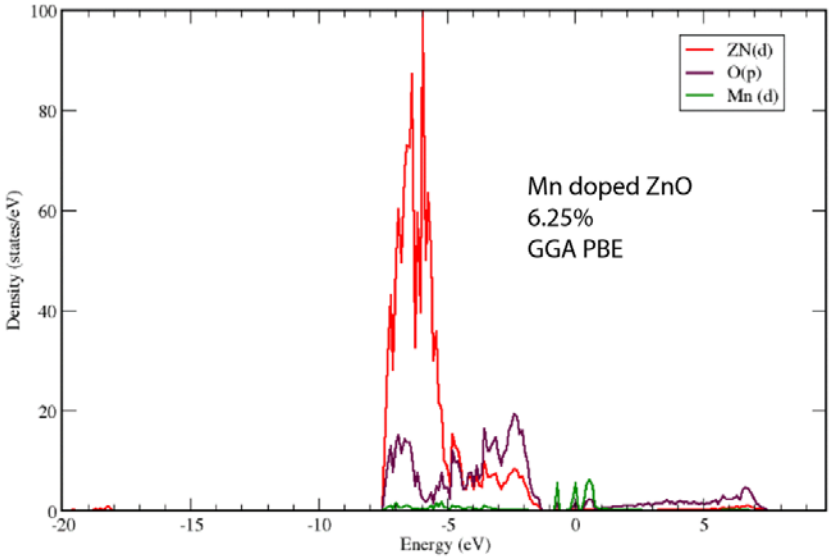

Figure 3.13 PDOS of Mn doped ZnO by GGA PBE

Conclusions:

We have discussed various tools to investigate the electronic structure of solid. We have investigated the lattice parameters, charge density, bandstructure and density states of ZnO unitcell, suppercell and Mn-doped ZnO supercell. Our results suggest that Mn doping at low concentrations can reduce the band gap of ZnO. Due to the reduced band gap and high charge transfer Mn-Doped ZnO can be used for electro photochemical splitting of water for hydrogen production. Interestingly, our experimental collaborators could synthesize this material at low Mn concentrations. They have found good photo electrochemical activity of this material for splitting of water.

References:

[1] R. Hoffmann, Solids and Surfaces - A chemist's view of bonding in extended structures, VCH Publishers, 1998

[2] S. Liang, J. He, Z. Sun, Q. Liu, Y. Jiang, H.Cheng, B. He, Z. Xie and S. Wei, *J. Phys. Chem. C* **2012**,116, 9049.

[3] X.Yang, A. Wolcott, G. Wang, A. Sobo, R.C. Fitzmorris, F. Qian, J. Z. Zhang, Y. Li, *Nano let*. **2009**, 9, 2331.

[4] J. H. Bang, P. V. Kamat, *ACS Nano*. **2010**, 5, 9421.

[5] K. Sivula, R. Zboril, F.L. Formal, R. Robert, A. Weidenkaff, Tucek, J. Frydrych, M. Gratzel, *J. Am. Chem. Soc.* **2010**, 132, 7436.

[6] N.A. Kelly, T.L. Gibson, *Int. J. Hydrogen Energ.* **2008**, 33, 6420.

[7] Z. Chen, T.F. Jaramillo, T.G. Deutsch, A. Kleiman-Shwarsctien, A.J. Forman, N. Gaillard, R. Garland, K. Takanabe, C. Heske, M. Sunkara, E.W. Mcfarland, K. Domen, E. L. Miller, J. A. Turner, H. N. Dinh, *J. Mater. Res.* **2010**,25,3.

[8] A. Fujishima, K. Honda, *Nature*. **1982**, 238, 37.

[9] Gerischer H, (1981), In: F. Cardon, W.P Gomes, W. Dekeyser, (Ed.), *Photovoltaic and photoelectrochemical solar energy conversion.* **1981,** 263, Plenum, New York,1981, p 199 .

[10] A. J. Nozik, Annual. *Rev. Phys. Chem*. **1978**, 29, 189.

[11] A Heller, *Acc. Chem. Res.* **1981**, 14, 154.

[12] M. Tonezzer, R.G. Lacerda, *Sensors and Actuators B: Chemical. **2010***, 150, 517.

[13] Y. Ding, Z.L. Wang, *Micron*. **2009,** 40, 335.

[14] U. Ozgur, Y.I Alivov, C. Liu, A. Teke, M.A. Reshchikov, S. Dogan, V. Avrutin, S.J. Cho, H.A. Morkoc, *J. Appl. Phys.* **2005,** 98, 041301.

[15] A.A. Tahir, K.G.U. Wijayantha, *J. Photochemistry and Photobiology A: Chemistry* **2010**,216, 119.

[16] V. Sharma, P. Kumar, N. Singh, S. Upadhyay, V.R. Satsangi, S. Dass, R. Shrivastav, *Int. J. Hydrogen Energ.* **2012**, 37, 2012, 12138.

[17] V. Sharma, P. Kumar, J. Shrivastava, A. Solanki, V.R. Satsangi, S. Dass, R. Shrivastav. *Int. J. Hydrogen Energy.* **2011**, 36, 4280.

[18] V. Sharma, P. Kumar, J. Shrivastava, A. Solanki, V.R. Satsangi, S. Dass, R. Shrivastav, *J. Mater. Sci.* **2011**, 46, 3792.

[19] R.R. Prabhakar, N. Matheus, K.B. Jinesh, K.B. Jinesh, K.R.G. Karthik, S.S. Pramana, B. Varghese, C.H. Sow, S. Mhaisalkar. *J. Mater. Chem*. **2012**, 22 , 9678.

[20] C Roining, P. X. Gao, Y. Ding, Z.L. Wang, D. Schwen, *Appl. Phys Lett*. 2004, 84, 783.

[21] Y.W. Hong, J.H. Kim, *Ceramics International*. **2004**, 30, 1301.

[22] M. Liu, A.H. Kitai, P. Mascher, J. Lumin. **1992,** 54, 35.

[23] B. S. Venkataprasad, F.L. Deepak, *Solid State Commun.***2005,**135, 345.

[24] L. W. Yang, X. L. Wu, G. S. Huang, T. Qiu, Y. M. Yang, J. Appl. Phys. **2005**, 97, 014308

[25] R. W. G. Wyckoff, Crystal Structures, Vol 1, 2nd Edition, Wiley, New York, **1986**, p. 112.

[26] K. Sato and H. Katayama-Yoshida. *Physica E*. **2001,** 10, 251.

[27] H. Schulz and K. H. Thiemann, *Solid State Commun.* **1979**, 32, 783.

[28] I. V. Maznichenko, A. Ernst, M. Bouhassoune, J. Henk, M. Däne, M. Lüders, P. Bruno, W. Hergert, I Mertig, Z. Szotek and W. M. Temmerman, *Phys. Rev. B* **2009,** 80, 144101.

[29] R. A. Powell, W. E. Spicer, and J. C. McMenamin. *Phys.Rev. Lett*. **1971,** 27, 97.

CHAPTER 4

Light Metal Decorated MOF-5

The effect of light metal (M =Li, Be, Mg, and Al) decoration on the stability of metal organic framework MOF-5 and its hydrogen adsorption is investigated by ab initio and periodic density functional theory (DFT) calculations by employing models of the form BDC:M_2:nH_2 and MOF-5:M_2:nH_2, where BDC stands for the benzenedicarboxylate organic linker and MOF-5 represents the primitive unit cell. The suitability of the periodic DFT method employing the GGA-PBE functional is tested against MP2/6-311+ G* and MP2/cc-pVTZ molecular calculations. A correlation between the charge transfer and interaction energies is revealed. The metal-MOF-5 interactions are analyzed using the frontier molecular orbital approach. Difference charge density plots show that H_2 molecules get polarized due to the charge generated on the metal atom adsorbed over the BDC linker, resulting in electrostatic guest-host interactions.

Our solid state results show that amongst the four metal atoms, Mg and Be decoration does not stabilize the MOF-5 to any significant extent. Li and Al decoration strengthened the H_2-MOF-5 interactions relative to the pure MOF-5 exhibited by the enhanced binding energies. The hydrogen binding energies for the Li- and Al-decorated MOF-5 were found to be sensible for allowing reversible hydrogen storage at ambient temperatures. A high hydrogen uptake of 4.3 wt.% and 3.9 wt.% is also predicted for the Li- and Al-decorated MOF-5, respectively.

4.1. Introduction

Depletion of fossil fuels as well as environmental concerns has led to a widespread research for finding new and renewable energy sources. Hydrogen (H_2), with its high chemical energy content (142 MJ/kg), that is at least three times larger than that of other chemical fuels (for example, the equivalent value for liquid hydrocarbons is 47 MJ/kg), abundance and non-polluting nature has generated tremendous interest [1]. Hydrogen economy offers an alternative to our dependence on fossil fuels and provides an environmentally clean source of energy. However, the application of hydrogen economy for practical applications requires efficient H_2 storage with high gravimetric and volumetric density. In comparison to storage of H_2 in a high-pressure tank and cryogenic liquefaction of hydrogen, hydrogen adsorption in solid materials is much safer [2]. A number of research efforts have been made to find new storage materials which are capable of exhibiting reversible H_2 storage at high densities, reasonably fast adsorption/ desorption kinetics and long life time [3]. However, till date no material has been found to have all the above stated properties. Solid state hydrogen adsorption is currently pursued by two main strategies: strong chemical associations (chemisorption) and weak dispersive interactions (physisorption). As an example, the chemisorption approach applies to the class of simple and complex metal hydrides. Although these materials show high H_2 storage, they suffer from large dehydrogenation activation barriers. Using periodic density functional theory (DFT) calculations, Kelkar et al. [4] have shown that doping different phases of MgH_2 with Al and Si can result in a lowering of its activation energy barriers associated with the direct desorption of H_2 from its (001) surface. With regard to physisorption of H_2, materials with large surface areas and low densities, such as metal organic frameworks (MOFs), are attractive. MOFs are crystalline hybrid organic/inorganic nanoporous materials which can adsorb guest molecules, and thus are potential candidates for H_2 storage [5]. There are predominantly Van der Waals interactions between the hydrogen molecules and the MOFs. Due to these weak forces, the adsorption energies of H_2 are normally as low as ~2.26-5.2 kJ/mol [6-8]. As a result, MOFs showcase rapid adsorption and desorption kinetics. The drawback is that significant hydrogen adsorption is achieved only at low temperatures. A study by Lochan

and Head-Gordon [9] has shown at, room temperature, that desired H_2 binding energy should be in the range of 28-40 kJ/mol. Thus, clearly there is a significant need to enhance the H_2 binding energy ($E_{binding}$) as well as increase H_2 adsorption and storage capacity of MOFs in order to render them useful for practical and mobile applications. The various approaches to improve hydrogen adsorption in MOFs include the optimization of pore size [10], adding another guest molecule in the pore of crystal [11] and catenation [10]. Li et al. [12] have recently exploited the idea of optimization of the pore size. To enhance the $E_{binding}$, introduction of electron donating groups and inclusion of open metals sites [13] have been attempted.

It is necessary to develop an understanding of the fundamental interactions involved in hydrogen adsorption in order to be able to tune H_2 storage in MOFs. Ab inito and DFT studies on the molecular linker have been successful to identify the hydrogen binding sites. The first theoretical study on MOF-5 was carried out by Hubner et al. [14] by investigating simplistic model systems. Their calculations carried out by the second-order Møller-Plesset (MP2) method revealed that the $E_{binding}$ increased with increase in ring size. In a similar work Sagara et al.[15] studied both the organic linker part and zinc oxide part of MOF-5 using MP2 method. They concluded that H_2 preferably binds between two zinc clusters. In another study [16] it is shown that the H_2 top site is favorable when compared to the edge site of BDC linker in MOF-5. In a series of landmark papers from 2007 to 2009, Han et al. [17-19] shown that the force fields based on accurate quantum chemical calculations like CCSD(T) calculations cab be used for GCMC simulations to determine the H_2 loading. They demonstrated that this very accurately reproduces the experimental loading curve for MOF-5 and other MOF and COF systems. Mulder et al. [20] and Mueller and Ceder [21] carried out a full periodic DFT study of MOF-5 and found five symmetrically unique adsorption sites, their results indicated that the sites with the strongest interaction with hydrogen are located near the Zn_4O clusters.

The recent advances in studying MOFs and covalent organic frameworks (COFs) using quantum calculations, Monte-Carlo (MC) simulations and molecular dynamics simulations have been critically reviewed in Ref. [22]. The authors have also discussed the different strategies being pursued for improving hydrogen storage in these materials.

One such particularly interesting method involves decoration of the organic linker part of the MOFs with a metal. Previously, various authors have studied the interaction of H_2 molecules with transition metal ions [23-26]. In an important study [27] authors have shown that transition metals, and their ions bind with upto six H_2 molecules. Consequently, it was shown that s-block metal cations cab bind with eight H_2 molecules with high binding energies [29]. These reports suggest that metals can enhance the H_2 binding energies. Nevertheless, synthesizing such bare metal cations is difficult. To overcome this problem metals can be adsorb on the materials with high electron affinity so that atoms can acquire desired charge via charge transfer. Recently, nanomaterials like nanotubes [30], nanofibers [31] and nanospheres [32] are used to adsorb metal atoms, adsorbed metals acquire the desired charge, resulting a significant enhancement in the H_2 binding energies.

Transition metal decorated systems materials show very high binding energy [33-37]. However, transition metals show a tendency to bind with each other. This decreases the H_2 storage capacity [38-45]. A possible solution of this problem is to use elements with low cohesive energy, like s-block metals.

The light metal decoration approach has been investigated theoretically on several systems [33,35,46-57].

The interaction of MOF-5 with H_2 are primarily due to the dispersive interactions and weak electrostatic forces associated with metal oxide clusters ($O_{13}Zn_4$). Kuc et al. [58,59] have shown that the physisorption of H_2 in MOFs is due to LDI between linkers and connectors with hydrogen. However, electrostatic interactions were unimportant due to low charge separation in the MOF, this low charge separation is not sufficient to induce dipole moments in H_2. They have also shown that correlation methods and large basis sets are necessary to correctly include LDI in these systems. Clearly, DFT is unable correctly describe LDI. But ab initio methods are not practical for application to the full structure. Motivated by the above facts, herein we have studied metal (M)-decorated MOF-5, where M= Li, Be, Mg and Al, using both periodic DFT based calculations employing the PBE functional and molecular quantum chemical computations with MP2 methods to test the accuracy of the former for predicting the structures and H_2 binding energies of the metal-decorate MOF-5s. Further, we have analyzed which light metal

atom will be the best for increasing the strength of H_2 adsorption and amount of H_2 storage in MOF-5 for making it suitable forambient H_2 storage applications. To this end we have examined the optimized geometries, atomic charges, interaction energy of the metal atoms with MOF-5 and the hydrogen binding energies.

4.2. Computational methodology

It has been reported by Mueller and Ceder [17] that studies on a truncated part of MOF like BDC linker alone can yield misleading results. In order to investigate this effect, in this work we have performed calculations on two sets of systems: (i) the full primitive cell of MOF-5 and (ii) the molecular benzenedicarboxylate (BDC) linker. In the paper the pure and metal decorated MOF-5 unit cells are referred to as MOF-5 and MOF-5:M_2, respectively and the corresponding molecular counterparts are referred as BDC and BDC:M_2, respectively, where M=Li, Be, Mg, and Al. The interaction energy (ΔE) of the metal atom M with MOF-5 is calculated as follows:

$$\Delta E(MOF-5:M)=\frac{1}{2}[E_{Tot}(MOF-5:M_2)-2*E_{Tot}(M)-E_{Tot}(MOF-5)] \qquad (4.2.1)$$

Different numbers of H_2 molecules were allowed to interact with Li-decorated BDC and M-decorated MOF-5. These are represented as BDC:Li_2:nH_2 and MOF-5:M_2:nH_2, respectively, where n is the number of H_2 molecules adsorbed. The corresponding H_2 binding energies per H_2 are calculated by the equations:

$$E_{binding}(MOF-5:M_2:H_2)=\frac{1}{n}[E_{Tot}(MOF-5:M_2:nH_2)-2*E_{Tot}(MOF-5:M_2)-nE_{Tot}(H_2)] \qquad (4.2.2)$$

$$E_{binding}(BDC:M_2:H_2)=\frac{1}{n}[E_{Tot}(BDC:M_2:nH_2)-2*E_{Tot}(BDC:M_2)-nE_{Tot}(H_2)] \qquad (4.2.3)$$

Density functional theory (DFT) [60] is capable of scaling well with system size. It, however, unfortunately fails to calculate magnitude of weak interactions accurately because these interactions depend strongly on electron correlation. Within the local density approximation (LDA) these weak interactions get overestimated [61-64]. In comparison the generalized gradient approximation within the Perdew, Bruke and Ernzerhof (PBE) [65] exchange correlation functional is known to give reasonably accurate results [61,63]. However, it is still important to test the reliability of using DFT for the systems under study. For this purpose we have implemented three computational methods : gas-phase and periodic DFT calculations with the PBE functional using a plane wavepseudopotential approach and molecular calculations with MP2 and other DFT functionals and 6-311+G* and cc-pVTZ basis-sets.All the DFT planewave-pseudopotential based calculations have been performed using the Vienna ab initio simulations package (VASP) [66,67]. We have used the projector augmented wave (PAW) [68,69] approach to evaluate all the properties. An energy cut-off of 520 meV was employed throughout our periodic DFT calculations. All geometry optimizations were carried out without any geometry constraint. All forces were calculated using Hellmann-Feynman theorem. Geometries considered optimized with maximum force found smaller than 0.01 eV/Å. Real space projections were used to evaluate PAW character of wavefunctions. The valence states for all the potentials used here are 4s and 3d for Zn, 2s and 2p for both O and C and 1s for H. The primitive cell of MOF-5 was built from the crystal structure of MOF-5 that was taken from experimental data [70] and a 2 X 2 X 2 k-point grid generated by MonkhorstePack scheme [71] was applied to it. For the gas phase calculations of pure and decorated BDCs using VASP a large cell size of 20 X 20 X 20 was chosen to avoid interaction between successive BDC molecules. These calculations were carried out at gamma-point. For obtaining the atomic charges Bader analysis [72] was performed. Our quantum chemical calculations with MP2 and other DFT functionals with the 6-311þ G* and cc-pvtz basis sets were carried out with the Gaussian 09 package [73]. For all super-molecules basis set superposition error (BSSE) correction was evaluated by the counterpoise method [74]. The atomic charges were derived by the CHELPG ESP method [75]. All our calculations are 0 K calculations and do not include zero-point energy contribution.

4.3 Results and discussion
4.3.1 Structure

Herein we begin with a comparison of the structures of BDC and BDC:M_2 (M = Li, Al, Be and Mg) systems optimized from MP2/6-311 + G* and GGA-PBE/plane wave methods. The MP2 optimized geometry of the model BDC linker is displayed in Fig. 4.1. Selected bond distances of the bare and metal decorated organic linker calculated from the two methods are presented in Table 1. It can be seen that in all cases there is a reasonable agreement between the structural parameters obtained from the two methods. These results suggest that using the PBE exchange correlation functional is reliable for structural investigations of this class of molecules. The effect of adsorption of metal on BDC can be understood by comparing the corresponding bond distances in Table 1.

Clearly, except for C_2-C_3 bond distances predicted by MP2 method for BDC:Li_2 and BDC:Al_2, there is a marked increase in all other C-C bond lengths in the different systems obtained from both the GGA-PBE and MP2 methods. Overall the C-C elongation is most pronounced in case of BDC:Be_2. The distance of metal atom from center of mass of BDC (BDC_{com}) is also listed in Table 1 and it exhibits the order: BDC:Be_2 < BDC:Li_2 < BDC:Mg_2 < BDC:Al_2. To determine the effect of going from a gas phase to a solid-state calculation on the structural parameters of MOF- 5 we performed periodic DFT calculations with the PBE-GGA functional on the full primitive unit cell of MOF-5 consisting of 106 atoms. The optimized structure thus obtained is shown in Fig. 4.2. Table 2 lists the selected structural parameters calculated from this work, a previous theoretical study [21] and experiment [5]. It also presents the ratio of our calculated values with respect to the experimental results for each structural parameter of MOF-5. Our results show strong agreement with both theory and experiment. The latter is depicted by the high average ratio of 0.995. In the table we have also given the average C-C bond lengths in the BDC linker obtained from our GGA-PBE/plane wave and MP2/6- 311 + G* calculations. A comparison with the experimental data shows that these values do not show as good an agreement. This tells us that for an

accurate study of the structures of MOF-5 the primitive unit cell GGA-PBE computations are most suited.

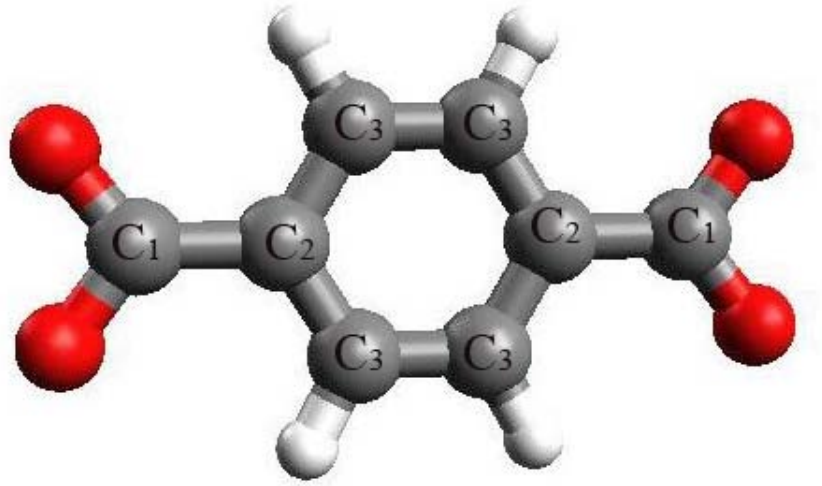

Figure 4.1 MP2 optimized geometry of the BDC linker and the schematic numbering of the C atoms.

System	Method	C_1-C_2	C_2-C_3	C_3-C_3	M-BDC$_{COM}$
BDC	MP2	1.505	1.419	1.396	
	GGA-PBE	1.478	1.402	1.395	
BDC:Li_2	MP2	1.583	1.413	1.411	1.814
	GGA-PBE	1.571	1.418	1.415	1.777
BDC:Be_2	MP2	1.619	1.426	1.425	1.584
	GGA-PBE	1.576	1.428	1.440	1.584
BDC:Mg_2	MP2	1.581	1.420	1.418	2.209
	GGA-PBE	1.558	1.425	1.414	2.241
BDC:Al_2	MP2	1.578	1.418	1.414	2.325
	GGA-PBE	1.570	1.418	1.416	2.295

Table 4.1. Selected bond distances in pure and metal-decorated BDC linker calculated by MP2/6-311G* and GGA-PBE/plane wave methods. All bond distances are in A and charges in atomic units.(See Fig. 4.1 for labeling of C atoms)

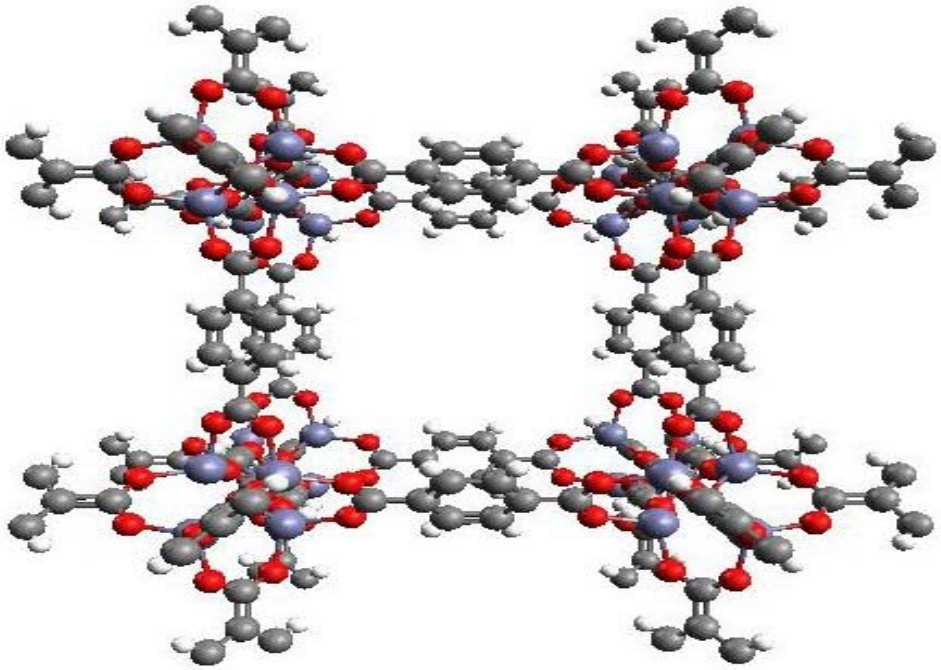

Figure 4.2 The full unit cell of MOF-5 optimized from GGA-PBE calculations within the Plane wave-pseudopotentials approach. The gray, red, purple and white colored balls represent carbon, oxygen, zinc and hydrogen atoms respectively.

As a next step light metals were decorated on the top of the benzene ring (on both its sides) of MOF-5. Following metal decoration different numbers of H_2 molecules were allowed to interact with MOF- 5. Selected structural parameters of MOF-5:M_2, MOF-5:Li_2:nH_2 and MOF-5:Al_2:nH_2 are listed in Table 3. The labeling of C atoms in the organic linker part of MOF-5 is the same as shown for BDC in Fig.4.1 . The table shows that the C-C bond lengths seem to remain unaffected in case of Mg. But in all other MOF-5:M_2 systems, there is an elongation of C_2-C_3 bond and a contraction of the C_1-C_2 and C_3-C_3 bonds relative to the pure MOF-5. A look at the distances of the metal atoms to the COM of the BDC in the decorated MOF-5s reveals that Mg is more than twice the distance away from the BDC than the other atoms. The large values of Mg-BDC_{com} (3.754A°) suggest that there is little interaction between Mg and MOF-5.

It is further evident from Table 4.3 that addition of H_2 molecules does not change the MOF-5 structure much. However, as number of H_2 molecules increases the M-BDC_{com} distance and the highest H_2-M distance also increase along with a slight decrease in H-H bond length in the adsorbed H_2 molecules suggesting a weakening of interactions

with MOF-5. Though the M-BDC_{com} distances in MOF-5:Li_2:nH_2 and MOF-5:Al_2:nH_2 for the same n are similar, the H_2 molecules are further away from Al than Li implying a relatively weaker interaction with Al. On this basis we expect the Al-decorated MOF-5 to exhibit a lesser H_2 binding energy than Li-decorated MOF-5.

Comparing Table 4.3.3 to the values for BDC:M_2 computed using the MP2/6-311 + G* method presented in Table 1, it can be seen that the C-C bond lengths show a wide variation. For all M the C_1-C_2 and C_3-C_3 bonds in MOF-5:M_2 are shorter and the C_2-C_3 bonds relatively longer than predicted for the BDC:M_2 molecular systems. The magnitudes M-BDC_{COM} also differ for the solid state and gas phase systems. The MBDC_{COM} order in MOF-5:M2 is Be < Al ≈ Li < Mg as opposed to Be < Li < Mg < Al in BDC:M_2. As shown by Mueller and Ceder [21], our results also indicate that limiting studies to simply BDC:M2 may not yield accurate structural results and that it is more appropriate to examine the metal decorated MOF-5s using primitive unit cells.

Method	**Lattice constant**	**Zn-Zn**	**C-C(average)**	**O-C-O**
	(Å)	**(Å)**	**(Å)**	**(deg)**
Calculated	26.139	3.202	1.399	126.2
(our work)			(1.425)	
			{1.440}	
Calculated [17]	26.137	3.220	1.400	126.1
Experiment [69]	25.911	3.181	1.396	125.8
Ratio	0.991	0.993	0.998	0.997
(our calculated: experiment)				

Table 4.2. Selected structural parameters of the primitive unit cell of MOF-5 calculated in this work by the GGA-PBE/plane wave method, in a previous theoretical study [17] and obtained from experiment [71]. The ratio of our theoretical values with respect to the experimental results for each parameter is also listed. The values in ( ) and { } are the average C-C bond distances in the BDC linker obtained from GGA-PBE and MP2/6-311+G* methods, respectively.

4.3.2. Charge transfer and interaction energy variation

It is understood that metal atoms, when adsorbed over a surface with high electron affinity such as benzene, will donate their valence electrons to it thereby resulting in a charge generation. The H_2 molecules then bind to these metal cations in the decorated MOFs. The extent of electron density transfer depends up on the ionization potential (IP). IP increases across a row and decreases down a column in the periodic table, so that amongst the metal atoms investigated herein Li has the least value (5.4 eV) followed by Al (6.0 eV), then Mg (7.6 eV) and Be has the highest IP (9.3 eV). The atomic charges on each metal atom [Q(M)] in MOF-5:M_2 and BDC:M2 systems calculated from GGA-PBE/planewave method and MP2/6-311+G* method, respectively are presented in Table 4. Based on the IP values, the expected Q(M) order is Li > Al > Mg > Be while the exhibited order is Li > Al > Be > Mg in MOF-5:M_2 and Li > Mg > Al >Be in BDC:M_2. Recalling the discussion in Section 3.1, adsorption of Mg on MOF-5 had little effect on its structural parameters. The Mg-BDCcom distance in MOF-5:Mg_2 was w70% larger than in BDC:Mg_2. Clearly, periodic GGA-PBE calculations predict a nonionic interaction between Mg and MOF-5 and so a direct comparison of charge transfer in the two systems would be incorrect. Removing Mg from the above series both calculation methods yield the same order of Q(M). Baker and Head-Gordon [76] have studied the interaction of Li with other polycyclic aromatic hydrocarbons with various electronic structure methods and observed an artificial electron transfer in some cases when using DFT due to the self-interaction error. They found that for the ionic system $Li^+(C_6H_6)^-$ the B3LYP and BLYP density functionals produced partial charge transfer of only 0.69 and 0.46 respectively for as opposed to 0.88 with the CCSD method However, in our analysis the atomic charge for Li in MOF-5:Li_2 derived from MP2 and GGA-PBE methods illustrated good agreement. For the other metals Table 4 shows that compared to MP_2, DFT overestimates the charge transfer in MOF-5:Be_2 and MOF-5:Al_2 by nearly 50% and underestimates by the same percentage for MOF-5:Mg_2.

System	C_1-C_2	C_2-C_3	C_3-C_3	M-BDC$_{COM}$
MOF-5	1.499	1.404	1.391	
MOF-5:Li_2	1.428	1.475	1.379	1.674
MOF-5:Be_2	1.441	1.480	1.381	1.430
MOF-5:Mg_2	1.498	1.403	1.389	3.754
MOF-5:Al_2	1.438 1.453 (1.446)	1.426 1.497 (1.462)	1.379	1.651
MOF-5:Li_2:2H_2	1.428	1.473	1.380	1.940
MOF-5:Li_2:4H_2	1.425	1.469	1.380	2.145
MOF-5:Li_2:6H_2	1.424	1.471	1.377	2.215
MOF-5:Al_2:2H_2	1.433 1.478	1.476 1.435	1.379	1.932
MOF-5:Al_2:4H_2	1.434 1.475	1.475 1.434	1.378	2.085
MOF-5:Al_2:6H_2	1.452 1.478	1.456 1.460	1.383	2.252

Table 4.3. Optimized structural parameters of MOF-5:M_2 (all M) and MOF-5:M_2:nH_2 (M = Li, Al) primitive unit cells obtained using the GGA-PBE/plane wave method. The labeling of C atoms is the same as in Fig. 4.1. The values in ( ) are the average bond distances. All bond distances are in Å.

Furthermore, Bader charges have previously been shown to be substantially in error in a study of charge quadrupole interactions for H_2 adsorption and diffusion in CuBTC [77]. Thus, whether the interaction energies between the metal atoms and MOF-5 conform to the amount of charge transfer predicted needs to be explored. The interaction energies (ΔE(MOF-5:M)) between the metal atom and MOF-5 in MOF-5:M_2 calculated using Eq. (1) are also presented in Table 4.4. The calculated values of MOF-5:Be_2 and MOF-5:Mg_2 are much smaller in magnitude than those of MOF-5:Li2 and MOF-5:Al_2. The ΔEs of MOF-5:Mg_2, MOF-5:Li_2 and MOF-5:Al_2 are in accordance to the GGA-PBE/plane-wave calculated atomic charges, while ΔE of MOF-5:Be_2 can only be a result of low charge transfer as predicted by MP2/6-311+G* for BDC:Be_2. This discussion suggests that except for Be decorated MOF-5, the GGA-PBE functional within the planewave-pseudopotential approach can be applied to accurately model the charge transfer between the metal atoms Li, Mg and Al and MOF-5. A negative ΔE implies that the interaction between the metal atom and MOF-5 is exothermic and that the decoration

stabilizes the MOF-5. A positive value tells that interaction is endothermic and that metal decoration destabilizes the system. All the ΔEs in Table 4 are negative but those of MOF-5:Be_2 and MOF-5:Mg_2 are nearly close to zero while MOF-5:Li_2 and MOF-5:Al_2 are considerably larger. Therefore, at room temperature Be and Mg may not remain adsorbed to MOF-5. These results suggest that out of the four metals investigated herein only Li and Al will stabilize MOF-5 to a significant extent and hence, H_2 interactions are investigated only in the Li- and Al-decorated systems.

Metal	Q(M) (a.u.) MP2	Q(M) (a.u.) GGA-PBE	ΔE (kJ/mol) GGA-PBE
	BDC:M_2	MOF5:M_2	MOF5:M_2
Li	0.84	0.90	-151.48
Be	0.18	0.45	-4.72
Mg	0.59	0.26	-1.35
Al	0.38	0.66	-128.32

Table 4.4. Calculated atomic charge of metal atom M in BDC:M_2 (MP2/6-311G* method) and in MOF-5:M_2 systems (GGA-PBE/plane wave method) and calculated and interaction energies (ΔE) in MOF-5:M_2 systems.

4.3.3 Nature of metal-MOF-5 and metal-H_2 interactions

In this section we first correlate the nature of interactions between the metal atoms and MOF-5 to the observed structural parameters and interaction energies. It is understood that the effective strength of the metal-MOF-5 interaction will be a net result of the competing attractive metal-pi-arene type interaction (due to the charge generated on the metal) and the mutual repulsion between the total electron densities of the metal atoms and benzene rings of MOF-5. To gain insight into the attractive interactions we have used the Frontier Molecular Orbital approach. It is known that the highest occupied

molecular orbital (HOMO) and the lowest unoccupied molecular orbital (LUMO) are the best global descriptors of reactivity [78,79]. In Fig. 4.4(a)-(e) we have illustrated the HOMOs of the four metal atoms and the LUMO of pure MOF-5. The HOMOs of the resulting metal decorated MOF-5s are displayed in Fig. 4.5(a)-(d). It can be seen that the HOMO of Li, Be and Mg is s type and of Al is p type. In MOF-5 the doubly degenerate unoccupied p-type orbital of benzene splits into two components because of the two carboxylic groups attached to it. The orbital component with a large density on the two ipso carbon atoms interacts constructively with the p* orbitals of the carboxylic groups, forming the MOF-5 LUMO (Fig. 4.4(e)) which is not completely delocalized over the benzene ring due to nodal planes. When the metal atoms are adsorbed over the BDC linker the HOMO of the metal atoms will interact with the LUMO of MOF-5. The HOMOs of the resulting metal-decorated MOF-5s are shown in Fig. 4.5(a)-(d). It can be seen that in case of MOF-5:Be_2 and MOF-5:Mg_2 HOMO the electron density is localized around the metal atoms displaying that they have little interaction with MOF-5. So at room temperature these metal atoms may get desorbed from the metal-organic framework. In comparison the Li- and Al-decorated MOF-5 HOMO are of the p type, delocalized around the benzene rings, similar to the LUMO of MOF-5 illustrating a transfer of electron density from the metal to the organic linker. Further, as there is no directional electron density between the metal and BDC, it can be inferred that the metal-MOF-5 interaction is ionic in nature and of the form $M^{\delta+}(BDC)^{\delta-}$ where $\delta+$ is the charge generated on the metal due to electron transfer. The greater cloud distribution around the carbon atoms in the Li decorated MOF-5 than in the Al-decorated MOF-5 is indicative of a greater electron transfer and hence, a stronger interaction of MOF-5 with Li than with Al. Based on the above discussion, the strength of the metal-parene attraction in MOF-5:M_2 systems decreases as follows: Li > Al >>Be > Mg. As the electron density depends on the number of electrons, the mutual repulsion between the electron densities of the metalandMOF-5will increase in the order: Li < Be < Mg < Al. Clearly, the ΔE of MOF-5:Li will be the largest. Though a greater repulsion is expected between electron densities of Al and MOF-5, the contribution of the attraction on

account of charge transfer is much higher than Be and Mg and therefore, MOF-5:Al_2 will exhibit the next highest ΔE. Both Be and Mg HOMOs have poo r attraction for the MOF-

5 LUMO, but Mg has larger number of electrons. Therefore, the MOF-5:Mg interaction will be the weakest. This conforms to the metal- MOF-5 interaction energy order (MOF-5:Li< MOF-5:Al <<MOF-5:Be< MOF-5:Mg) predicted in Section 3.2. At this point we would like to recall that the atomic charge on Li and Al in MOF-5:Li_2 and MOF-5:Al_2 was predicted to be +0.90 and +0.66 a.u., respectively (see Table 4). Therefore, when H_2 molecules are added to these decorated MOF-5s they interact not with a neutral metal atom but with a metal ion. The transfer of electrons from metal ions to the H^+ molecules is energetically not favorable because removing electrons from a positive ion is difficult by virtue of its much higher second ionization potential compared to the first ionization potential. The H_2 adsorption therefore, takes place by a charge polarization mechanism in which the metal ion polarizes the nearby hydrogen molecules. The bonding between the metal ion and H_2 molecule thereby proceeds through a simple electrostatic interaction. For understanding the above mechanism of charge polarization, we derived charge density difference surfaces of MOF- 5:Li_2:$2H_2$ (MOF-5:Li_2:$4H_2$) relative to the charge densities of MOF-5:Li_2 and two H_2 molecules (four H_2 molecules). The charge density calculation for MOF-5:Li_2 and two H_2 molecules (four H_2 molecules) was carried out by keeping the constituent atoms at the same positions as in MOF-5:Li_2:$2H_2$ (MOF-5:Li2:$4H_2$) and using the unit cell dimensions of the hydrogenated decorated MOF-5.

The charge density difference plots, thus obtained, are showcased in Fig. 6. In these plots, red regions imply electron loss and blue regions indicate electron gain. It is noticeable that the change in electron density is occurring only around the H atoms. Around each H atom there is a blue region toward the Li ion and a corresponding red region on the other site. In this manner this picture depicts that due to polarization by the Li ion there is a shift of electron density in the H_2 causing part of the H atoms to become positively charged (red region) and another part to become negatively charged (blue region). 0.756A°. Thus, in the Liand Al-decorated MOF-5 hydrogen molecules are bonded in molecular form. The slight increase in bond length is an artifact of the polarization of the H_2 molecule by the metal ion.

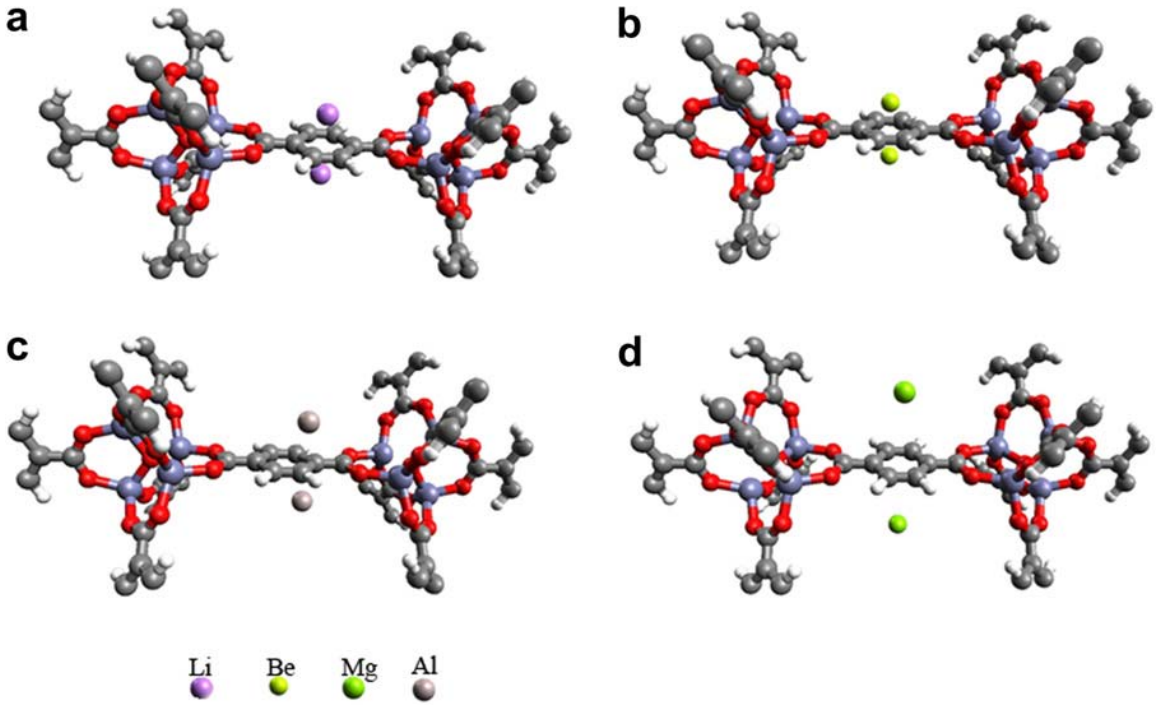

Figure 4.3 The optimized structures of Li-, Be-, Mg- and Al-decorated primitive cells of MOF-5.

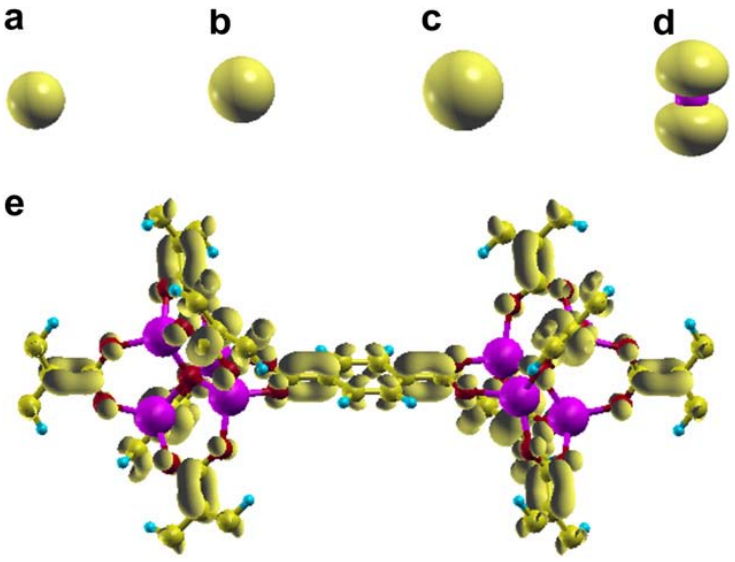

Figure. 4.4. Frontier molecular orbitals of metals and MOF-5, (a) HOMO of Li atom, (b) HOMO of Be atom, (c) HOMO of Mg atom, (d) HOMO of Al atom, and (e) LUMO of MOF-5.

The experimental bond length of H_2 molecule is 0.741A°. The H-H distances in MOF 5:Li_2:nH_2 and MOF-5:Al_2:nH_2, as listed in Table 3, are between 0.750 and

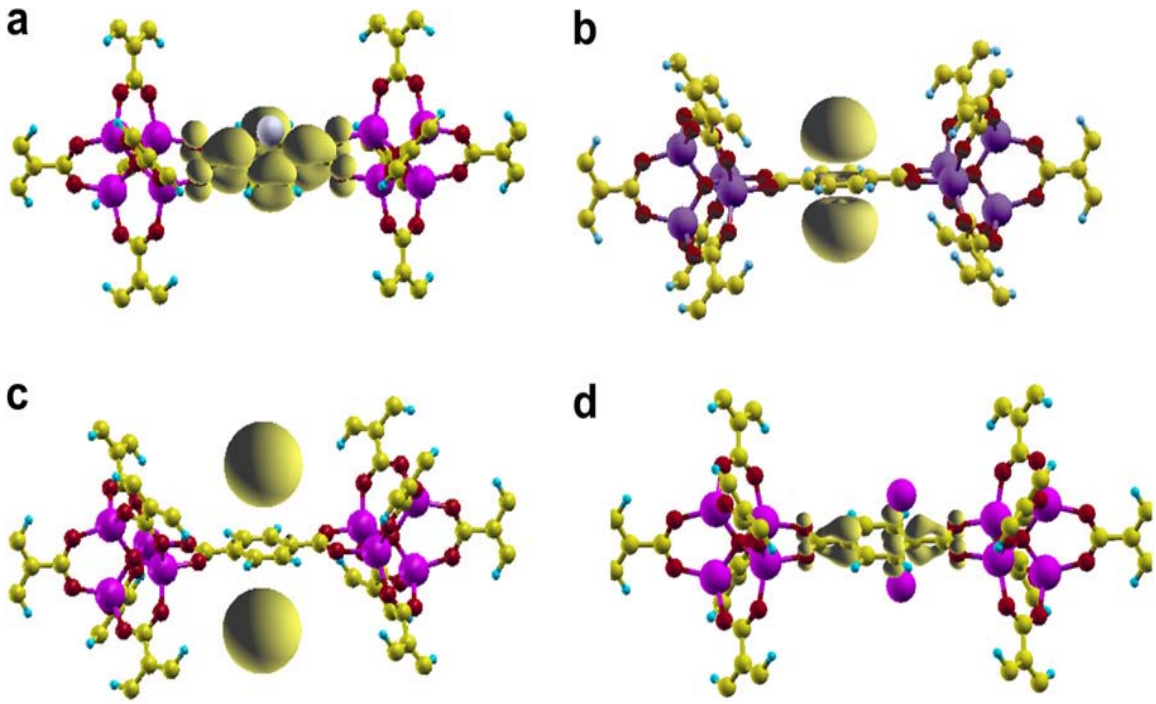

Figure 4.5. Frontier molecular orbitals of decorated MOF-5, (a) HOMO of MOF-5:Li_2, (b) HOMO of MOF-5:Be_2, (c) HOMO of MOF-5:Mg_2, and (d) HOMO of MOF-5:Al_2.

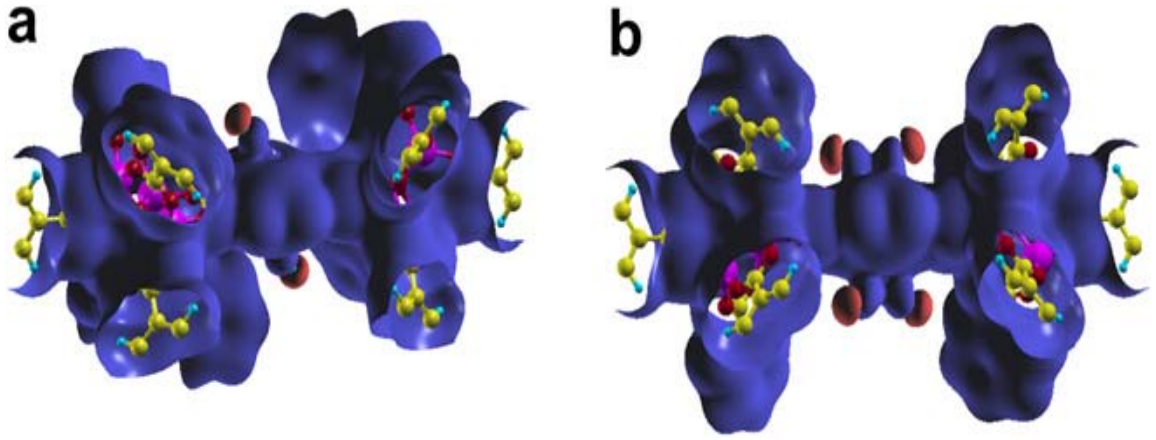

Figure 4. 6. Charge density difference plots of (a) MOF-5:Li_2:2H_2 and MOF-5:Li_2 and 2H_2 molecules and (b) MOF-5:Li_2:4H_2 and MOF-5:Li_2 and 4H_2 molecules, at an isovalue of 0.01.

4.3.4. Hydrogen binding energies and gravimetric storage

In order to systematically investigate the suitability of DFT functionals for the calculation of H2 binding energies for the metal decorated MOF-5s we first compare the BSSE corrected $E_{binding}$ for the BDC:Li_2:nH_2 molecular models evaluated using MP2 and different DFT functionals available with Gaussian 09 and using the GGA-PBE functional with the periodic DFT code VASP. $E_{binding}$ calculations utilizing 6-311 + G* are shown in Fig. 4.7(a). It can be seen from Fig. 4.7(a) that there is considerable difference in the Ebinding by MP2 method and by GGA-PBE (VASP). This figure also suggests that B3LYP and PBEPBE functional underestimates binding energy while PW91PW91, PBE1PBE and GGA-PBE (VASP) functionals overestimates the binding energy. To consider long range interactions 6-311+G* basis set does not have sufficient polarizations functions and leads to unphysical large basis set errors [80]. To avoid such unphysical large basis set error, we have used cc-pvtz basis set. The results for $E_{binding}$ are shown in Fig. 4.7(b). In comparison, the H_2 binding energies computed using the GGA-PBE functional along with the plane wave approach show excellent agreement with ccpvtz/ MP2 results for each n number of H_2 molecules adsorbed. B3LYP Functional is found to underestimate $E_{binding}$, while PW91PW91, PBEPBE and PBE1PBE functionals are found to highly overestimate $E_{binding}$. The $E_{binding}$ for PBEPBE and PW91PW91 functionals are found to mach up to second decimal digit. The optimized geometries of the corresponding n = 2-6 H_2 adsorbed Li-decorated MOF-5s are shown in Fig. 4.8. The total H_2 binding energy and binding energy per H_2 molecule of MOF- 5:Li2:nH_2 and MOF-5:Al2:nH_2 from the solid-state calculations of the full primitive unit cells are listed in Table 5. Our $E_{binding}$ per H_2 for MOF-5:Li_2:nH_2 (n=2-6) show an excellent agreement with the previously reported theoretical results of Blomqvist et al. [53] also presented in Fig.4.7(b), as well as with the MP2 values calculated for the BDC:Li_2:nH_2 models in Fig. 4.7(b). This agreement depicts that the solid-state GGA-PBE methodology can be used to calculate with good precision the $E_{binding}$ for the Li- and Al-decorated MOF-5s studied in this work.

It is evident from both Table 4.5 and Fig. 4.7(b) that $E_{binding}$ decreases as the number of hydrogen molecules increases. This decrease is a result of the increased repulsion between the H_2 molecules, the reduced sigma donation of the H_2 molecules, and the consequent reduced effective charge on the metal atoms. Adding more number of H_2 molecules would therefore decrease $E_{binding}$ still further. From Table 4.5 it can be seen that $E_{binding}$ of Li-decorated MOF-5 and Al-decorated MOF-5 lies between -18.00 kJ/mol and -11.70 kJ/mol and between -13.87 kJ/mol and -9.77 kJ/mol, respectively. These are much higher in magnitude than the usual pure MOF-H_2 interaction strengths between 2.26-5.2 kJ/mol [6-8] mentioned earlier. Recalling the hydrogen binding energy range of ~24-34 kJ/mol estimated by Lochan and Head- Gordan [9] at room temperature, we do not expect more than three H_2 molecules per metal atom to remain adsorbed to Li- and Al-decorated MOF-5s. Assuming that only sites near the metal-decorated BDCs are occupied and three H_2 molecules per M atom implies 18 H_2 molecules per formula unit of $Zn_4(BDC)_3M_6$. This corresponds to a hydrogen uptake of 4.3 wt.% and 3.9 wt.% for Li- and Al-decorated MOF-5, respectively. Thus, on basis of increased H_2 binding energies and increased H_2 storage capacities, we expect Li- and Al decorated MOF-5s to have potential for room temperature hydrogen storage applications.

System	**Total $E_{binding}$ (This work)**	**Ebinding per H_2 (This work)**	**Ebinding per H_2 (Ref. [53])**
MOF:Li2:2H2	-36.00	-18.00	-18.00
MOF:Li2:4H2	-62.36	-15.59	-16.00
MOF:Li2:6H2	-70.20	-11.70	-12.00
MOF:Al2:2H2	-27.74	-13.87	-
MOF:Al2:4H2	-50.40	-12.06	-
MOF:Al2:6H2	-58.62	-9.77	-

Table 4. 5. Calculated total H_2 binding energies and binding energies per H_2 of MOF-5:Li_2:nH_2 and MOF-5:Al_2:nH_2 systems and previously reported theoretical binding energies [53] per H_2 of MOF- 5:Li_2:nH_2. All energies are in kJ /mol.

4.4 Conclusions

Herein we have studied the effect of light metal atom (M= Li, Be, Mg and Al) decoration on the H_2 storage properties of MOF-5 by calculations on the molecular benzenedicarboxylate (BDC) models and on the primitive unit cells. Our systematic investigations revealed that using the GGA-PBE density functional based planewave-pseudopotential methodology is reliable for accurate evaluation of structural parameters, atomic charges and H_2 binding energies of the systems under study, particularly for Li- and Al-decorated MOF-5s. The nature of the interactions between the metal atoms and MOF-5 and between H_2 molecules and metal-decorated MOF-5 was analyzed. The calculated metal-MOF-5 interaction energies illustrated that only Li and Al atoms stabilize MOF-5. Furthermore, the predicted enhanced H_2 binding energies as well as gravimetric capacities suggest that these Li- and Al-decorated MOF-5s will be suitable for storage of H_2 at ambient conditions.

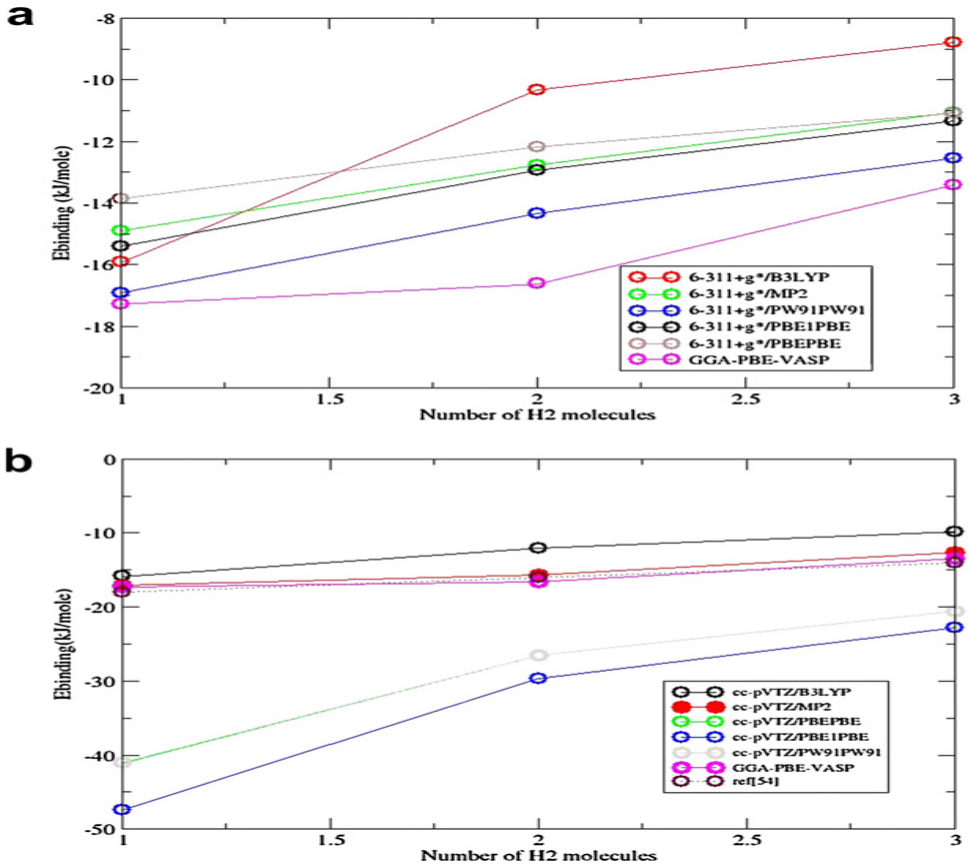

Figure 4.7. Curves for $E_{binding}$ verses number of H_2 adsorbed on BDC.(a) calculated $E_{binding}$ using 6-311+G* basis set.(b) calculated $E_{binding}$ using cc-pvtz basis set.

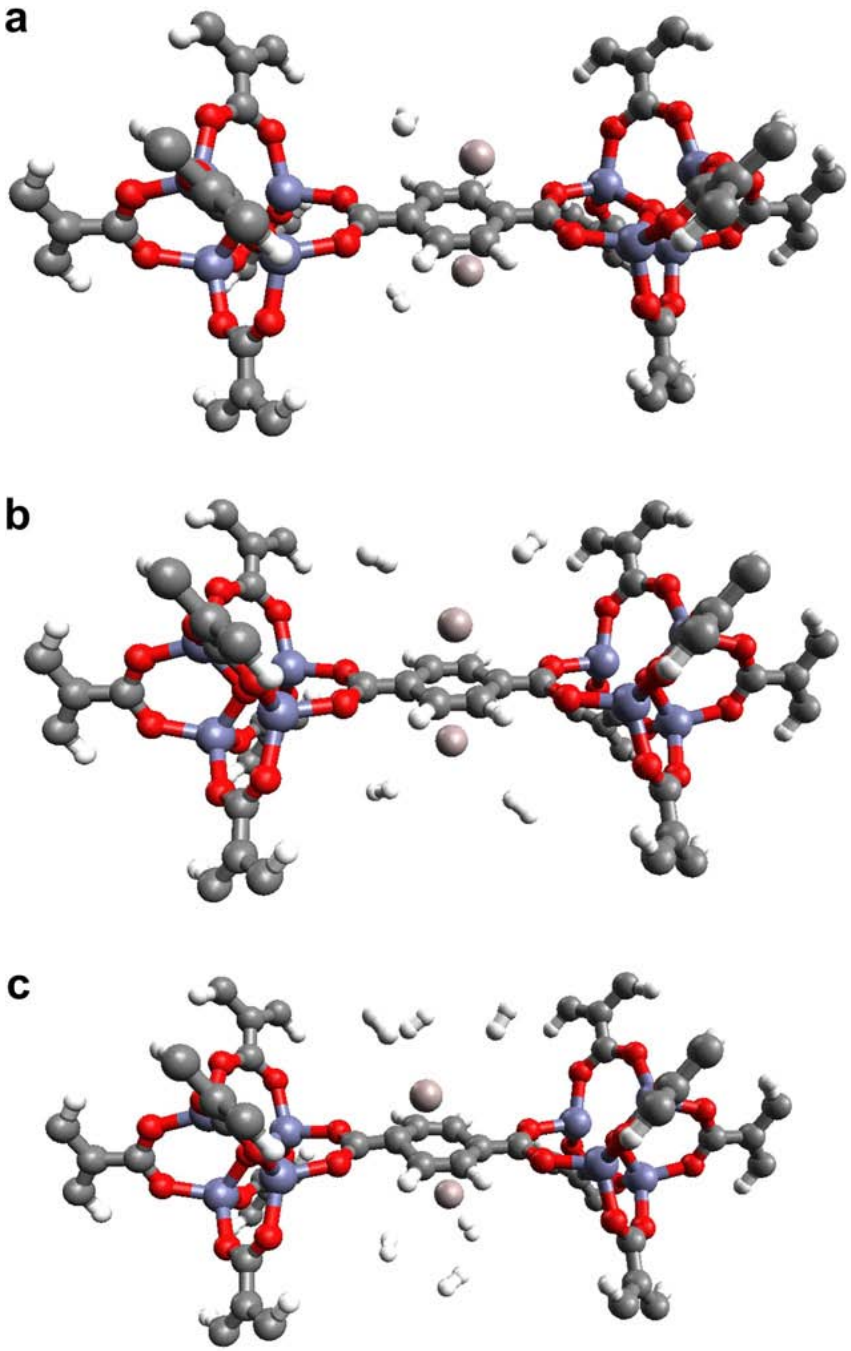

Figure 4.8. The optimized geometries of the corresponding n=2-6 H_2 adsorbed Al decorated MOF-5.

.

References:

[1] Schlapbach L, Zuttel A. *Nature*,**2001**, 414, 353.

[2] Seayad ATM, Antonelli DTM. *Adv*. *Mater*. **2004**, 16, 765.

[3] http://www1.eere.energy.gov/hydrogenandfuelcells/storage/pdfs/targets_onboard_hydro_storage.pdf.

[4] Kelkar T, Pal S, Kanhere DG. *Chem*. *Phys*. *Chem*.**2008**, 9, 928.

[5] M. Eddaoudi, H. Li, T. Reineke, M. Fehr, D. Kelley, T. L. Groy, and O. M. Yaghi, *Top. Catal.* **1999**, *9*, 105.

[6] J. L. C. Roswell, A. R. Milward, K. S. Park, and O. M. Yaghi, *J. Am. Chem. Soc.* **2004**, *126*, 5666.

[7] Bordiga S, Vitillo JG, Ricchiardi G, Regli L, Cocina D, Zecchina A, et al. *J Phys Chem B.* **2009**,109,18237.

[8] Kaye SS, Long JR. *J. Am. Chem. Soc.* 2005.127,6506.

[9] Lochan RC, Head-Gordon M. *Phys. Chem.Chem. Phys.* **2006**,8,1357.

[10] Yaghi OM, Chen B, Ockwig NW, Millward AR, Contreras DS. *Angew. Chem. Int. Ed.* **2005**,44,4670.

[11] Chae HK, Siberio-Perez DY, Kim J, Go Y, Eddaoudi M, Matzger AJ, et al. *Nature.* **2004**, 427, 523.

[12] Li J, Cheng S, Zhao Q, Long P, Dong J. *Int. J. Hydrogen. Energy.* **2009**, 34, 1377.

[13] Chen B, Eddaoudi M, Reineke TM, Kampf JW, O'Keeffe M, Yaghi OM. *J. Am. Chem. Soc.* **2000**, 122, 11559.

[14] Hubner O, Gloss A, Fichtner M, Klopper W. *J. Phys. Chem. A.* **2004**, 108, 3019.

[15]Sagara T, Klassen J, Ganz E. *J. Chem. Phys.* **2004**, 121, 12543.

[16] Buda C, Dunietz BD. *J. Phys. Chem. B.* **2006**, 110, 10479.

[17] Han SS, Deng WQ, Goddard W. *Angew. Chem. Int. Ed.* **2007**, 119, 6405.

[18] Han SS, Furukawa H, Yaghi OM, Goddard WA. *J. Am. Chem. Soc.* **2008**, 130, 11580.

[19] Han SS, Goddard WA. High *J. Phys. Chem. C.* **2008**, 112, 13431.

[20] Mulder F, Dingemans T, Wagemaker M, Kearley G. *Chem. Phys.* **2005**, 317, 113.

[21] Mueller T, Ceder G. *J. Phys. Chem. B.* **2005**, 109, 17974.

[22] Han SS, Mendoza-Corte´s JL, Goddard III WA. *Chem. Soc. Rev*. 2009, 38, 1460

[23] Niu J, Rao BK, Jena P. Phys. Rev. Lett. **1992**, 68, 2277.

[24] Charles J, Bauschlicher W, Walch SP. *J. Chem. Phys.* **1982**, 76, 4560.

[25] Niu J, Rao BK, Khanna SN, Jena P. *Chem. Phys. Lett*. **1991**, 230, 299.

[26] Maseras F, Lledos A, Clot E, Eisenstein O. *Chem. Rev*. **2000**, 100, 601.

[27] Gagliardi L, Pyykko P. J. Am. Chem. Soc. **2004**, 126, 15014.

[28] Maark TA, Pal S. *Int. J. Hydrogen. Energy*. **2010**, 35, 12846.

[29] Chandrakumar KRS, Ghosh SK. *Chem. Phys. Lett* **2007**, 447, 208.

[30] 111.Y. Liu, H. Kabbour, C. M. Brown, D. A. Neumann, and C. C. Ahn, *Langmuir* **2008**, *24*, 4772.

[31] Suttisawat Y, Rangsunvigit P, Kitiyanan B, Williams M, Ndungu P, Lototskyy M, et al. *Int. J. Hydrogen. Energy*. **2009**, 34, 6669.

[32] Kim BJ, Lee YS, Park SJ. *Int. J. Hydrogen. Energy*. **2008**, 33, 4112.

[33] Zubizarreta L, Menndez J, Pis J, Arenillas A. *Int. J. Hydrogen. Energy*. **2009**, 34, 3070.

[34] Zhao Y, Kim YH, Dillon AC, Heben MJ, Zhang SB. Phys. Rev. Lett. **2005**, 94, 155504.

[35] Yildirim T, Ciraci S. *Phys. Rev. Lett*. **2005**, 94, 175501.

[36] Lee H, Choi WI, Ihm J. Phys. Rev. Lett. **2006**, 97, 056104. Meng S, Kaxiras E, Zhang Z. *Nano. Lett*. **2007**, 7, 663.

[37] Kim G, Jhi SH, Park N. *Appl. Phys. Lett*. **2008**, 92, 013106.

[38] Sun Q, Wang Q, Jena P, Kawazoe Y. *J. Am. Chem. Soc.* **2005**, 127, 14582.

[39] Forster PM, Eckert J, Heiken BD, Parise JB, Yoon JW, Jhung SH, et al. *J. Am. Chem. Soc.* **2006**, 128, 16846.

[40] Ma S, Zhou H-C. *J. Am. Chem. Soc.* **2006**, 128, 11734.

[41] Dinca M, Dailly A, Liu Y, Brown CM, Neumann DA, Long JR. *J. Am. Chem. Soc.* **2006**, 128, 16876.

[42] Dinca M, Han WS, Liu Y, Dailly A, Brown CM, Long JR. *Angew. Chem. Int. Ed.* **2007**, 46, 1419.

[43] Dinca M, Long JR. *J. Am. Chem. Soc.* **2007**, 129, 11172.

[44] Vitillo JG, Regli L, Chavan S, Ricchiardi G, Spoto G, Dietzel PDC, et al. *J. Am. Chem. Soc.* **2008**, 130, 8386.

[45] Hamaed A, Trudeau M, Antonelli DM. *J. Am. Chem. Soc.* **2008**, 130, 6992.

[46] Patchkovskii S, Tse JS, Yurchenko SN, Zhechkov L, Heine T, Seifert G. *Proc. Natl. Acad. Sci.* **2005**, 102, 10439.

[47] Heine T, Zhechkov L, Seifert G. *Phys. Chem. Chem. Phys.* **2004**, 6, 980.

[48] Sun Q, Jena P, Wang Q, Marquez M. *J. Am. Chem. Soc.* **2006**, 128, 9741.

[49] Chandrakumar KRS, Ghosh SK. Nano. Lett. **2007**, 8, 13.

[50] Forst CJ, Slycke J, Van Vliet KJ, Yip S. *Phys. Rev. Lett.* **2006**, 96, 175501.

[51] Kim YH, Zhao Y, Williamson A, Heben MJ, Zhang SB. *Phys. Rev. Lett.* **2006**, 96, 016102.

[52] Chen P, Wu X, Lin J, Tan KL. *Science*. **1999**, 285, 91.

[53] Blomqvist A, Arajo CM, Srepusharawoot P, Ahuja R. *Proc. Natl. Acad. Sci.* **2007**, 104, 20173.

[54] Han SS, Goddard WA. *J. Am. Chem. Soc.* **2007**, 129, 8422.

[55] Venkataramanan N, Sahara R, Mizuseki H, Kawazoe Y. *Int. J. Mol. Sci.* **2009**, 10, 1601.

[56] Sun YY, Lee K, Kim YH, Zhang SB. *Appl. Phys. Lett.* **2009**,95,033109

[57] Zou X, Cha M-H, Kim S, Nguyen MC, Zhou G, Duan W, et al. *Int. J. Hydrogen. Energy.* **2010**, 35, 198.

[58] Kuc A, Heine T, Seifert G, Duarte HA. *Chem. Eur. J.* **2008**,14,6597.

[59] Kuc A, Heine T, Seifert G, Duarte HA. *Theor. Chem. Accounts.* **2008**,120,543.

[60] Hohenberg P, Kohn. *Phys. Rev*. **1964**, 136, B864.

[61] Zhang Y, Pan W, Yang W. *J. Chem. Phys.***1997**, 107, 7921.

[62] Perez-Jorda J, Becke AD. *Chem. Phys. Lett*. **1995**, 233, 134.

[63] Wesolowski TA, Parisel O, Ellinger Y, Weber J. *J. Phys. Chem. A.* **1997**, 101, 7818.

[64] Patton DC, Pederson MR. *Phys. Rev. A.* **1997**; 56,R2495-8.

[65] Perdew JP, Burke K, Ernzerhof M. *Phys. Rev. Lett*. **1996**,77, 3865.

[66] Kresse G, Furthmuller *J. Comp. Mater. Sci.* **1996**, 6, 15.

[67] Kresse G, Furthmuller *J. Phys. Rev. B.* **1996**, 54, 11169.

[68] Kresse G, Joubert D. *Phys. Rev. B.* **1999**, 59, 1758.

[69] Blochl PE. *Phys. Rev. B.* **1994**, 50, 17953, 79.

[70] Li H, Eddaoudi M, O'Keeffe M, Yaghi OM. *Nature* **1999**, 402, 276.

[71] Monkhorst HJ, Pack JD. Phys Rev B, 1976, 13, 5188.

[72] Henkelman G, Arnaldsson A, Jonsson H. *Comp. Mat. Sci.* **2006**, 36, 354.

[73] Gaussian 09, Revision A.1, Frisch MJ, Trucks GW, Schlegel HB, Scuseria GE, Robb MA,Cheeseman JR et al. Gaussian Inc., Wallingford CT, **2009**.

[74] Simon S, Duran M, Dannenberg JJ. *J. Chem. Phys.* **1996**, 105, 11024.

[75] Breneman CM, Wiberg KB. *J. Comp. Chem*. **1990**, 11, 361073.

[76] Baker TA, Head-Gordon M. *J. Phys. Chem. A.* **2010**, 114, 10326-33.

[77]Liu J, Rankin RB, Johnson JK. *Mol. Simulat*. **2009**, 35, 60-9.

[78] Parr RG, Yang W. *J. Am. Chem. Soc.* 1984, **106**, 4049-50.

[79] Yang W, Parr RG. *Proc. Natl. Acad. Sci. USA* **1985**, 82, 6723-6.

[80]Youhwa O, Yong-Hyun K, Yousung J. *Phys. Rev. Lett*. **2010**,104, 179601.

CHAPTER 5

Transition Metal as Novel Dopants of MOFs

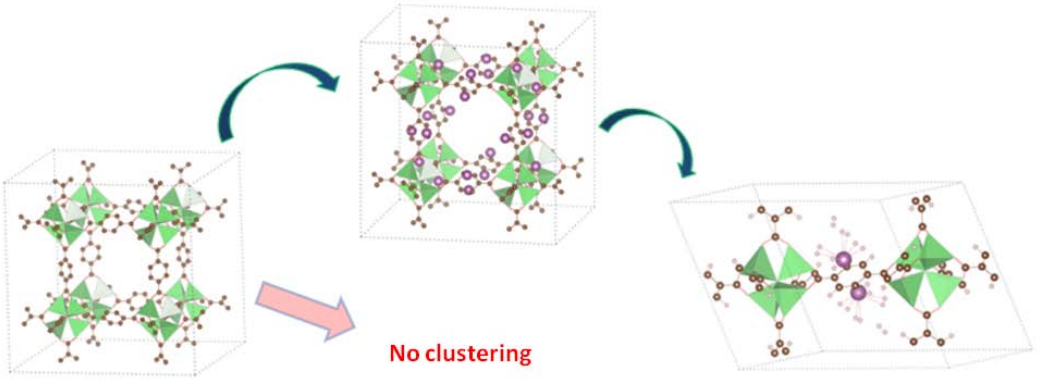

Transition metal based systems show promising binding energy for hydrogen storage but suffer from clustering problem. The effect of light transition metal (M = Sc, Ti) decoration and boron substitution on the hydrogen storage properties of MOF-5 and clustering problem of metals have been investigated using ab-initio density functional theory (DFT). Our results of solid state calculations reveal that while Ti cluster strongly, Sc atoms do not suffer from this problem when decorating MOF-5. Boron substitution on metal decorated MOF-5 enhances the interaction energy of both the metals with MOF-5.

Sc decorated MOF-5 shows a hydrogen storage capacity of 5.81 wt% with calculated binding energies of 20-40 kJ/mol which ensures the room temperature applicability of this hydrogen storage material. To exploit ZIFs for hydrogen storage it is essential to investigate the primary adsorption sites. Herein, we investigate ZIF-72 unique adsorption sites are obtained using ab inito molecular dynamics (MD) techniques. Furthermore, our results suggest that the binding energy of and gravimetric storage can be improved significantly via metal decoration of the pore site.

5.1 Introduction

Due to the high energy density, efficient burning within fuel cell technology, high abundance and environmentally clean nature, hydrogen has attracted vast research interest [1] as an alternative to our dependence upon fossil fuels. However, the need of safe and competent (high gravimetric and volumetric density) storage system is the key challenge for practical commercialization of hydrogen powered mobile or static applications. Technical targets established by U.S. Department of Energy (DOE) require 5.5 wt. % gravimetric and 40 g of H_2/L volumetric storage by the year 2015. O ver the past decade, a number of research efforts have been made to find new storage materials in order to achieve the established storage targets.

Simple and complex metal hydrides are promising materials for hydrogen storage. Although, these materials exhibit a high H_2 storage capacity, they suffer from large dehydrogenation activation barriers. In an interesting study, Kelkar et al.[1] have shown that doping different phases of MgH_2 with Al and Si can result in a lowering of its activation energy barriers associated with the direct desorption of H_2 from its (001) surface.

A variety of porous materials have been widely tested experimentally and theoretically[3], including covalent organic frameworks (COFs) and metal organic

frameworks (MOFs). MOFs are crystalline hybrid organic/inorganic nanoporous materials, which can adsorb guest molecules, and thus are potential candidates for H_2 storage [4]. Due to the predominant contribution of van der Waals interactions between the physisorbed H_2 molecules and the host MOFs the resulting H_2 adsorption enthalpies are typically in the range of 2.2-5.2 kJ/mol[5-7]. As a result, MOFs exhibit fast adsorption/desorption kinetics. The drawback is that significant hydrogen adsorption can only be achieved at a low temperature of 77 K.

A study by Lochan and Head-Gordon[8] depicts that the ideal H_2 binding energy range is 20-40 kJ/mol for storage at established target conditions (-20˚C to 50˚C and at 100 bar). H_2 binding energies in this range ensure reversibility and fast adsorption/desorption kinetics. A major challenge is thus, to tune the H_2 binding energy as well as the increase H_2 adsorption of MOFs in order to render them useful for practical and mobile applications. For this, the introduction of interactions other than van der Waals is necessary in MOFs. A widely accepted strategy is the introduction of charged species in MOFs for achieving the desired H_2 binding energy [9,10].

Many theoretical studies have been focused upon the interaction of H_2 molecules with metal ions[10-15]. Many research studies explored extensively the possibility of storing hydrogen via the Kubas interaction transition metal (TM) decorated graphitic nanostructures[16-24] (nanotubes, fullerenes, and graphene). In a well-known study of TM decoration, Yildirim et al.[20] illustrated that Ti-decorated nanotubes can adsorb upto 8 H_2 per Ti with a high binding energy of 0.43 eV/H_2 with hydrogen uptake upto 8 wt %.

Decoration of alkali and alkaline earth metals have also been investigated theoretically on several systems, including carbon nanotubes (CNTs), graphene and fullerenes[25-40]. The prime problem with TM based materials is the tendency of metal atoms to cluster among each other[41,42]. It has been shown[41] that TM atoms cluster on the surface of C_{60}, which significantly reduces the storage capacity. To prevent the clustering of metal atoms, the doping of carbon nanostructures by boron has also been proposed[18].

It is well known that methods based on DFT are unable to correctly describe dispersion forces and van der Waals interactions face challenges in studying pure MOFs. Furthermore, ab initio methods such as MP2 and CCSD (T) are not practical for

application to the full structure. However, in metal decorated systems the electrostatic contributions are predominant. Thus, DFT methods provide reasonably accurate results for such systems. In a recent study[43], we have shown that PBE-PAW plane wave method gives reasonable H_2 binging energy for metal decorated MOF-5 when compared to cc-pVTZ/MP2.

The objective of this study is three fold: first, to identify potential hydrogen storage candidate with incorporation of Kubas interaction. Second, to search for the best light transition metal atom which can, increase the strength of H_2 adsorption, enhance the amount of H_2 storage in MOF-5 and does not suffer from the well-known clustering problem in MOFs. Third, to investigate whether boron substitution can avoid the clustering problem of TMs. Thus, herein we investigate Sc- and Ti-decorated MOF-5 systems and their hydrogen binding energies ($E_{binding}$) and storage capacities using periodic DFT based calculations employing the PBE functional. Furthermore, 1,4 boron substituted metal decorated MOF-5 are also investigated.

5.2. Computational methodology

All the calculations have been performed using the Vienna ab initio simulations package (VASP)[46,47] with DFT planewave-pseudopotential based approach. We have used the projector augmented wave (PAW)[48,49] approach to evaluate all the properties. The PAW potentials with the valence states 3p4s3d for Sc, d3s1for Ti 2s2p for C, 2s2p for O, d10p2 for Zn, 1s for H and s2p1 for B were used. A kinetic energy cut-off of 520 eV was employed for primitive cell calculations while 400 eV cut-off was taken for full-unit cell calculations. For Sc-nH_2 systems 330 eV cut-off was taken with spin polarized calculations. All geometry optimizations were carried out without any geometry constraint. All forces were calculated using Hellmann-Feynman theorem. Geometries considered optimized with maximum force found smaller than 0.01 eV/Å. Real/space projections were used to evaluate PAW character of wave-functions. The primitive cell of MOF-5 was built from the crystal structure of MOF-5 that was taken from experimental data[50] and a 2x2x2 k-point grid generated by Monkhorst Pack

scheme[51] was applied to it. For obtaining the atomic charges Bader analysis[44] was performed. Molecular DFT calculation of SC_2-BDC were performed at the B3LYP[52,53]/6-311+g(d) level using Gaussian09 program package[54]. Solvent effects were introduced using the polarizable continuum solvation model (PCM)[55].

5.3 Results and Discussion

We first investigate individual interactions of the bare metal atoms with up to n = 8 H_2 molecules. The corresponding structures are displayed in Figure 5.1 and Figure 5.2 while the $E_{binding}$ and charge on the metal atoms are presented in Table 5.1. H_2 binding energies are found to be between -113.31 to -33.02 kJ/mol for Sc-nH_2 and between -95.59 to -41.12 kJ/mole for Ti-nH_2. These results confirm that both Sc and Ti have potential for hydrogen storage.

5.3.1 Structural features of M-nH_2 systems

It is clear from figure 5.1 and figure 5.2 that for n = 1 case both metal atoms chemisorb H_2 dissociatively as H atoms (referred hereon as type "A" interaction) with high $E_{binding}$ and small H-H distances as given in Table 1. When n = 2 the interactions differ vividly for the metals. Sc chemisorbs one H_2 dissociatively (type "A") and the other in a combined chemi-physisorption type "B" manner with a higher binding energy (69.30 kJ/mol per H_2) than Ti (32.17 kJ/mol) which shows only type "B" interactions.

Interactions of three H_2 molecules with Sc and Ti are comprised of 2 type of interactions: two H_2 molecules are chemi-physisorbed (or physisorbed for Ti) "A" and another H_2 molecule is strongly chemisorbed "B" giving reasonable binding energies for both the metals [Table. 5.1]. Four H_2 molecules interacts with Sc and hence shown to be physisorbed "A" resulting a reasonable binding energy of 34.95 KJ/mol, while interactions of Ti with four H_2 molecules are of two types: two H_2 molecules are

physisorbed “A” and other two H_2 molecules are strongly chemisorbed “B” forming four Ti-H bond having a large binding energy of 62.99 kJ/mol per H_2. Ti-$(H_2)_5$ shows slightly distorted square pyramidal structure and having four equivalent equatorial semi planar “A” H_2 molecules and a slightly distorted axial “B” H_2 molecule. Equatorial Ti-H distances are in between chemisorption and physisorption range and the axial Ti-H distance is in the physisorption range. Sc-$(H_2)_5$ cluster is almost structurally similar to that of Ti-$(H_2)_5$ but possessing far lower binding energy of 39.92 kJ/mol per H_2 than that of Ti-$(H_2)_5$ (52.01 kJ/mol per H_2). Sc-$(H_2)_6$ and Ti-$(H_2)_6$ both hold distorted octahedral structures with four semi equatorial equivalent “A” H_2 molecules and two semi axial equivalent “B” H_2 molecules. All the Sc-H distances are in almost physisorption range while the equatorial Ti-H distances and axial Ti-H distances account for the chemi-physisorbed and physisorbed type of interactions respectively. Ti-$(H_2)_7$ possess a complex structure having almost seven equivalent “A” chemi-physisorbed Ti-H_2 binding positions giving a binding energy of 51.80 kJ/mol per H_2 range. Sc-$(H_2)_7$ structure differs greatly from that of Ti$(H_2)_7$ with four types of Sc-H_2 binding positions: two equivalent equatorial “A” positions [Fig.5.2], two equivalent equatorial “B” positions, two equivalent di-axial “C” positions and one mono axial “D” position. Sc-H bond lengths in “A” and “B” positions attribute in favor of chemi-physisorbed type of interactions , while “C” and “D” positions strongly recommend physisorption type of interactions. The differential binding strategies result in a reasonable differences in binding energies for Sc-$(H_2)_7$ and Ti$(H_2)_7$ [Table. 5.1]. Both Sc$(H_2)_8$ and Ti$(H_2)_8$ clusters show similar kind of structures possessing four different H_2 binding sites “A” , “B”, “C” and “D” respectively. In both the structures, all the M-H distances (M=Sc,Ti) imply physisorption kind of binding, resulting a moderately high binding energy for Ti (B.E/H_2=41.12kJ/mol) and a accessible binding energy for Sc (B.E/H_2=33.2kJ/mol). From the above discussion (also see Table 5.1) it is clear that total binding energies of bare Sc metal are in the accessible range for n = 3-8H_2, while of bare Ti metal show slightly large values for all n except n = 2 and 8. Based on this it can be suggested that Sc may be a better candidate than Ti for decorating MOF-5.

System	Binding energy/H_2	Bader charge on metal
Sc-1H_2	-113.31	1.15
Sc-2H_2	-69.30	1.14
Sc-3H_2	-44.02	1.15
Sc-4H_2	-34.95	1.20
Sc-5H_2	-39.92	1.15
Sc-6H_2	-38.25	1.16
Sc-7H_2	-37.90	1.19
Sc-8H_2	-33.02	1.23
Ti-1H_2	-95.59	1.02
Ti-2H_2	-32.17	0.35
Ti-3H_2	-43.40	0.75
Ti-4H_2	-62.99	1.50
Ti-5H_2	-52.01	0.89
Ti-6H_2	-51.03	0.91
Ti-7H_2	-51.80	0.92
Ti-8H_2	-41.12	1.01

Table 5.1. Binding energies (in kJ/mol) and Bader charges on metals atoms of M-nH_2 systems.

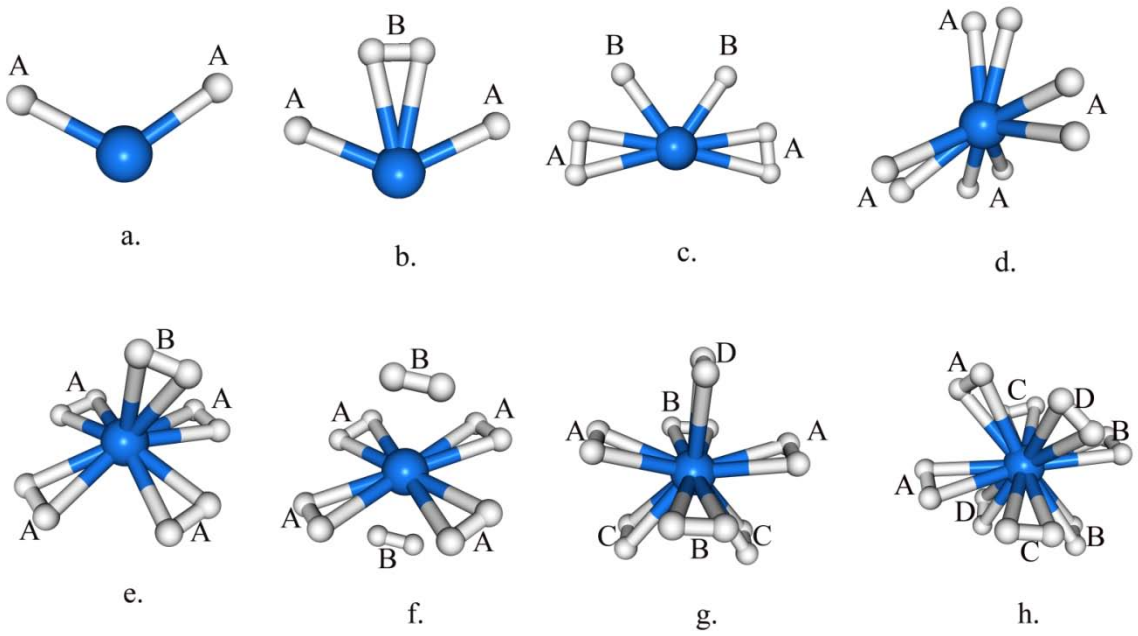

Figure 5.1. Relaxed structures of Sc-nH_2 (a) 1H_2, (b) 2H_2, (c) 3H_2, (d) 4H_2, (e) 5H_2 (f) 6H_2 (g) 7H_2 (h) 8H_2. Labels A, B, C and D represent the symmetrically equivalent positions.

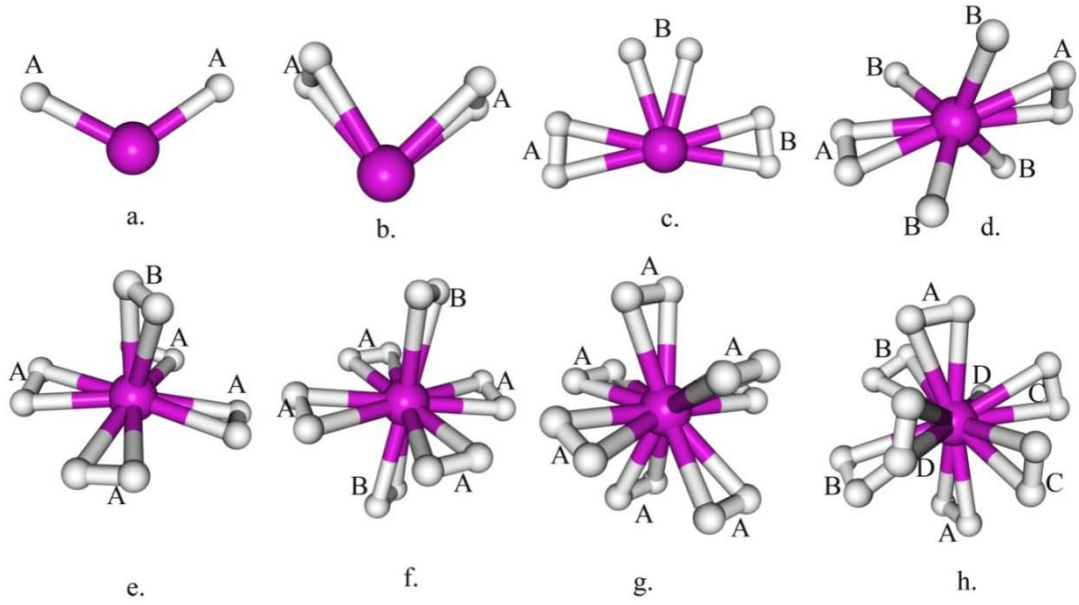

Figure 5.2. Relaxed structures of Ti-nH_2 (a) 1H_2, (b) 2H_2, (c) 3H_2, (d) 4H_2, (e) 5H_2 (f) 6H_2 (g) 7H_2 (h) 8H_2. Labels A, B, C and D represent the symmetrically equivalent positions.

As a next step we analyzed the corresponding metal-decorated MOF-5s (MDMs). The adsorption of metal atoms (Sc and Ti) on the MOF-5 was investigated by fully optimizing the structures with metal atoms initially placed close to the aromatic ring center of MOF-5. Both Sc and Ti show high interaction energy with MOF-5 of -281.32 and -244.04 kJ/mol, respectively.

The geometrical changes induced on MOF-5 as a result of metal decoration can be understood by comparing the C–C bond lengths of the aromatic ring listed in Table 5.2. It is clear from the table that both metal atoms induce a stretching of the aromatic ring with a shortening of C_1–C_2 and an increase in C_2–C_3 and C_3–C_3 distance, indicating that a charge transfer takes place from metal atoms to the MOF-5 framework. The C_1–C_2 bond contractions in particular become more predominant when more H_2 molecules are allowed to interact with the MDM.

Bader analysis[44] of the self-consistent charge density revealed that Sc and Ti atoms carry a charge of 1.12 and 1.1 e per metal, respectively (See Figure 5.3). This implies that a e^- charge has been produced due to the large difference in the electronegativities of the metal atoms and MOF-5. This charge will be critically beneficial in raising the H_2 binding affinity.

It is well known that TMs prefer to cluster among each other this clustering then reduces their binding energy as well as H_2 storage capacity. Thus, we have studied the clustering of these TMs on MOF-5. As shown in Fig. 5.3 initially three metal atoms were decorated on each side of benzene ring in MOF-5(six metals atoms on primitive cell) at a close M-M distance of 1.51Å from each other. On relaxation Sc atoms were found to be far apart (3.1 Å) while the Ti atoms were relatively close to each other at 2.10 Å. This

SYSTEM	**C_1-C_2**	**C_2-C_3**	**C_3-C_3**	**M-BZ_{COM}**	**M-H_2**	**M-H_2**	**M-H_2**	**M-H_2**	**H-H(Average distace)**
MOF-5	1.498	1.403	1.391						
MOFSc_2	1.476	1.472	1.461	1.767					
MOF:Sc_2:2H_2	1.471	1.477	1.467	1.760	2.12				0.81
MOF:Sc_2:4H_2	1.466	1.469	1.465	1.790	2.11	2.11			0.81

MOF:Sc_2:6H_2	1.466	1.469	1.460	1.819	2.18	2.15	2.21		0.79
MOF:Sc_2:8H_2	1.460	1.469	1.448	1.834	2.22	2.29	2.24	2.29	0.77
MOF:Sc_2:10H_2	1.459	1.469	1.446	1.830	2.25	2.26	2.23	2.82	0.77(0.75)
MOF:Ti_2	1.485	1.479	1.463	1.631					
MOF:Ti_2:2H_2	1.475	1.466	1.460	1.72	1.72				1.95
MOF:Ti_2:4H_2	1.479	1.451	1.447	1.760	1.87	1.87			0.90
MOF:Ti_2:6H_2	1.487	1.451	1.454	1.769	1.9	1.9	1.9		0.85
MOF:Ti_2:8H_2	1.467	1.460	1.433	1.792	1.9	2.0	1.95	1.96	0.81
MOF:Ti_2:10H_2	1.465	1.461	1.433	1.785	2.0	1.99	2.0	2.0(3.86)	0.80(0.75)
MOF:2B									
MOF:2B:Sc_2	1.547	1.570	1.472	1.652					0.78
MOF:2B:Sc_2:2H_2	1.548	1.577	1.478	1.668	2.22				0.78
MOF:2B:Sc2:4H_2	1.549	1.564	1.475	1.698	2.19	2.19			0.78
MOF:2B:Sc_2:6H_2	1.552	1.558	1.465	1.747	2.17	2.17	2.22		0.78
MOF:2B:Sc_2:8H_2	1.567	1.544	1.446	1.898	2.0	2.0	2.0	2.1	0.80
MOF:2B:Sc_2:10H_2	1.556	1.552	1.450	1.819	2.12	2.11	2.16	2.17(3.83)	0.78

Table 5.2. Structural parameters of MOF-5, MOF-M_2, MOF:M_2:nH_2, MOF:2B, MOF:2B:Sc_2 and MOF:2B:Sc_2:nH_2 systems.Values given in ( ) are corresponds to fifth hydrogen per metal. M-BZ_{COM} is the distance of metal atom from benzene of MOF-5.

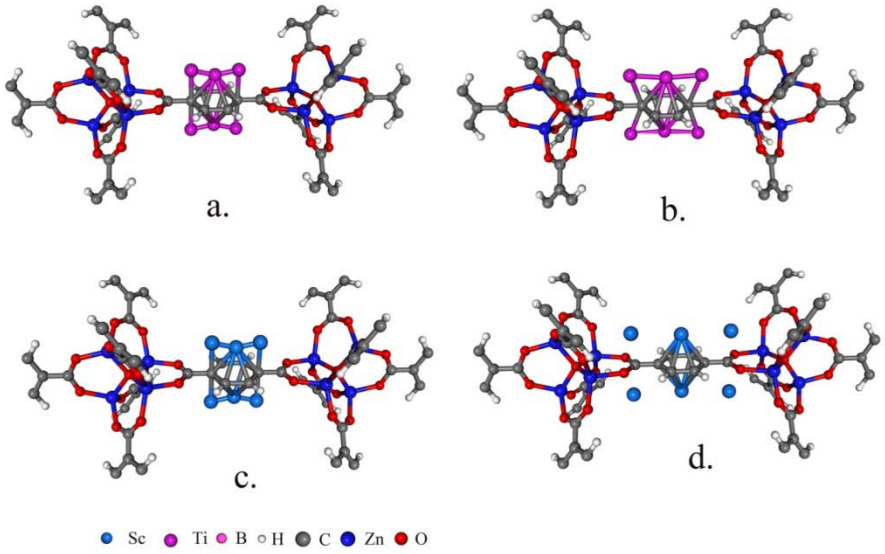

Figure 5.3. (a) Initial geometry of MDM where 6 Ti metals are decorated on MOF-5. (b) Relaxed geometry of MDM where 6 Ti metals are decorated on MOF-5 (c) Initial geometry of MDM where 6 Sc metals are decorated on MOF-5 (d) Relaxed geometry of MDM where 6 Sc metals are decorated on MOF-5

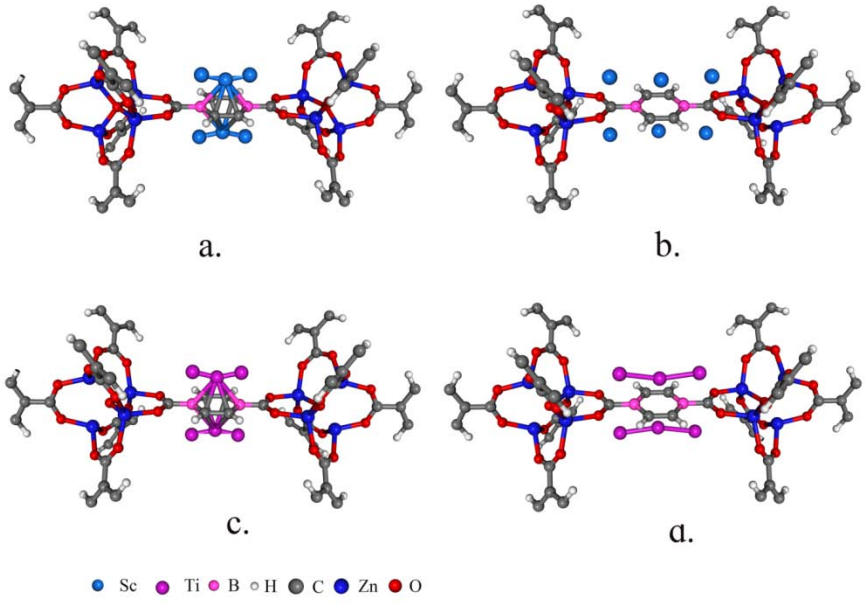

Figure 5.4. (a) Initial geometry of system where 6 Ti metals are decorated on 1,4 boron substituted MOF-5. (b) Relaxed geometry of system where 6 Ti metals are decorated on 1,4 boron substituted MOF-5 (c) Initial geometry of system where 6 Sc metals are

decorated on 1,4 boron substituted MOF-5 (d) Relaxed geometry of system where 6 Sc metals are decorated on 1,4 boron substituted MOF-5

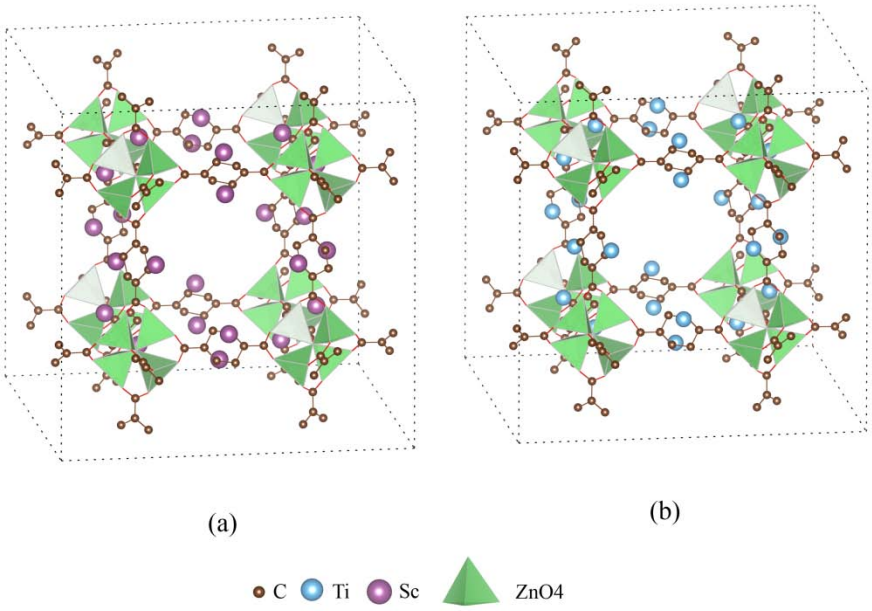

Figure 5.5. (a) Optimized geometry of full-MDM where 24 Sc metal atoms are decorated on MOF-5. (b) Optimized geometry of full-MDM where 24 Ti metal atoms are decorated on MOF-5.

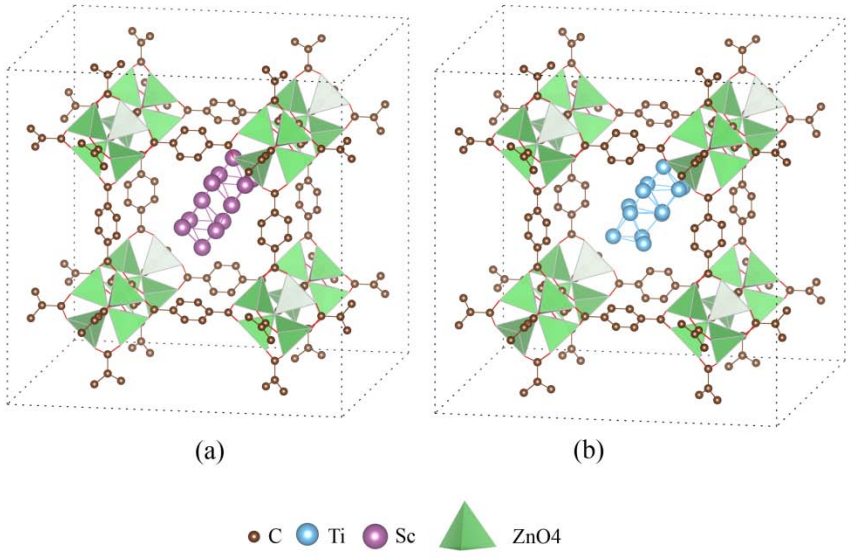

Figure 5.6. (a) Optimized geometry of full-MOF-5 where a cluster of 12 Sc metal atoms relaxed inside the pore. (b) Optimized geometry of full-MOF-5 where a cluster of 12 Ti metal atoms relaxed inside the pore.

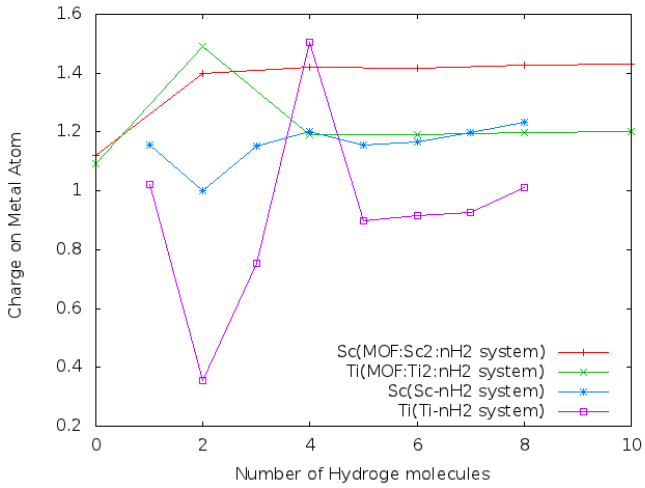

Figure 5.7. The Bader charge on metal atoms on different systems.

confirms that Sc atoms do not cluster on MOF-5 but Ti atoms do. Further affirmation of this comes from the Bader charge analysis. Sc atoms in MOF-5:Sc_6 maintain their charge of 0.9 e, but the charge on Ti atoms in MOF-5:Ti_6 (0.45 e) is much reduced compared to MOF-5:Ti_2.

To confirm that Sc atoms do not cluster on MOF-5, we have optimized the full unit-cell of MOF-5, full metal decorated MOF-5 (MOF:M_{24}) (Fig. 5.5a and Fig. 5.5b), M_{12} cluster inside the MOF-5 (MOF:M_{12})(Fig. 5.6a and Fig. 5.6b). In full unit cell of MOF-5 there are 12 BDC facing towards inside, thus we have taken M_{12} cluster inside the MOF-5 pore. The difference in the formation energy of both atomic and clustered configuration indicates that whether the metal clusters inside the MOF or remains in atomic non-clustered form. The formation energy per metal of clustered configuration is given as:

$$E_f^c = \frac{1}{12}\left[E_T(MOF:M_{12}^c) - E_T(MOF) - 12E_T^a(M)\right] \qquad (5.1)$$

While the formation energy per metal of atomic non-clustered configuration is given as:

$$E_f^a = \frac{1}{24}\left[E_T(MOF:M_{24}^a) - E_T(MOF) - 24E_T^a(M)\right] \quad (5.2)$$

The difference in the formation energy of both atomic and clustered configuration is given as:

$$\Delta E_a^c = E_f^a - E_f^c \quad (5.3)$$

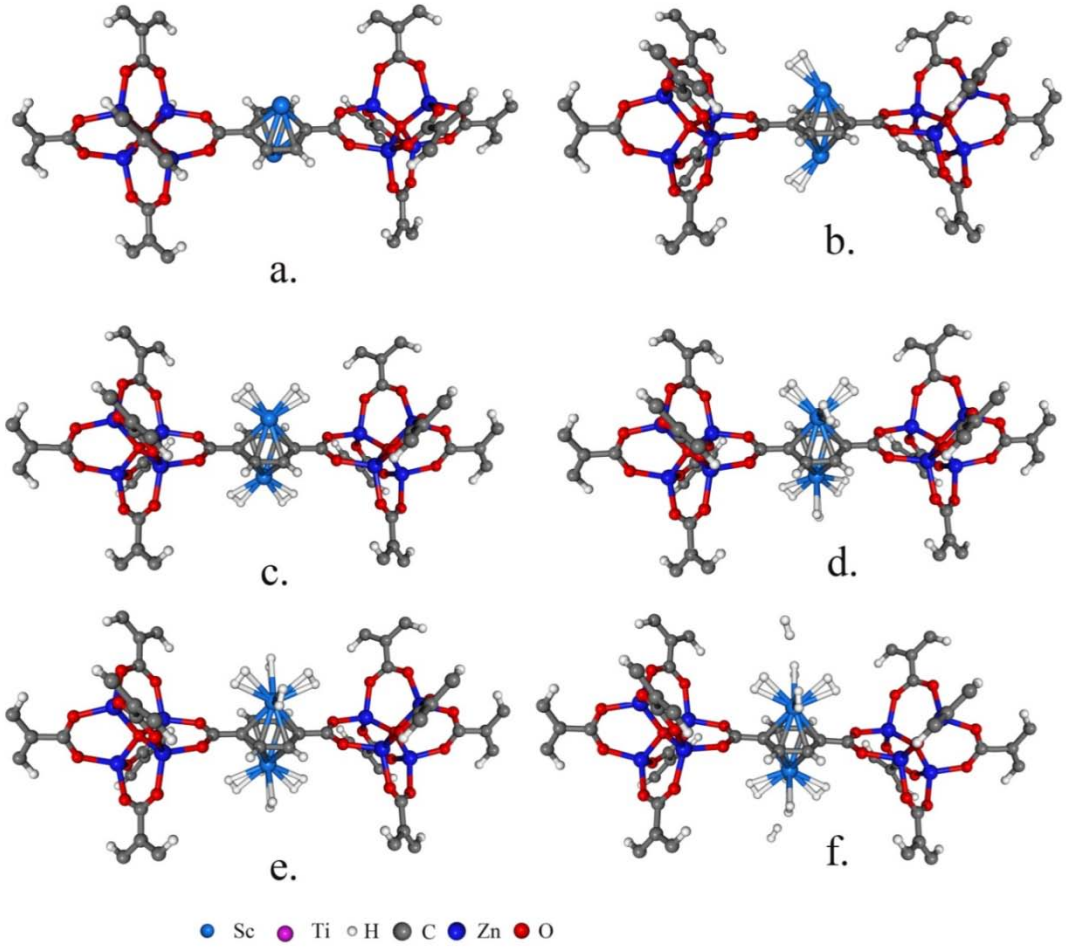

Figure 5.8. Relaxed structures of (a) MOF:Sc_2 and MOF:Sc_2:nH_2 (b) 2H_2, (c) 4H_2, (d) 6H_2, (e) 8H_2, (f) 10H_2

If ΔE_a^c is positive, clustering is favored and if ΔE_a^c is negative, non-clustered atomic configuration is favored. $\Delta E_a^c(Sc)$ is found to be -0.31 eV while $\Delta E_a^c(Ti)$ found to

be 1.29 eV. These results clearly prove that Ti clusters strongly inside MOF while Sc does not cluster within MOF. In a recent study[45], it was shown that lithium decorated MOF has been prepared via impregnating MOF with an ethanol solution of $LiNO_3$, followed by heat treatment in the vacuum. Similar strategy can be followed for synthesizing Sc decorated MOF-5.

System	Total Binding energy(kJ/mole)	BE/H_2
MOF:Sc_2:2H_2	-40.55	-20.27
MOF:Sc_2:4H_2	-129.82	-32.45
MOF:Sc_2:6H_2	-178.02	-29.67
MOF:Sc_2:8H_2	-194.28	-24.28
MOF:Sc_2:10 H_2	-209.29	-20.92
MOF:Ti_2:2H_2	-196.13	-98.06
MOF:Ti_2:4H_2	-298.00	-74.500
MOF:Ti_2:6H_2	-401.04	-66.84
MOF:Ti_2:8H_2	-398.37	-49.79
MOF:Ti_2:10H_2	-393.57	-39.35
MOF:2B:Sc_2:2H_2	-47.74	-23.87
MOF:2B:Sc_2:4H_2	-111.85	27.96
MOF:2B:Sc_2:6H_2	-153.88	-25.64
MOF:2B:Sc_2:8H_2	-217.85	-27.23
MOF:2B:Sc_2:10 H_2	-199.80	-19.88

Table 5.3. Binding energies of MOF:M_2:nH_2 and MOF:2B:Sc_2:nH_2 systems.

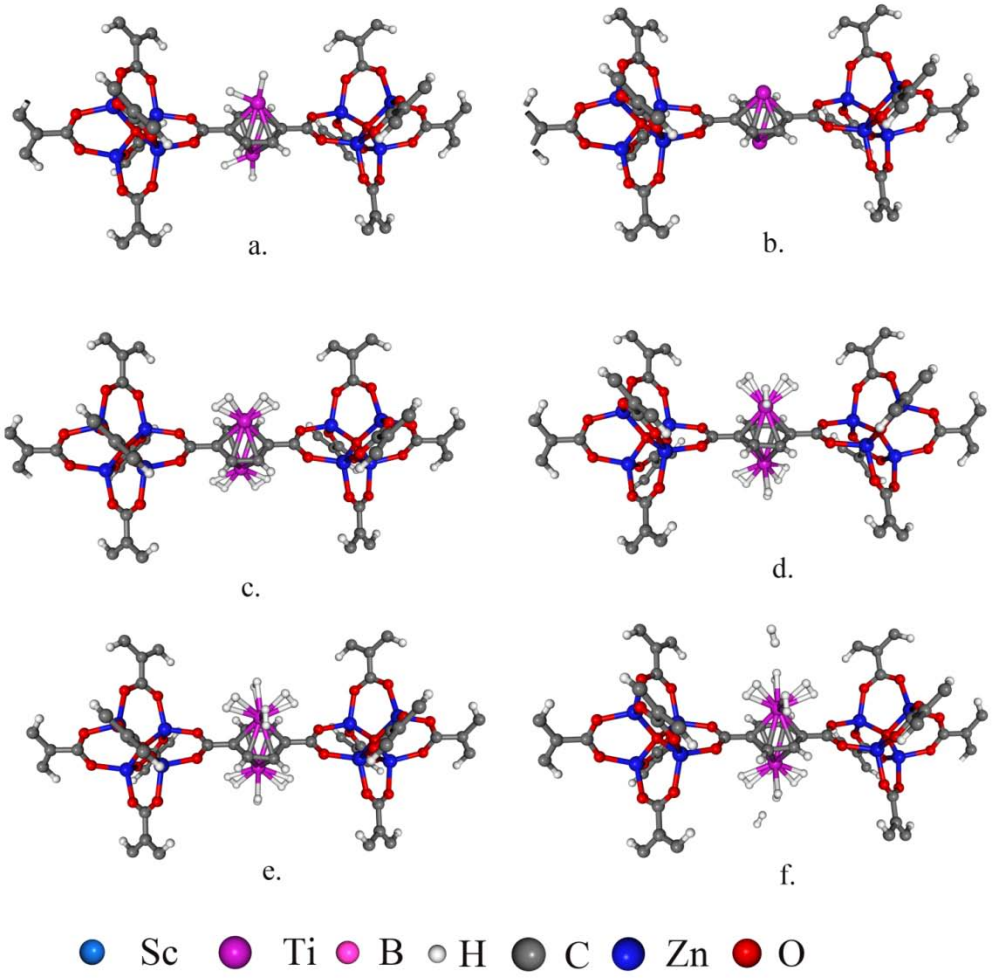

Figure 5.9. Relaxed structures of (a) MOF:Ti_2 and MOF:Ti_2:nH_2 (b) 2H_2, (c) 4H_2, (d) 6H_2, (e) 8H_2, (f) 10H_2.

The molecular frequency calculations on Sc_2-BDC units suggested that Sc_2-BDC correspond to stable minima (fig. 5.10.a and fig 5.10.b) in both ethanol and water.

The above results open up a possibility to realize a TM (Sc) decorated MOF-5 as a potential hydrogen storage candidate which does not suffer from the clustering

problem. Therefore, we also perform a comparative study of MOF-5:M_2 (where M = Sc and Ti) with regard to their interaction with increasing number of H_2. The fully optimized geometries of MOF-5:M_2:2nH_2 (where n =1, 2…, 5) are displayed in Fig. 5.8 and Fig. 5.9

The adsorption energies were calculated as:

$$E_{binding} = \frac{1}{2n}\{E_T(MOF:M_2:2nH_2) - E_T(MOF:M_2) - 2nE_T(H_2)\} \quad (5.4)$$

where $E_T(MOF:M_2:2nH_2)$, $E_T(MOF:M_2)$, and $E_T(H_2)$ are the total energies of $MOF:M_2:2nH_2$, $MOF:M_2$, and H_2 molecule, respectively. The $E_{binding}$ are listed in Table 5.3. We found binding energies of 20.27 kJ/mol H_2 for n = 1, 32.45 kJ/mol H_2 for n = 2, 29.67 kJ/mol H_2 for n = 3, 32.29 kJ/mol H_2 for n = 4 and 19.46 kJ mol H_2 for n = 5 for Sc decorated MOF. The binding energies of Ti decorated MOF-5 were found to be higher lying in range of -98.06 to -39.35 kJ/mol H_2 for n=1-5. Though for both MDMs $E_{binding}$ decreases with increasing number of H_2 molecules, the decrease in $E_{binding}$ is more significant in case of Sc. Furthermore its binding energies for all n are well within the range (20-40 kJ/mol H_2) resulting in H_2 storage at ambient temperature.

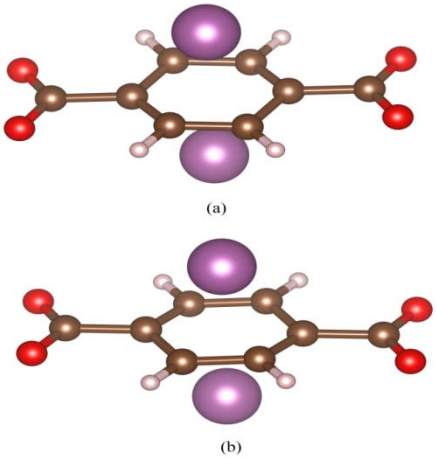

Figure 5.10: (a) Optimized geometry of Sc2-BDC in water solvent (b) Optimized geometry of Sc2-BDC in ethanol solvent.

Typically H_2 binds to transition metals through charge Kubas interactions. Such electrostatic interactions are consistent with small changes in the H–H bond length which is true for our systems as well as seen from Table 5.2 (our calculated value for the H–H

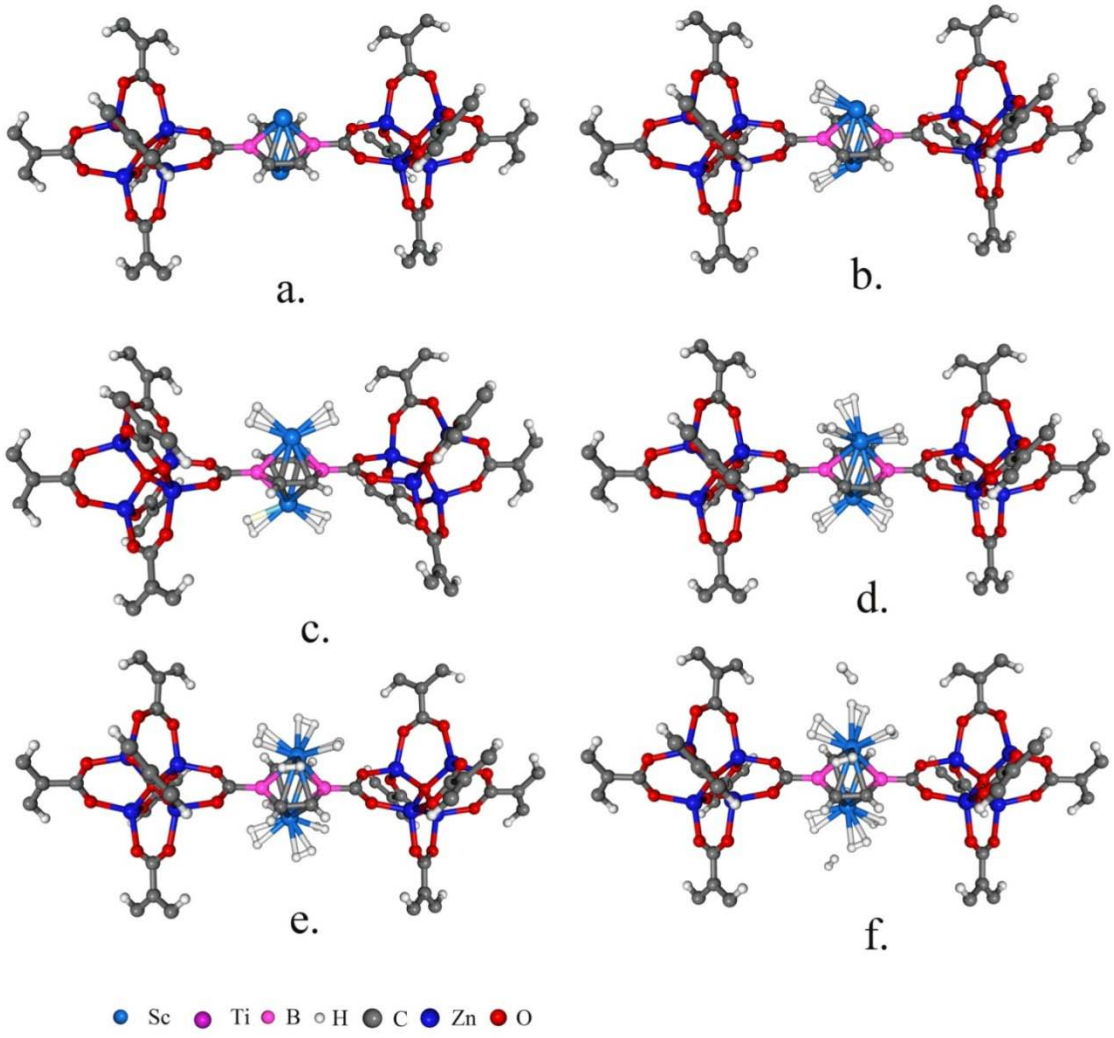

Figure 5.11. Relaxed structures of (a) MOF:2B:Sc_2 and MOF:2B:Sc_2:2nH_2 (b) 2H_2, (c) 4H_2, (d) 6H_2, (e) 8H_2, (f) 10H_2

bond distance in the free molecule is 0.750 Å). This decrease in H-H distances with n can be attributed to electron donation from hydrogen sigma bonding orbital to d orbital of metal. But as the number of H_2 molecules increase electron donation from sigma bonding

orbital of each H_2 to d orbitals of metal reduces due to competition of more H_2 molecules. Consequently the H_2 bond length starts approaching its equilibrium value when significant numbers of H_2 molecules interact with MOF-5:M_2.

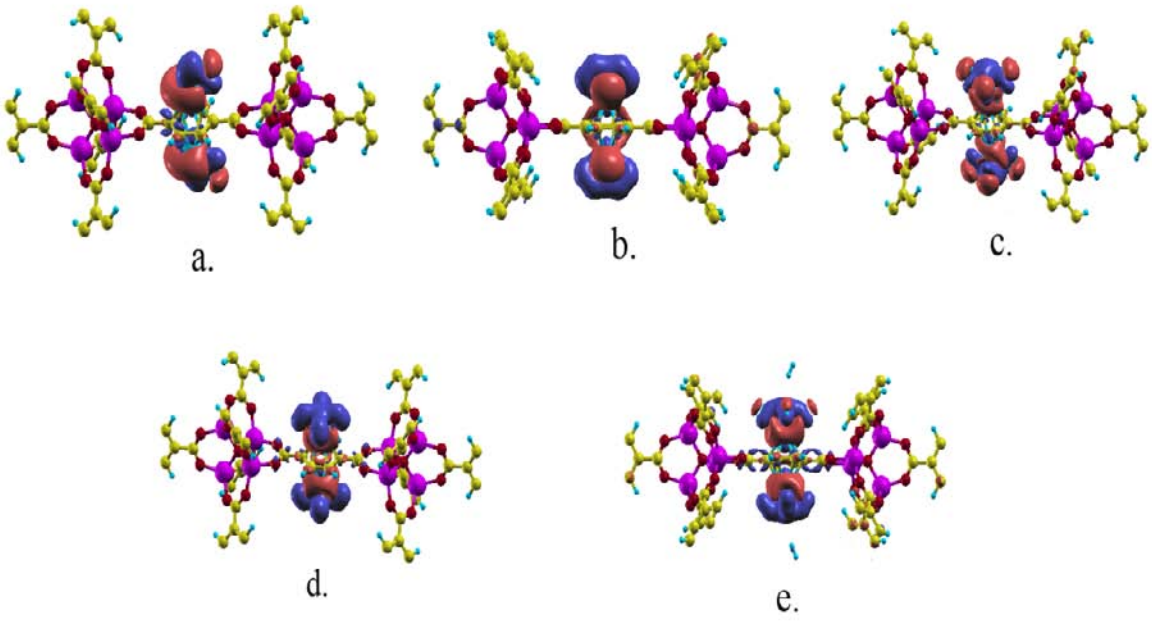

Figure 5.12. Difference charge density plots of MOF:Sc:2nH_2 (a) $2H_2$, (b) $4H_2$, (c) $6H_2$, (d) $8H_2$, (e) $10H_2$.

Lately many studies are focused on Boron substituted metal decorated MOFs[44-45]. Their results prove that B substitution increases the interaction energy of these metals with MOFs and carbon based nanomaterials. We have also studied 1,4 boron substituted Sc- and Ti-decorated MOF-5 and found in agreement with these results that boron substitution of MOF-5 increases its interaction energy by almost 100% with Sc and Ti (to -484.9 and -502.75 kJ/mol, respectively). To investigate whether boron substitution can further, avoid the transition metal clustering problem in our systems, to start with three Sc and Ti atoms were decorated on 1,4 boron substituted MDMs on each side of benzene

ring at low M-M distance of 1.511 Å. As in case of MOF-5:Sc_6 up on relaxation Sc atoms were found to be significantly apart (3.1Å) with a Bader charge of 1.13 e/Sc. Interestingly the Ti-Ti distances and charge increased to 2.42Å and 0.71 e/Ti in 1,4-B substituted MOF-5 compared to MOF-5:Ti_6. But these are still not large enough to completely avoid clustering (Fig 5.4).

As Sc atoms continue to not cluster even in presence of B atoms we have further studied adsorption of up to $5H_2$ molecules per metal (see Fig. 5.11). The calculated $E_{binding}$, presented in Table 5.3, are decreased slightly by B substitution. The only noticeable difference is in the orientation of H_2 molecule: parallel in B-substituted Sc-decorated MOF-5 and perpendicular in non B-substituted Sc decorated MOFs.

Above discussions suggest Sc to be a potential dopant for MOF-5 in the view of H_2 storage. Charge Density calculations have been done to investigate the charge distribution over the entire systems for all the MOF:Sc:$2nH_2$ structures (n=1-5). DCD plots of show the charge transfer; blue reign indicates the charge gain while red reign indicates charge loss. Electron transfer from hydrogen to metals can be clearly identified from DCC plots of these systems [Fig 5.12].

To estimate the storage capacity in the systems under investigation we assume that all metal sites are saturated, i.e., $5H_2$ are adsorbed around every metal atom, and that no other sites are populated. As each formula unit (f.u.) contains six metal atoms, $Zn_4O(BDC)_3M_6$ this corresponds to a total adsorption of 30 H_2 molecules equivalent to a hydrogen uptake of 5.81, 5.72 and 5.86 wt % for Sc decorated MOF-5, Ti decorated MOF-5 and Sc decorated 1,4 boron substituted MOF-5 respectively. Thus, Sc-decorated MOF-5s with their avoidance of metal clustering, suitable H_2 binding energies and high gravimetric H_2 storage capacities are excellent candidates for achievement of practical applications of H_2 storage at ambient conditions.

5.4 ZIF-72 as a potential hydrogen storage material

Zeolitic imidazolate frameworks (ZIFs) are porous materials consisting of tetrahedral clusters of MN_4 (M = Co, Cu, Zn, etc.) linked by imidazolate linkers [56,57]

The basic structure of ZIFs is based on classical zeolites. When compared to MOFs, ZIFs possess higher chemical stability with large structural diversity [58]. Due to these features ZIFs are very promising hydrogen storage materials.

There are only few studies are pursued the investigations of hydrogen storage in ZIFs[57-61]. In a well known experimental study Yaghi et al.[57] have suggested that ZIF-8 and ZIF-11 show reversible hydrogen storage. The hydrogen uptakes of both ZIF-8 and ZIF-11 are fond to be similar. In a Neutron powder diffraction study by Yildirim et al.[60] on ZIF-8, they suggested that the imidazolate linker represents the primary adsorption site for H_2. Furthermore, they obtained a hydrogen storage capacity of 4.2 wt % at low temperature. To design to materials with improved performance and to enhance the potential of known materials with superior storage capacities, it essential to develop an understanding of the H_2 interaction and hydrogen adsorption sites in ZIFs. Theoretical studies such as ab-inito MD can explore the interactions, mechanisms and hydrogen adsoption sites of these materials. Therefore, we have employed the ab-intio MD and DFT to investigate the hydrogen adoption sites on ZIF-72. We have also studied the enhancement of hydrogen binding energies and gravimetric capacities via metal decoration.

5.4.1 ZIF-72 structure

To relax the lattice parameter of ZIF-72, the primitive cell was chosen. This primitive cell was optimized without any constraints. The calculated lattice parameters of primitive cell are found to be in good agreement with the lattice parameters of experimental primitive cell. The calculated geometrical parameters are give in table5.5,

there is good agreement obtained with the geometrical parameters of experimental unit cell.

Lattice Parameter	a	b	c	α	β	γ
Experimental	14.255	14.255	14.225	107.249	107.249	107.249
Calculated	14.437	14.436	14.437	107.238	107.254	107.249

Table 5.4 Lattice parameters of ZIF-72.

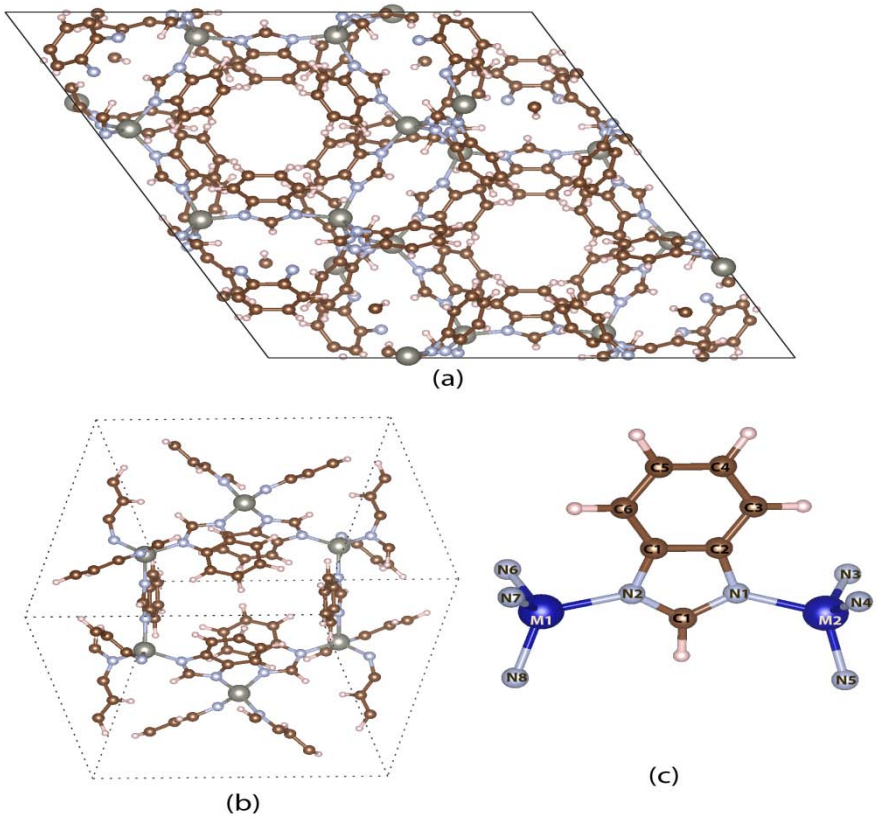

Figure 5.13. (a) ZIF-72 full unit cell, (b) ZIF-72 primitive cell and (c) the numbering scheme of ZIF-72

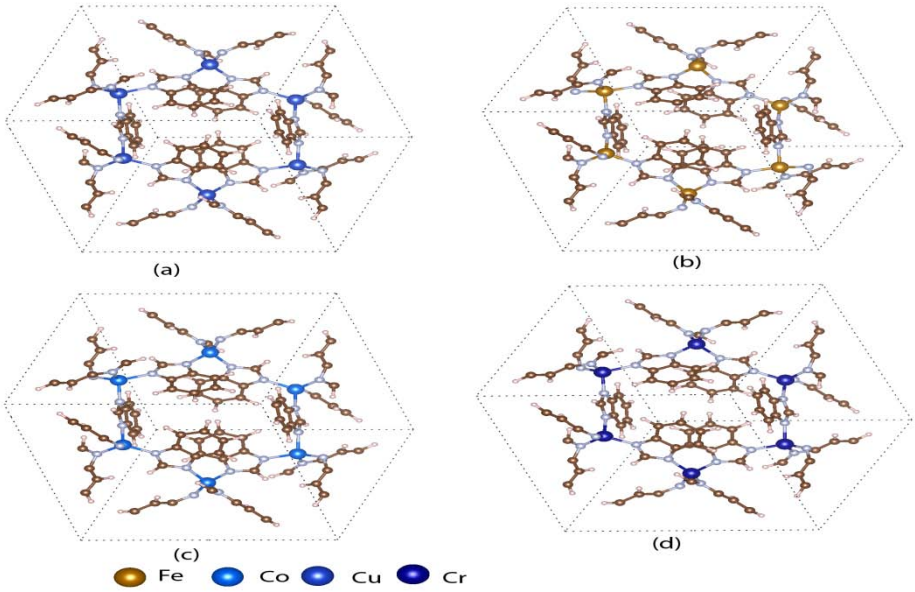

Figure 5.14. Metal substituted ZIFs (a) Cu-ZIF-72 unit cell, (b) Fe-ZIF-72 unit cell, (c) Cu-ZIF-72 unit cell, and (d) Cr-ZIF-72 unit cell.

System	Zn-Zn	Zn_1-N_2	Zn_2-N_1	**N_1-Zn_2-N_3**	**N_1-Zn_2-N_4**	N_1-Zn_2-N_5
ZIF(Zn)Experimental	6.07	1.96	2.0	108.68	100.69	115.95
ZIF(Zn)Calculated	6.18	2.02	2.03	106.16	106.18	115.05
ZIF(Co) Calculated	6.14	2.0	2.0	103.85	98.88	118.68
ZIF(Cu) Calculated	6.18	2.02	2.03	102.9	102.49	117.0
ZIF(Fe) Calculated	6.0	1.92	1.92	100.35	94.91	145.87
ZIF(Cr) Calculated	6.13	1.97	1.97	106.24	103.26	117.58

Table 5.5. Geometrical parameters of metal(Co, Cu, Cr, Fe and Zn) based ZIF.

ZIF-72 possesses as interesting structure which can be broken down to its primitive structure. Therefore, The primitive cell can studies using quantum mechanical methods like DFT. Motivated by these facts we have investigated other transition metal based M-ZIF(M=Cu, Co, Cr, Fe) various structural parameter are given in the table Z.

The above table clearly suggest the highest pore volume can be achieved with Zn based ZIF (highest Zn-Zn distance). Consequently, we have further studied Zn-based ZIF for hydrogen storage properties.

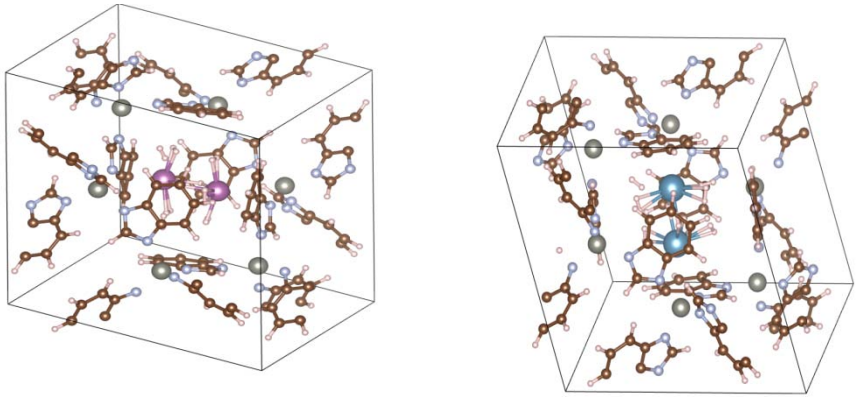

Figure 5.15. The structure of Sc and Ca decoreated ZIF-72

To exploit ZIF for hydrogen storage it is necessary to investigate the various adsorption sites. A molecular Dynamics method offers a powerful tool to investigate varius adsoption sites. We have allowed 12 H_2 molecules to interact with ZIF-72 structure. The system was subjected to simulated annealing from 100K to 25K for 2ps. The resulting structure was further allowed to anneal from 25K to 4K for 2ps. Five unique sites were selected from final structure. The sites with highest binding energies are “pore site” and site near the imadazole ring.

However, the hydrogen binding energies are as low as ~2-5 kJ/mol. For practical hydrogen storage material, these binding energies should be enhanced significantly. The investigation of H_2 binding sites suggest that pore sites can accommodate more H_2 molecules. Therefore, we attempt the introduction of electrostatic interaction via metal decoration approach.

We have decorated 2 benzene ring of ZIF-72 with Sc and Ca atoms. Several H_2 molecules are allowed to interact with these decorated metals.

Interestingly, both Sc and Ca atoms bind with 8 H_2 molecules and the resulting H_2 binding energies are -32.76 and -12.70 kJ/mol(per H_2). The calculated H_2 binding energies Sc-decorated ZIF-72 are suitable for room temperature hydrogen storage.

5.5 Conclusions:

Thus, we have analyzed light transition metal decoration of MOF-5 and its subsequent effect on its hydrogen storage properties. Our results suggest that in these systems Ti suffers from clustering but Sc avoids this problem. The calculated binding energies are found to be in the desired range for hydrogen storage at room temperature. Boron substitution increases the interaction energy. Both Sc and Ti decorated MOF-5 adsorb $5H_2$ per metal atom, with gravimetric storage of 5.81 and 5.72 wt%, respectively. Due to high storage and desired binding affinity Sc decorated MOF-5 is found to be an excellent hydrogen storage candidate for room temperature applications.

The lattice parameters and structural parameters of ZIF-72 have been calculated. The structure of other transition metal based ZIF-72 have also been investigated. H_2 adsorption sites of ZIF-72 have been calculated, Sc decoration in ZIF increases the H_2 binding energy, making this material suitable for room temperature hydrogen storage.

References

[1] Schlapbach, L.; Zuttel,A. *Nature* **2001**,414,353-353

[2] Kelkar T.; Pal S; Kanhere D.G. *Chem.Phys.Chem* **2008**,9,928-934

[3] Kumar, R. Mahesh; Subramanian, V. *Int. J. Hydrogen Energy* **2011,**36(17), 10737-10747

[4] Eddaoudi M.; Li H.; Reineke T.; Fehr M.; Kelley D.; Groy, T.L.;Yaghi, O.M. *Top.Catal* **1999**,9,105-111.

[5] Rowsell, J.L.C.; Yaghi, O.M. *J. Am. Chem. Soc.* **2006**,128,1304-1315.

[6] Bordiga, S.; Vitillo, J.G.; Ricchiardi, G.; Regli, L.; Cocina, D.; Zecchina, A.; BjØrnar, A.;Morten

[7]B.;Jasmina, H.; Lillerud, K.P. *J Phys Chem* B **2009**,109,18237-18242.

[8] Kaye, S.S.; Long, J.R. *J. Am. Chem. Soc.* **2005**,127,6506-6507.

[9] Lochan, R.C.; Head-Gordon, *Phys.Chem.Chem.Phys.* **2006**,8,1357-1370.

[10] Niu, J.; Rao, B.K.; Jena, P. *Phys. Rev. Lett.* **1992**,68,2277-2280.

[11] Rao, B. K.; Jena, P. *Europhys. Lett.* **1992**, 20, 307-312

[12] Niu, J.; Rao, B.K.; Khanna, S.N.; Jena, P. *Chem. Phys. Lett.* **1991**,230,299-305.

[13] Maseras, F.; Lledos, A.; Clot, E.; Eisenstein O. *Chem. Rev.* **2000**,100,601-636.

[14] Gagliardi, L.; Pyykko, P. *J. Am. Chem. Soc.* **2004**,126,15014-15015.

[15] Maark, T.A.; Pal, S. *Int. J. Hydrogen Energy* **2010**, 35,12846-12857.

[16] Chandrakumar, K.R.S.; Ghosh, S.K.; *Chem. Phys. Lett.* **2007**,447,208-214.

[17] Kiran, B.; Kandalam, A. K.; Jena, P. *J. Chem. Phys.***2006**, 124, 224703.

[18] Durgun, E.; Jang, Y.-R.; Ciraci, S. *Phys. Rev. B* **2007**, 76, 073413.

[19] Zhao, Y.; Kim, Y.H.; Dillon, A. C.; Heben, M. J.; Zhang, S. B. *Phys. Rev. Lett.* **2005**, 94, 155504.

[20] Phillips, A. B.; Shivaram, B. S. *Phys. Rev. Lett.* **2008**, 100, 105505.

[21] Yildirim, T.; Ciraci, S. *Phys. Rev. Lett.* **2005,** 94, 175501.

[22] Zhou, W.; Yildirim, T.; Durgun, E.; Ciraci, S. *Phys. Rev. B* **2007**, 76, 085434.

[23] Suttisawat, Y.; Rangsunvigit, P.; Kitiyanan, B.; Williams, M.; Ndungu, P.; Lototskyy, M.; Nechaev, A.; Linkov, V.; Kulprathipanja S. *Int.J. Hydrogen.Energy* **2009**,34,6669-6675.

[24] Kim, B.J.; Lee, Y.S.; Park, S.J. *Int. J.Hydrogen Energy* **2008**,33,4112-4115.

[25] Zubizarreta, L.; Menndez, J.; Pis, J.; Arenillas, A. *Int. J. Hydrogen Energy* **2009**,34,3070-3076.

[26] Lee, H.; Choi, W.I.; Ihm, J. *Phys. Rev. Lett.* **2006**,97,056104.,

[27] Patchkovskii, S.; Tse, J.S.; Yurchenko, S.N.; Zhechkov, L.; Heine, T.;Seifert, G. *Proc. Natl. Acad. Sci. USA* **2005**,102,10439-10444.

[28] Heine T.; Zhechkov, L.; Seifert, G. *Phys. Chem. Chem. Phys.* **2004**,6,980-984.

[29] Sun, Q.; Jena, P.; Wang, Q.; Marquez M. *J. Am. Chem. Soc.* **2006**,128,9741-9745.

[30] Chandrakumar, K.R.S.; Ghosh, S.K. *Nano. Lett.* **2007**,8,13-9.

[31] Forst, C.J.; Slycke, J, Van Vliet, K.J.; Yip, S. *Phys. Rev. Lett.* **2006**,96,175501.

[32] Kim, Y.H.; Zhao, Y.; Williamson, A.; Heben, M.J.; Zhang, S.B. *Phys. Rev. Lett.* **2006**,96,016102.

[33] Chen, P.; Wu, X.; Lin, J.; Tan, K.L. *Science* **1999**,285,91-93.

[34] Blomqvist, A.; Arajo, C.M.; Srepusharawoot, P.; Ahuja, R. *Proc. Natl. Acad. Sci. USA* **2007**,104,20173-20176.

[35] Han, S.S.; Goddard, W.A. *J. Am. Chem. Soc.* **2007**,129:8422-8423.

[36] Venkataramanan, N.; Sahara, R.;, Mizuseki, H.; Kawazoe, Y. *Int. J. Mo.l Sci.* **2009**,10,1601-1608.

[37] Sun, Y.Y.; Lee, K.; Kim, Y.H.; Zhang, S.B. *Appl. Phys. Lett.* **2009**,95,033109.

[38] Zou,X.; Cha, M.H.; Kim, S.; Nguyen, M.C.; Zhou, G.; Duan, W; Ihm, J. *Int. J. Hydrogen Energy* **2010**,35,198-203.

[39] Han, S.S.; Mendoza-Corte´s, J.L.; Goddard III, W.A. *Chem. Soc. Rev* **2009**,38,1460-1476.

[40] Srinivasu, K.; Ghosh, S.K. *J. Phys. Chem. C* **2011**,115 (34), 16984–16991

[41] Han, S.S.; Goddard, W.A. *J. Phys. Chem. C* **2008**,112, 13431-12436.

[42] Sun, Q.; Wang, Q.; Jena, P.; Kawazoe, Y. *J. Am. Chem. Soc.* **2005**, 127, 14582–14583.

[43] Krasnov, P. O.; Ding, F.; Singh, A. K.; Yakobson, B. *J.Phys.Chem. C* **2007**, 111, 17977–17980.

[44] Dixit, Mudit; Maark, T.A.; Pal, S. *Int. J. Hydrogen Energy* **2011**,36(17),10816-10827

[45] Henkelman, G.; Arnaldsson, A.; Jonsson, H. *Comp. Mat. Sci.* **2006**,36,354-360.

[46] Kubo, M.; Shimojima, A.; Okubo, T. *J.Phys.Chem C* **2012**,116,18,10260-10265.

[47] Kresse, G.; Furthmuller, J. *Comp. Mater. Sci.* **1996**,6,15-50.

[48] Kresse, G.; Furthmuller. J. *Phys. Rev. B.* **1996**,54,11169-11186.

[49] Kresse, G.; Joubert, D. *Phys. Rev. B.* **1999**,59, 1758-1775.

[50] Blochl, PE. *Phys. Rev. B.* **1994**,50,17953-17979.

[51] Li, H.; Eddaoudi, M.; O'Keeffe, M.; Yaghi, O.M. *Nature* **1999**,402,276-279.

[52] Monkhorst, H.J.; Pack, J.D. *Phys. Rev. B.* **1976,**13,5188-5192.

[53] Becke, A. D. *J. Chem. Phys.* **1993**, 98, 5648–52.

[54] Stephens, P. J.; Devlin, F. J.; Chabalowski, C. F.; Frisch, M. J. *J. Phys. Chem.* **1994**, 98, 11623–11627

[55] Frisch, M. J.; Trucks, G. W.; Schlegel, H. B.; Scuseria, G. E.; Robb, M. A.; Cheeseman, J. R.; Scalmani, G.; Barone, V.; Mennucci, B.; Petersson, G. A. et al. Gaussian 09, Revision A.1; Gaussian, Inc.: Wallingford, CT, 2009.

[56] Cossi, M.; Scalmani, G.; Rega, N.; Barone, V. *J. Chem. Phys.* **2002**,117, 43–54

[57] Zuttel, A. *Naturwissenschaften* **2004**, *91*, 157–172.

[58] Park, K. S.; Ni, Z.; Cote, A. P.; Choi, J. Y.; Huang, R. D.; Uribe Romo, F. J.; Chae, H. K.; O'Keeffe, M.; Yaghi, O. M. *Proc. Natl. Acad. Sci. U.S.A.* **2006**, *103*, 10186–10191.

[59] Huang, X.-C.; Lin, Y.-Y.; Zhang, J.-P.; Chen, X.-M. *Angew. Chem., Int. Ed.* **2006**, *45*, 1557–1559.

[60] Hayashi, H.; Cote, A. P.; Furukawa, H.; O'Keeffe, M.; Yaghi, O. M. *Nat. Mater.* **2007**, *6*, 501–506.

[61] Wu, H.; Zhou, W.; Yildirim, T. *J. Am. Chem. Soc.* **2007**, *129*, 5314–5315.

[62] Zhou, W.; Wu, H.; Hartman, M. R.; Yildirim, T. *J. Phys. Chem. C* **2007**, *111*, 16131–16137.

CHAPTER 6

Why Boron Substitution Increases the Interaction Energies of Metals with Benzene Based MOFs

We have investigated the role of boron to enhance the interaction energies of metals. To tune the interaction energies of metals with host materials and their H_2 binding energies ($E_{binding}$), boron substitution in the framework has been widely pursued. The investigation of role of boron substitution in enhancement of the interaction energies is necessary for designing new and potential storage materials. Our results demonstrate that boron substitution provides the proper symmetry in the framework to overlap with the metals orbitals. These orbital interactions increase the host-guest interactions, leading to increase in the interaction energies. We have also investigated the nature of interaction of H_2 molecules with metals in metal decorated-boron-substituted benzene as a model system for benzene based MOFs.

6.1 Introduction

In recent years, many research efforts have been made to find environmentally clean, renewable and efficient fuel. Hydrogen is promising fuel due to its high energy content and CO_2 free burning [1- 5].

The need for cost effective, efficient storage system is the prime problem for hydrogen based fuel technology [6-8]. To meet the performance and cost requirements, storage material must possess high gravimetric capacity as well as reversibility. Room temperature applicability and reversibility can be ensured via hydrogen binding energies in the range 20-40 kJ/mol [9, 10]. MOFs, due to their high surface area, non-dissociative hydrogen binding and fast kinetics [11], are good candidates for hydrogen storage applications. However, Van der Walls interactions involved with H_2 binding with MOFs, are not strong enough to hold hydrogen at ambient temperatures. To enhance the H_2 binding energies, introduction of electrostatic interactions are often pursued via metal decoration.

Theoretical studies have been carried out to understand the interaction of H_2 molecules with transition metal ions [14-18]. It has been shown [18] shown that neutral and cationic transition metals have the capacity to bind with six H_2 molecules.
. However, transition metals cluster with other and resulting in decrease in the H_2 storage capacity [26]. Light metals do not suffer form the clustering problem but the binding energies of alkali metals are significantly low to practically synthesize these systems.

Recently, it has been found that born substitution within the framework strengthens the metals-framework binding energy as well as the H_2 binding energy. Various research studies exploited the idea of boron substitution. Srinivasu et al. have attempted the improvement light metal adsorption energy using the boron substitution. They found that the interaction energies of metals have been increased significantly on boron substitution. Sankaran et. al.[34] have boron substitution in carbon nanotubes they have found that boron substitution enhances the hydrogen storage. Yu et al.[35] have studied the hydrogen spillover on B-doped graphene they found that by boron

substitution increases the adsorption energies for both H atoms and the metal cluster on graphene.

The approach of boron substitution followed by metals decoration has been successfully used by Pal and co-workers[12], they have shown that H_2 binding energies of boron substituted Sc decorated MOF-5 lie in the range of 20-40 kJ/mol with good gravimetric weight percent. To design new materials with improved H_2 capacity, role of boron substitution has to be clearly investigated. In this study we have focused on molecular level investigation of role of boron substitution in benzene based MOFs.
In this work we focus on the role of boron substitution to enhance the adsorption energies of benzene based MOFs.

6.2 Methodology

In this work we have performed ab-initioand DFT performed on boron substituted benzene based systems (Bz). The interaction energy (ΔE) of the metal atom M with BDC is calculated as follows:

$$\Delta E(Bz:M_2)=\frac{1}{2}[E_{Tot}(Bz:M_2)-2*E_{Tot}(M)-E_{Tot}(Bz)] \quad (6.2.1)$$

Different numbers of H_2 molecules were allowed to interact with M-decorated Bz systems. The corresponding H_2 binding energies per H_2 are calculated by the equations:

$$E_{binding}(Bz:M_2:H_2)=\frac{1}{n}[E_{Tot}(Bz:M_2:nH_2)-2*E_{Tot}(Bz:M_2)-nE_{Tot}(H_2)] \quad (6.2.2)$$

All calculations have been performed using the using Gaussian09 program package[27] and Vienna ab initio simulations package (VASP)[28,29] with DFT plane

wave pseudopotential based approach using PBE[30] exchange correlation functional . Our quantum chemical calculations were carried out with B3LYP functional with the 6-311G(d) and cc-pvtz basis sets. For all super-molecules basis set superposition error (BSSE) correction was evaluated by the counterpoise [31] method. We have used the projector augmented wave (PAW)[32,33] approach to evaluate all the properties. A kinetic energy cutoff of 400 eV was employed for DCD calculations. All geometry optimizations were carried out without any geometry constraint. All forces were calculated using the Hellmann Feynman theorem. Geometries were considered optimized with maximum force found smaller than 0.01 eV/Å. Frequency calculations are done to confirm the stable minimum for each structure.

6.3 Results and Discussions

6.3.1 Boron substituted systems

We have selected four model systems namely benzene (BZ), 1-boron substituted benzene (BZ:B), 1-4 di-boron substituted benzene(BZ:2B) and 1-3 diboron substituted benzene(BZ:1-3B). The optimized geometries at B3lyp/cc-pvtz are given in Figure 6.1 We have calculated interaction energies of four metals with our model systems. It is clear from table.1 Sc and Ti show highly exothermic interactions with large negative interaction energies with benzene, where as Li shows moderately exothermic interaction whereas Na binding is endothermic. Table 6.1. clearly shows that there is increase in the binding energies of all metals on boron substitution. The enhancement in binding energies of Li and Na decorated benzene is considerably high when compared to Sc and Ti decorated benzene, on boron substitution.

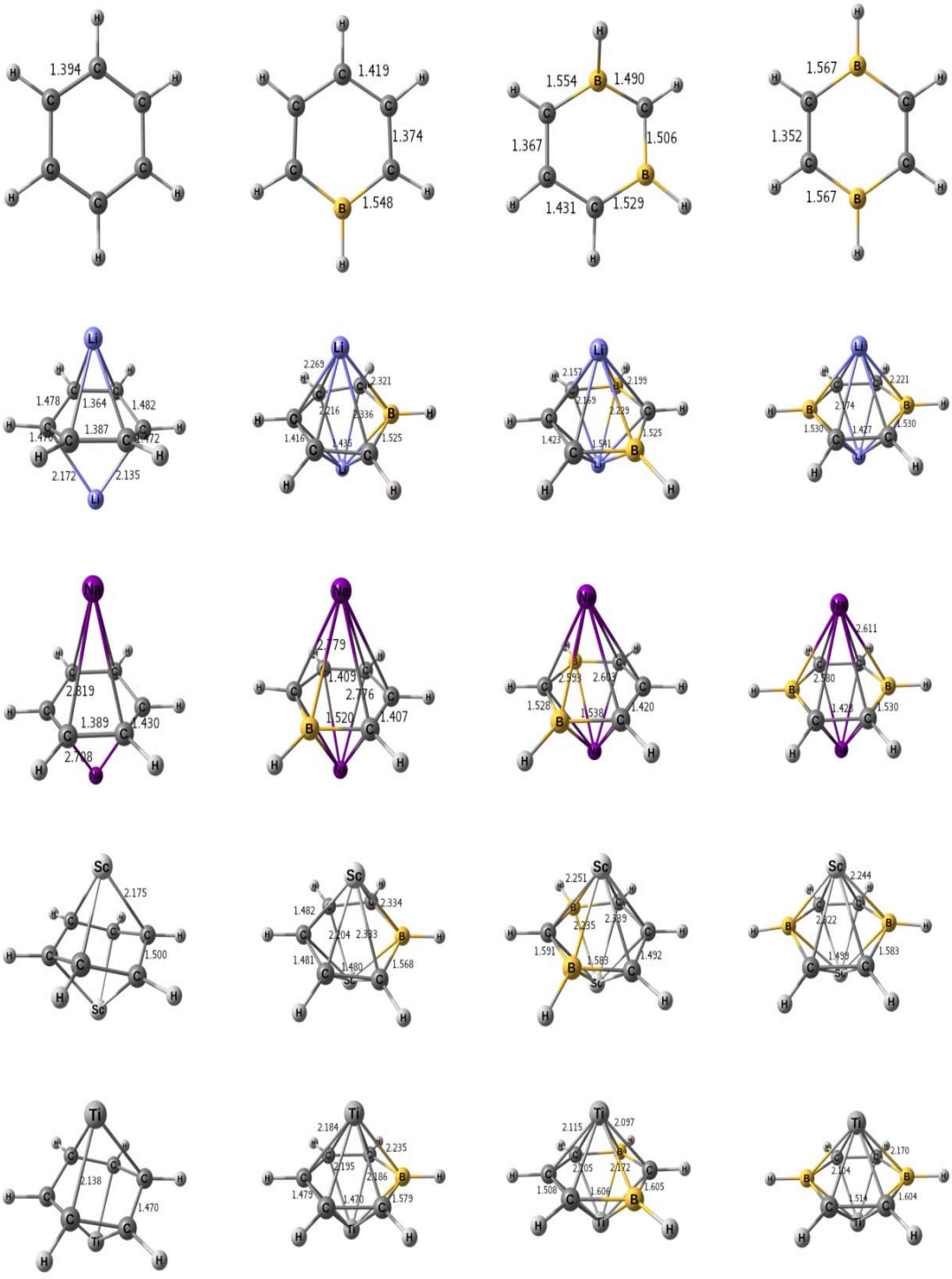

Figure 6.1. Optimized geometries of BZ, BZ:B, BZ:2B, BZ:1-3B and corresponding metals decorated counterparts.

6.3.2. Role of Aromaticity: Boron substituted model systems

On boron substitution, the number of pi electrons in boron substituted benzene decreases when compared to unsubstituted benzene, this decrease in electrons can be compensated by electron transfer by decorated metals, making the ring aromatic. Nucleus independent chemical shift (NICS) has been widely used as the indicator of aromaticity[NICS]. Table 6.2. demonstrate that the NICS values of all Li decorated boron substituted benzene are significantly negative. Hence, on Li decoration boron substituted benzene is getting aromatized. However, Na decoration does not show the similar trend. The NICS values of Sc and Ti decorated benzene are significantly negative for both boron substituted and unsubstituted benzene.

Table 6.1. Interaction energies of model systems with metals.

System	ΔE(B3LYP/6-311g(d))	ΔE(B3LYP/cc-pVTZ)
BZ:Li_2	-88.64	-86.69
BZ:B:Li_2	-383.10	-383.70
BZ:2B:Li_2	-595.02	-593.27
BZ:1-3B:Li_2	-730.92	-728.92
BZ:Na_2	10.83	18.27
BZ:B:Na_2	-285.68	-279.53
BZ:2B:Na_2	-384.40	-377.40
BZ:1-3:Na_2	-528.49	-521.56
BZ:Sc_2	-274.95	-266.18
BZ:B:Sc_2	-495.43	-664.12
BZ:2B:Sc_2	-590.65	-596.99
BZ:1-3:Sc_2	-704.86	-709.52
BZ:Ti_2	-455.33	-413.60
BZ:B:Ti_2	-719.05	-789.89
BZ:2B:Ti_2	-903.40	-868.72
BZ:1-3B:Ti_2	-849.77	-982.71

The NICS results are found to be inconclusive for Sc and Ti decorated model systems.

6.3.3. Difference charge density

Difference charge density (DCD) plots are useful to understand the charge transfer Figure 6.2. showcase the DCD plots for BZ:M_2 and BZ:2B:M_2. The red colour represents positive values or charge gain whereas green colour represents negative values or charge loss. It can be seen from figure that charge transfer from metal to benzene follows the order of Ti>Sc>>Li>>Na. This less charge transfer of Na is can also be seen in non aromatic NICS values of BZ:Na_2 systems. In boron substituted benzene the above order follows but the extent of charge transfer is considerably high when compared to unsubstituted benzene. In BZM_2 systems the charge transfer mainly occurs via p-orbitals of carbon where as in BZ:2B:M_2 systems charge transfer mainly occurs via p-orbitals centred at boron. Clearly, DCD plots explain that in boron substituted benzene systems, boron substitution strengthens the charge transfer. Figure 6.4. shows the DCD plots of BZ:2B:Sc_2:nH_2 systems, these clearly show the charge transfer from H_2 to Sc. The plots suggests that the interaction of H_2 and BZ:2B:Sc_2 to is Kubas type. The DCD plots and H-H bond lengths suggest that there is charge transfer from metal d-obitals to orbitals of hydrogen molecules.

System	**NICS**
BZ	-8.78
BZ:B	6.49
BZ:2B	12.79
BZ:1-3B	12.14
BZ:Li_2	5.70
BZ:B:Li_2	1.80

BZ:2B:Li_2	-8.70
BZ:1-3B:Li_2	-7.68
BZ:B:Na_2	-3.61
BZ:2B:Na_2	-0.97
BZ:1-3B:Na_2	-1.27
BZ:Sc_2	-37.81
BZ:B:Sc_2	-37.85
BZ:2B:Sc_2	-19.35
BZ:1-3B:Sc_2	-4.33
BZ:Ti_2	-73.32
BZ:B:Ti_2	-21.45
BZ:2B:Ti_2	-94.46
BZ:1-3B:Ti_2	-92.67

Table 6.2. NICS values of different model systems and their metal decorated counter parts.

System	**IP(eV)**	**EA(eV)**
Bz	9.22	-1.94
Bz:B	8.62	1.99
Bz:2B	9.62	-1.62
Bz:1-3B	8.19	-1.79

Table 6.3. EA and IP values of benzene substituted model systems.

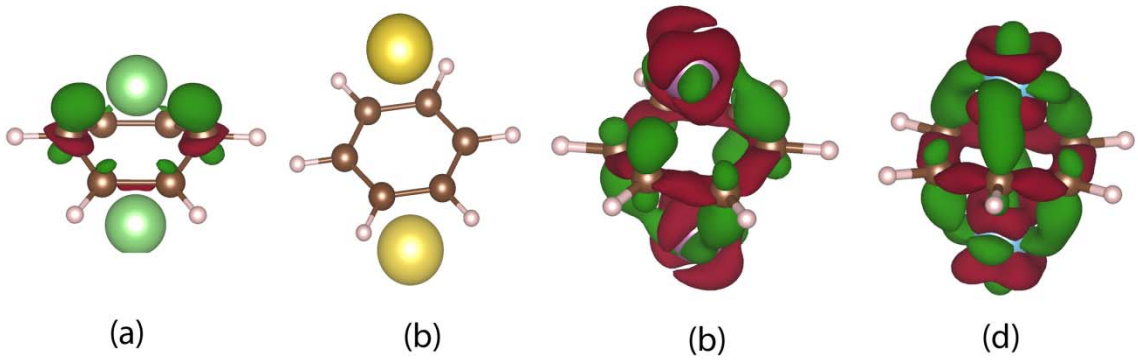

Figure 6.2. Charge density difference plots (iso value=0.01) for $BZ:M_2$ systems.(a)$Bz:Li_2$,(b)$Bz:Na_2$,(c)$Bz:Sc_2$,(d) $Bz:Ti_2$

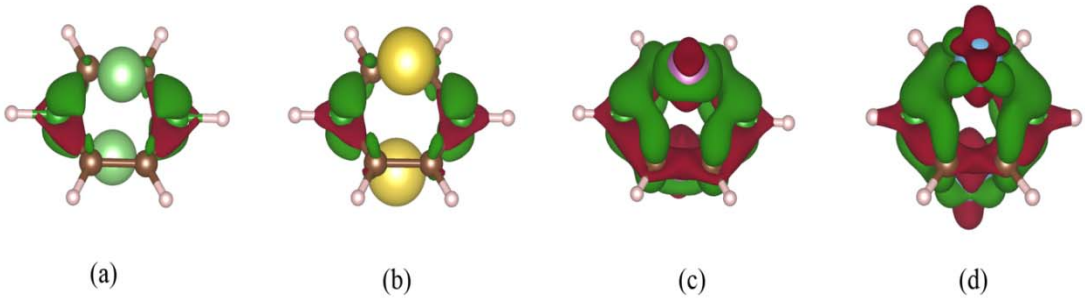

Figure 6.3. Charge density difference plots (iso value=0.01) for $BZ:2B:M_2$ systems. (a)$Bz:2B:Li_2$,(b) $Bz:2B:Na_2$, (c)$Bz:2B:Sc_2$, (d) $Bz:2B:Ti_2$

System	**VASP(PBE)**	**B3lyp/6-311g(d)**
$BZ:2B:Sc_2:H_2$	-33.95	-27.38
$BZ:2B:Sc_2:2H_2$	-36.78	-26.91
$BZ:2B:Sc_2:3H_2$	-32.07	-32.48
$BZ:2B:Sc_2:4H_2$	-33.56	-26.05
$BZ:2B:Sc_2:5H_2$	-28.15	--

Table 6.4. Binding energies of $BZ:Sc_2:nH_2$ systems.

6.3.4 MO Analysis

The Molecular Orbital (MO) analysis can provide the details of various interactions involved in binding.

To understand the role of substitution boron in the enhancement of interaction we have studied the frontier orbitals Bz, Bz:M_2, Bz:2B, and Bz:2B:M_2 system. Fig. 6.4 show the comparisons of MOs of benzene and Bz:2B system. On the boron substitution in the benzene, the HOMO and LUMO of Bz:2B on longer remain doubly degenerate, due to change in symmetry from D6H to D2H. Interestingly, the symmetry of one of HOMOs of benzene resembles to the LUMO of Bz:2B. This change in symmetry compared to benzene changes the nature of interactions involved in Bz:2B system and metals.

In the HOMO of Bz:Li_2 main atomic orbitals are Px on atom C_1 [0.302], Px on atom C_4 [0.302], S orbital on atom Li_{13} [-0.224], Px orbital on atom C_1 [0.178], Px orbital on atom C_4 [0.178]. These values suggest that the main interactions are due to the overlap between the two carbon atoms and one Li atom. The distorted structure of Bz:Li_2 system and the smaller distance between the C_1-Li_{13} C_4-Li_{13} also supports the molecular orbital analysis.

In contrast, In the HOMO of Bz:2B:Li_2, the highest contribution is of Pz on atom B [0.153 and 0.147], Py on atom Li atoms [0.145 and -0.145], and Pz on atom C [0.122, 0.122, -0.122, -0.122] the values suggest that there is strong interaction with Py orbital Li atoms and Pz orbitals of boron atoms. Also there is significant interaction between Pz of carbon atoms and Pz of Li atoms.

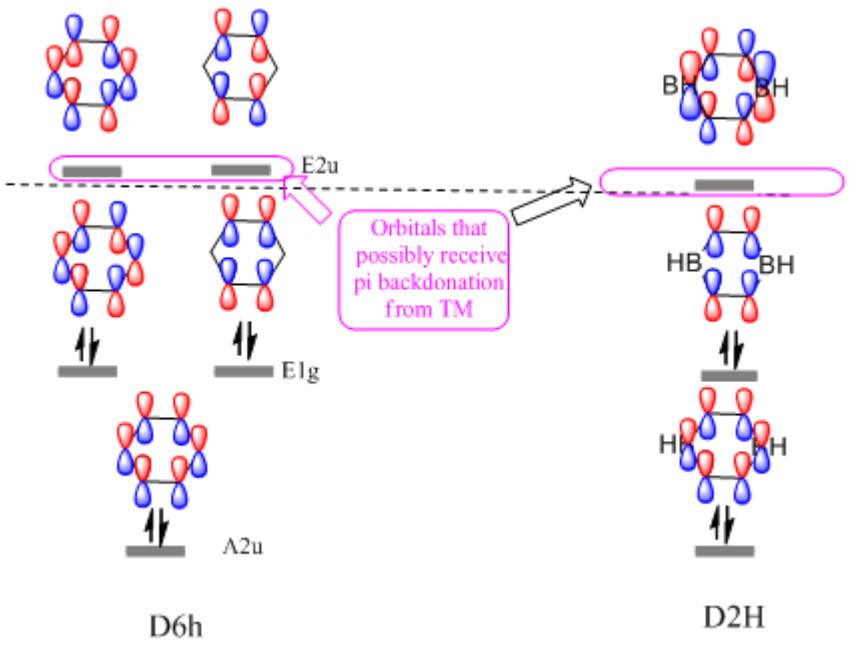

Figure 6.4. Comparison of change of MO diagram when going from D_{6h} to D_{2h} symmetry.

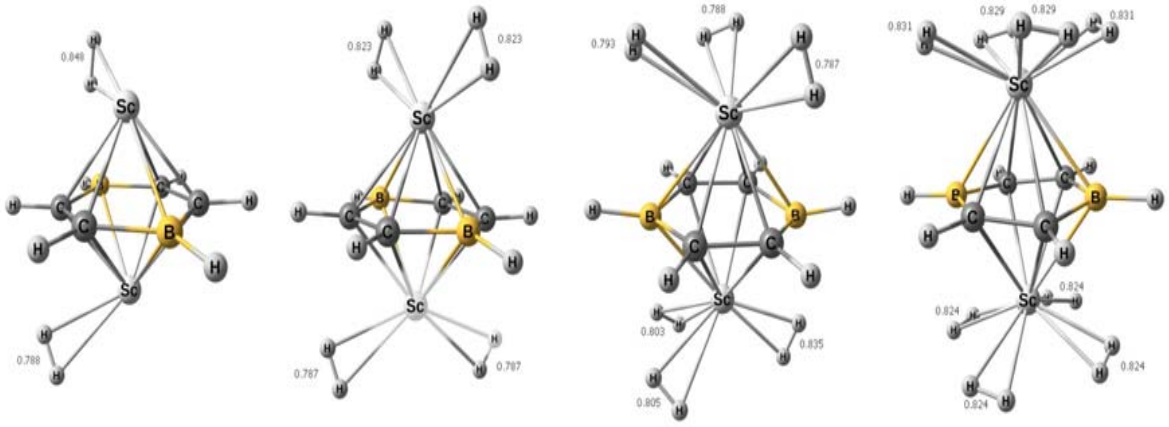

Figure 6.5. Optimized geometries of $BZ:Sc_2:nH_2$ systems.

Clearly, boron not only strongly interacts with Li atoms but also the boron substitution strengthens the interaction of Li-C atoms, this is attributed the imposed planarity in $Bz:2B:Li_2$ system when compared to $Bz:Li_2$ sytems. Similar results are a obtained for both $Bz:Na_2$ systems and $Bz:2B:Na_2$ systems. In the HOMO of $Bz:Sc_2$ main atomic orbitals are S on atom Sc[0.257, 0.257, -0.229and -0.229], Pz on atom Sc [0.225, -

0.225], Pz on atom C [0.066, -0.066, 0.066, -0.066, 0.066 and -0.066] the orbital contributions, molecular symmetry and structural distortions suggest that there is strong interactions with Pz of three carbon atoms and s orbital of Sc on both side of the ring. However, in the HOMO of Bz:2B:Sc_2 main atomic orbitals are Px on atom B [0.264 and 0.264], S on atom Sc [-0.222 and 0.222], Px on atom C[-0.166, -0.166, -0.166 -0.166], d on atom Sc [-0.163, 0.163, -0.161, 0.161, -0.144, 0.144], S on atom Sc [-0.136, 0.136, 0.132].

These orbital coefficients suggest that there is strong interaction between Px of boron atoms and d orbital of Sc atoms also there is considerable interaction between d orbital of Sc and Px orbitals of carbon atoms. The HOMO of Ti represents the Ti-Ti interactions. However, in the HOMO-1 of Bz:2B:Ti_2,the main orbitals are, d orbitals of atom Ti [0.237, -0.237, 0.190, -0.190], Px on atom B [-0.149, 0.149], Px on atom B [-0.131, -0.131], Px on atom B [-0.123, -0.123], d on atom Ti [0.107, -0.107], Px on atom C [0.061, 0.061, 0.061,0.061].

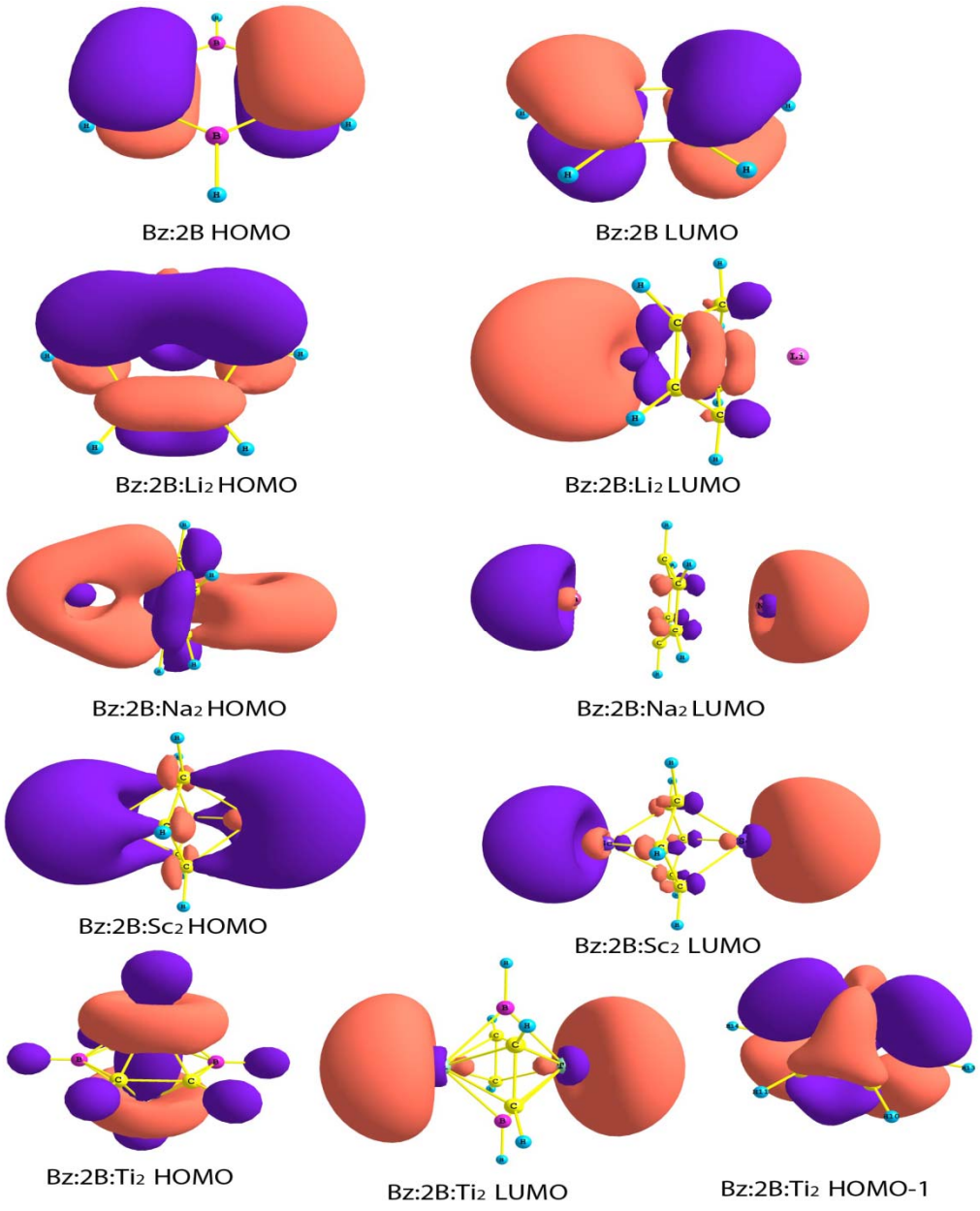

Figure 6.6. The molecular orbitals of Bz:2B and Bz:2B:M_2 systems.

The above molecular orbital analysis clearly suggests that the boron substituted systems have proper symmetry to overlap with the metal d or p orbitals. However, the unsubstituted systems interact with the metals only via s-obitals.

In the metals decorated benzene based systems the symmetry of benzene breaks and it no longer remains D_6H. This change in symmetry makes back bonding difficult because of improper orbital overlap with metal d-obitals and benzene of the framework. In Bz:2B:Sc_2 the HOMO represents the interaction of Sc perpendicular d-orbital with Bz:2B LUMO, where as in Bz:Sc_2 HOMO represents the interaction of s-orbitals of Sc with LUMO of benzene in D_{3d} symmetry. Careful analysis of MOs also suggests that high coefficient of pz orbital facilitates the interaction of M-d orbitals with Bz:2B system. It is clear from above discussion that the role of boron is three fold: (i) it provides proper orbital symmetry, via imposed planarity in the benzene ring, for metals d-obitals to interact via charge transfer.(ii) high p_z MO coefficient centered on boron facilitates the interactions. (iii) boron substitution makes benzene ring electron deficient.

6.3.5. BZ:Sc_2:nH_2 Systems

The optimized geometries at B3lyp/6-311g(d)of BZ:Sc_2:nH_2 are given in figure . We have given various structural parameters are given in table 6.4. It is clear from table the H-H bond lengths decease as more number of H_2 are allowed to interact with Sc metals The calculated binding energies lie in the range of 20-40kJ/mol of for BZ:2B:nH_2 systems. These results open up a possibility to use boron substitution and Sc decoration in benzene based MOFs. Our results are in good agreements with previous reported values of MOF-5[12]).

6.4. Conclusions

In this work we have analyzed the role of boron in strengthening the interaction of metals with boron substituted benzene using frontier molecular orbitals. Our results confirm that boron substitution enhances the interaction energy of metals with benzene. DCD plots clearly show the enhanced charge transfer on boron substitution. MO analysis suggests that boron substitution provides the proper symmetry to the MOs of framework to strongly interact with metals. Metals decoration breaks the symmetry of benzene and

resulting M-Bz interaction occurs primarily due to s-p overlap whereas boron substituted systems have proper symmetry to overlap with the metal through d or p orbitals. Large p-orbital coefficient centered on boron facilitates the interactions metal boron interactions.

References:

[1] L. Schlapbach, A. Zuttel, *Nature* **2001**,414, 6861

[2] N. L. Rosi, J. Eckert, M. Eddaoudi, D. T. Vodak, J. Kim,M. O'Kee_e, O. M. Yaghi, , *Science* **2003**, 300, 1127-1129.

[3] X. Zhao, B. Xiao, A. J. Fletcher, K. M. Thomas, D. Bradshaw, M. J. Rosseinsky, *Science* **2004**, 306, 1012-1015.

[4] J. L. C. Rowsell, E. C. Spencer, J. Eckert, J. A. K. Howard, O. M. Yaghi, , *Science* **2005**, 309, 1350.

[5] S. Han, W.-Q. Deng, W. Goddard *Angew. Chem. Int. Ed.* **2007**, 46, 6289

[6]DOErequirements(2010), url=http://www1.eere.energy.gov/hydrogenandfuelcells/storage/schallenges.html,.

[7] J. Graetz, *Chem. Soc. Rev.* **2009**, 38, 73-82.

[8] S. S. Han, J. L. Mendoza-Cortes, W. A. Goddard III *Chem. Soc. Rev*. **2009**, 381460.

[9] R. C. Lochan, M. Head-Gordon, *Phys. Chem. Chem. Phys.* **2006,** 8, 1357.

[10] P. Jena, *J. Phys.Chem. Lett.* **2011**, 2, 3

[11] S. Bordiga, J. G. Vitillo, G. Ricchiardi, L. Regli, D. Cocina, A. Zecchina, B. Arstad, M. Bjrgen, J. Ha_zovic, K. P. J. Lillerud, *J. Phys. Chem. B* **2005**,109, 18237.

[12] M. Dixit, T. Adit Maark, K. Ghatak, R. Ahuja, S. Pal, *J. Phys. Chem. C* **2012**,116, 33,17336.

[13] K. R. S.Chandrakumar, S. K. Ghosh, *Nano Lett.* **2008**, 8, 13.

[14] Niu J, Rao BK, Jena P. *Phys. Rev. Lett.* **1992**, 68,2277.

[15] Charles J, Bauschlicher W, Walch SP. *J. Chem. Phys.* **1982**, 76, 4560.

[16] Niu J, Rao BK, Khanna SN, Jena P. *Chem. Phys. Lett.* **1991**, 230, 299.

[17] Maseras F, Lledos A, Clot E, Eisenstein O. *Chem. Rev.* **2000**, 100, 601.

[18] Gagliardi L, Pyykko P. *J. Am. Chem. Soc.* **2004**, 126, 15014.

[19] Maark TA, Pal S. *Int. J. Hydrogen Energy* **2010**, 35, 12846.

[20] Chandrakumar KRS, Ghosh SK. *Chem. Phys. Lett.* **2007**, 447, 208.

[21] Suttisawat Y, Rangsunvigit P, Kitiyanan B, Williams M, Ndungu P, Lototskyy M, et al. *Int. J. Hydrogen Energy* **2009**,34, 6669.

[22] Kim BJ, Lee YS, Park SJ. *Int. J. Hydrogen Energy* **2008**, 33, 4112.

[23] Zubizarreta L, Menndez J, Pis J, Arenillas A. *Int. J. Hydrogen Energy* **2009**, 34, 3070.

[24] Zhao Y, Kim YH, Dillon AC, Heben MJ, Zhang SB. *Phys. Rev. Lett.* **2005**, 94, 155504.

[25] Yildirim T, Ciraci S. *Phys. Rev. Lett.* **2005**,94,175501.

[26] Sun Q, Wang Q, Jena P, Kawazoe Y. *J. Am. Chem. Soc.* **2005**, 127, 14582.

[27] Gaussian 09, Revision A.1, Frisch MJ, Trucks GW, Schlegel HB, Scuseria GE, Robb MA, Cheeseman JR et al. Gaussian Inc., Wallingford CT, **2009**.

[28] Kresse G, Furthmuller *J. Comp. Mater. Sci.* **1996**, 6, 15-50.

[29] Kresse G, Furthmuller J. *Phys. Rev. B.* **1996**, 54, 11169.

[30] Perdew JP, Burke K, Ernzerhof M. Phys. Rev. Lett. **1996**, 77, 3865.

[31] Kresse G, Joubert D. *Phys. Rev. B* **1999**, 59, 1758.

[32] Blochl PE. *Phys. Rev. B,* **1994**, 50 ,17953.

[33] Monkhorst HJ, Pack JD. Phys. Rev. B **1976**, 13, 5188.

[34] M. Sankaran, B. Viswanathan, S. Srinivasa Murthy, *Int. J. Hydrogen Energy*. **2008** 33, 393

[35] Hong-Yu Wu, Xiaofeng Fan, Jer-Lai Kuo, and Wei-Qiao Deng. *J. Phys. Chem. C* **2011,** *115*, 924.